(4)

Final Report

on

Fundamental Studies and Device Development In Beta Silicon Carbide

Supported by ONR Under Contract #N00014-82-K-0182 P00009

For the Period January 1, 1988 - December 31,1989

College of Engineering

North Carolina State University

Raleigh, North Carolina

4

Final Report

on

Fundamental Studies and Device Development In Beta Silicon Carbide

Supported by ONR Under Contract #N00014-82-K-0182 P00009

For the Period January 1, 1988 - December 31,1989

REPORT DOCUMENTATION PAGE

Form Approved
OMB No 0704-0188

1. AGENCY USE ONLY (Leave blank)	2. REPORT DATE	3. REPORT TYPE AND DATES COVERED
	28 Feb. 90	Final

4. TITLE AND SUBTITLE
Fundamental Studies and Device Development in Beta Silicon Carbide

5. FUNDING NUMBERS
N00014-82-K-0182/P00009
R&T Project Code:
414f043---04
21 Aug 1987; FRG:414f

6. AUTHOR(S)
Robert F. Davis

7. PERFORMING ORGANIZATION NAME(S) AND ADDRESS(ES)
North Carolina State University
Hillsborough Street
Raleigh,NC 27695

8. PERFORMING ORGANIZATION REPORT NUMBER
NCS-MAT/D-0014

9. SPONSORING/MONITORING AGENCY NAME(S) AND ADDRESS(ES)
Office of Naval Research
Electronics Program-Code 1114
800 North Quincy Street
Arlington, VA 22217

10. SPONSORING/MONITORING AGENCY REPORT NUMBER

11. SUPPLEMENTARY NOTES

12a. DISTRIBUTION/AVAILABILITY STATEMENT
Approved for Public Release; Distribution Unlimited

12b. DISTRIBUTION CODE

13. ABSTRACT (Maximum 200 words)

The dependence of growth rate of α-SiC on α-SiC substrates and surface morphology on temperature, source gas/carrier gas flow rate ratios, and the degree of off-axis tilt have been investigated. Theoretical and experimental studies of Al and N incorporation into 6H-SiC films during deposition have also been studied. Device research has involved studies of suitable ohmic and rectifying contacts, and the fabrication and characterization of Schottky and p-n junction diodes as well as MESFET, MOSFET and IMPATT structures.

14. SUBJECT TERMS
Alpha Silicon Carbide, growth rate, aluminum dopant, nitrogen dopant, ohmic contacts, Schottky contacts, MESFET, MOSFET, IMPATT

15. NUMBER OF PAGES
75

16. PRICE CODE

17. SECURITY CLASSIFICATION OF REPORT	18. SECURITY CLASSIFICATION OF THIS PAGE	19. SECURITY CLASSIFICATION OF ABSTRACT	20. LIMITATION OF ABSTRACT
UNCLAS	UNCLAS	UNCLAS	SAR

GENERAL INSTRUCTIONS FOR COMPLETING SF 298

The Report Documentation Page (RDP) is used in announcing and cataloging reports. It is important that this information be consistent with the rest of the report, particularly the cover and title page. Instructions for filling in each block of the form follow. It is important to ***stay within the lines*** to meet ***optical scanning requirements***.

Block 1. Agency Use Only *(Leave blank)*.

Block 2. Report Date. Full publication date including day, month, and year, if available (e.g. 1 Jan 88). Must cite at least the year.

Block 3. Type of Report and Dates Covered. State whether report is interim, final, etc. If applicable, enter inclusive report dates (e.g. 10 Jun 87 - 30 Jun 88).

Block 4. Title and Subtitle. A title is taken from the part of the report that provides the most meaningful and complete information. When a report is prepared in more than one volume, repeat the primary title, add volume number, and include subtitle for the specific volume. On classified documents enter the title classification in parentheses.

Block 5. Funding Numbers. To include contract and grant numbers; may include program element number(s), project number(s), task number(s), and work unit number(s). Use the following labels:

C	- Contract	**PR**	- Project
G	- Grant	**TA**	- Task
PE	- Program Element	**WU**	- Work Unit Accession No.

Block 6. Author(s). Name(s) of person(s) responsible for writing the report, performing the research, or credited with the content of the report. If editor or compiler, this should follow the name(s).

Block 7. Performing Organization Name(s) and Address(es). Self-explanatory.

Block 8. Performing Organization Report Number. Enter the unique alphanumeric report number(s) assigned by the organization performing the report.

Block 9. Sponsoring/Monitoring Agency Name(s) and Address(es). Self-explanatory.

Block 10. Sponsoring/Monitoring Agency Report Number. *(If known)*

Block 11. Supplementary Notes. Enter information not included elsewhere such as: Prepared in cooperation with...; Trans. of...; To be published in.... When a report is revised, include a statement whether the new report supersedes or supplements the older report.

Block 12a. Distribution/Availability Statement. Denotes public availability or limitations. Cite any availability to the public. Enter additional limitations or special markings in all capitals (e.g. NOFORN, REL, ITAR).

DOD	- See DoDD 5230.24, "Distribution Statements on Technical Documents."
DOE	See authorities.
NASA	- See Handbook NHB 2200.2.
NTIS	- Leave blank.

Block 12b. Distribution Code.

DOD	- Leave blank.
DOE	- Enter DOE distribution categories from the Standard Distribution for Unclassified Scientific and Technical Reports.
NASA	- Leave blank.
NTIS	- Leave blank.

Block 13. Abstract. Include a brief *(Maximum 200 words)* factual summary of the most significant information contained in the report.

Block 14. Subject Terms. Keywords or phrases identifying major subjects in the report.

Block 15. Number of Pages. Enter the total number of pages.

Block 16. Price Code. Enter appropriate price code *(NTIS only)*.

Blocks 17. - 19. Security Classifications. Self-explanatory. Enter U.S. Security Classification in accordance with U.S. Security Regulations (i.e., UNCLASSIFIED). If form contains classified information, stamp classification on the top and bottom of the page.

Block 20. Limitation of Abstract. This block must be completed to assign a limitation to the abstract. Enter either UL (unlimited) or SAR (same as report). An entry in this block is necessary if the abstract is to be limited. If blank, the abstract is assumed to be unlimited.

I. INTRODUCTION

Silicon Carbide is considered a superior candidate material for high temperature, high power and high frequency electronic devices due to its high melting point, high thermal conductivity (4.9W/cm°C)[1], wide bandgap (2.86 eV for 6H-SiC)[2] and high breakdown field (2 - 3 x 10^6 V/cm)[3]. Two additional reasons for the renewed interest in silicon carbide are the significant advances in the growth of monocrystalline thin films of this material by chemical vapor deposition (CVD) and the ability to dope this material with n- and p-type dopants during growth or via ion implantation. As a result, devices from this material have now become a reality.

Silicon carbide has been epitaxially grown on α-SiC substrates since the late 1960's. Several investigators have reported on the growth of α-SiC on α-SiC substrates in the temperature ranges 1773-2023K[4-6] and 1593-1663K[7] with growth directions parallel and perpendicular, respectively, to the [0001] axis. The growth of β-SiC on α-SiC and β-SiC substrates in the temperature ranges of 1773-1973K[8,9] and 1473-2073K[10], respectively, have also been studied.

The use of 6H-SiC {0001} substrates for the growth of β-SiC films in our laboratory resulted in a substantial reduction in the defect density at the interface of the films and the substrates[11]. High quality of 6H-SiC films grown on off-axis 6H-SiC substrates have also been grown in our laboratory by Kong et. al.[12]. Such films are very suitable for device fabrication. Therefore, a more thorough characterization of the film growth is of interest.

In this reporting period, the dependence of growth rate and surface morphology on temperature and source gases/carrier gas flow rate ratio have been investigated. The effect of the degree of off-axis tilt of the substrates on the surface morphology has also been studied. The results of these efforts are presented in Section II.

Theoretical and experimental studies of aluminum and nitrogen incorporation into 6H-SiC films during epitaxial growth via in situ CVD doping have also been conducted, as described in Section III. For the fabrication of devices, it is necessary to have viable ohmic and rectifying contacts. Research regarding this topic is described in Section IV.

Several devices in 6H-SiC including p-n junctions diodes, metal-semiconductor field-effect transistors (MESFETs), metal-oxide-semiconductor field-effect transistors(MOSFETs) and impact avalanche transit-time diodes(IMPATTs) have been fabricated and characterized at NCSU, as described in Section V. The final part (VI) of this report documents our new thrust in molecular beam epitaxy of SiC.

II. GROWTH OF 6H-SiC THIN FILMS VIA CVD

A. Experimental Procedure

High quality, Al-doped 6H-SiC wafers obtained from Cree Research, Inc. and black, industrial 6H-SiC crystals obtained from an Acheson furnace were employed as the substrates for the CVD growth of 6H-SiC films. The substrates from Cree Research, Inc. were cut such that the [0001] direction was oriented 3° off-axis toward the $[11\bar{2}0]$ orientation and terminated with either the Si face or the C face. The Acheson crystals were lapped 3°, 5.5°, 8.5°, 11.5° and 14.5° off the [0001] axis toward the $[11\bar{2}0]$ axis, respectively, and polished with 0.1 μm diamond paste. Each polished wafer was then oxidized at 1473K in flowing dry oxygen to form an approximately 50nm oxide layer which contained subsurface damage caused by the mechanical polishing. The Si face or the C face of the Acheson substrates was distinguished by the difference in the thickness of the resultant oxide layer. The oxide layer on each substrate was removed with an HF acid solution immediately prior to loading onto a SiC-coated graphite susceptor which held the samples during growth. A cold wall, barrel-type, rf-heated CVD system[13] was used for the deposition of the 6H-SiC films.

The substrates were initially heated to the growth temperature (1623-1873K) for 10 minutes in 1 atm of flowing H_2 (3000 sccm) to etch the surface of the substrates. The reactive gases of SiH_4 and C_2H_4 were subsequently introduced into the H_2 stream to start the SiC deposition under the same temperature and total pressure. The ratio of the sum of the SiH_4 and C_2H_4 flow rates (sccm) to the H_2 flow rate (sccm) was varied from 3:3000 to 1:3000. The ratio of the SiH_4 flow rate to the C_2H_4 flow rate was fixed at 2.

The as-grown surfaces of the thin films were examined by optical microscopy (OM) and scanning electron microscopy (SEM). The thickness of each film was measured by secondary ion mass spectrometry (SIMS). In order to get a thorough understanding of the growth kinetics, the growth rates on both the Si face and the C face of the substrates were determined. The results of this work are presented in the following subsection.

B. Results

1. CVD Growth Rate

The dependency of the growth rates on both the Si face and the C face on the temperatures at a $(SiH_4+C_2H_4)/H_2$ gas flow rate ratio of 1;3000 are shown in Fig. 1. The curves follow the Arrhenius equation:

$$R_g = R_o \exp\left(-\frac{\Delta E}{RT}\right)$$

where R_g is the growth rate perpendicular to the substrate surface, R_o is a pre-exponential factor, ΔE is the apparent activation energy and R is the ideal gas constant. From the slopes of the curves, ΔE was determined to be approximately 64 KJ/mol.(15 Kcal/mol.) for the Si face and 55 KJ/mol.(13 Kcal/mol.) for the C face, respectively. The lower activation energy value for the C face is evidence that the growth rate on the C face is higher than that on the Si face. By comparison, the activation energy values previously reported were 22 Kcal/mol. for the growth of α-SiC on an α-SiC $(000\bar{1})$ face in a C_3H_8 - SiH_4 - H_2 system by Wessels et. al.[4], while that calculated from Nishino and coworkers' data[5] was 13 Kcal/mol. for α-SiC grown on an α-SiC $(000\bar{1})$ C face using C_3H_8 and $SiCl_4$ in H_2. The value obtained for the C face in the present research is comparable with that calculated form Nishino and coworkers' data even though different reactants (C_2H_4 vs. C_3H_8 and SiH_4 vs. $SiCl_4$) were used. Kong and et. al.[14] previously reported an activation energy of 12 Kcal/mol. for β-SiC grown on the (0001) Si face of 6H-SiC using the same gases (C_2H_4 - SiH_4 - H_2) and deposition system as that used in the present research. There are no available comparative data for α-SiC grown on a 6H-SiC Si face.

The dependency of the growth rates on the $(SiH_4+C_2H_4)/H_2$ flow rate ratio at 1773K for 6H-SiC films on the off-axis Si face and C face of the 6H-SiC substrates is shown in Fig. 2. The growth rates for both faces increase linearly with the increase in the gas flow rate ratio. The correlation factor of each curve in Fig. 2 is 0.96.

2. Surface Morphology

The surface morphologies of the as-grown 6H-SiC epilayers were investigated with a Nomarski microscope and/or SEM. Figures 3 and 4 show the dependency of the surface morphologies on the temperatures for the Si face (Fig. 3) and the C face (Fig. 4). The films

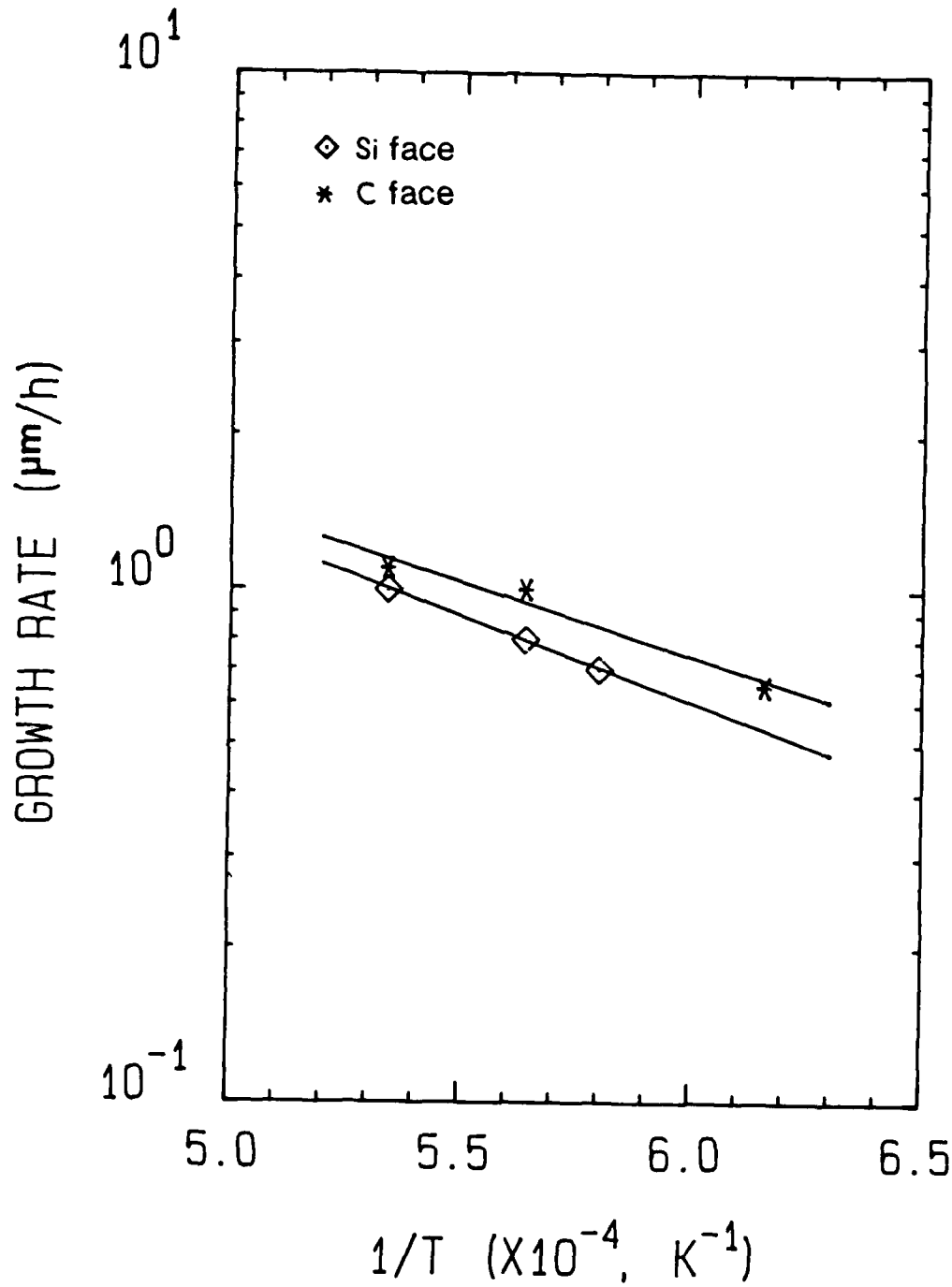

Figure 1: Growth rates of 6H-SiC on off-axis 6H-SiC substrates vs. the inverse of temperature. The activation energies calculated from the slopes of the curves are 64 KJ/mol for the Si face and 55 KJ/mol for the C face, respectively. The flow rate ratio of $(SiH_4 + C_2H_4)/H_2$ for the film deposition was 1:3000. The CVD reactor pressure was 1 atm.

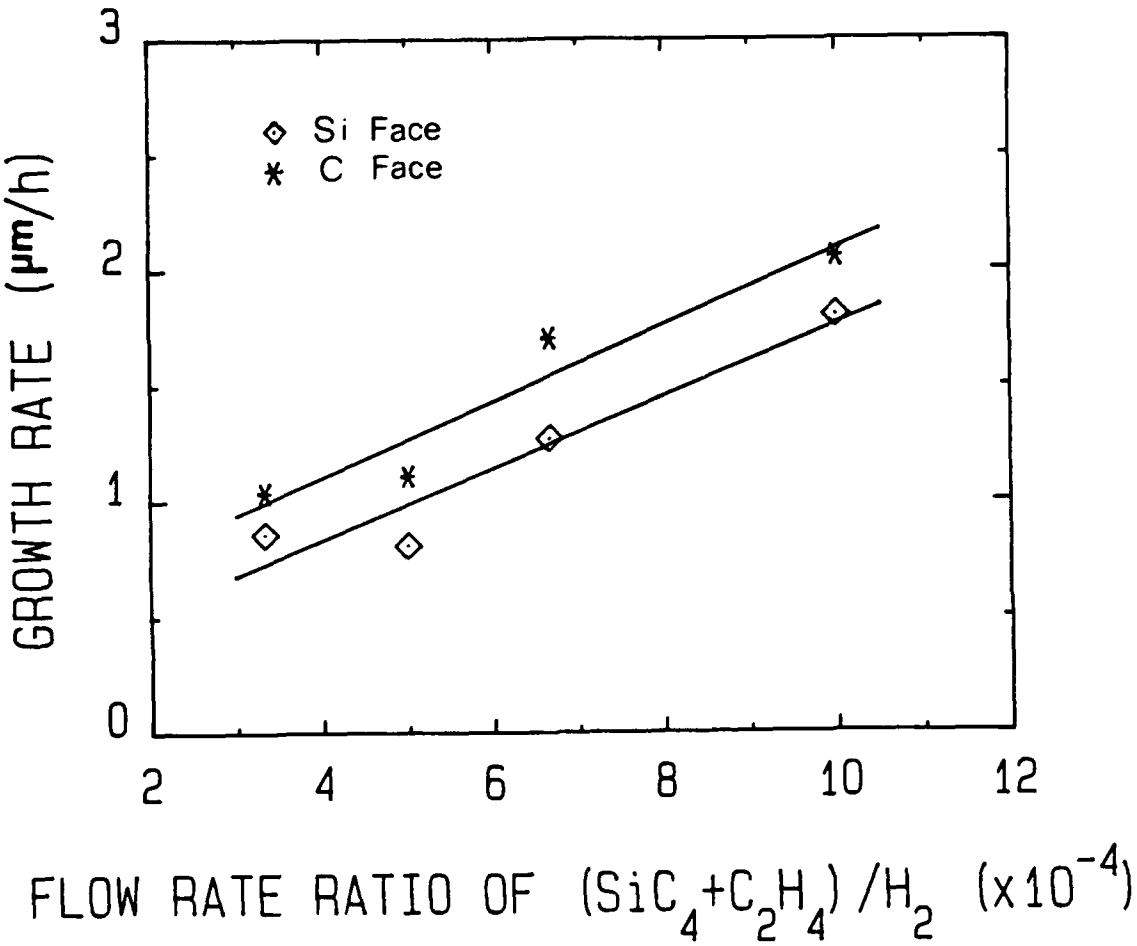

Figure 2: Linear relationship between growth rates and source/carrier gas flow rate ratio for 6H-SiC grown on off-axis 6H-SiC. The CVD deposition was carried out at 1773K and under 1 atm.

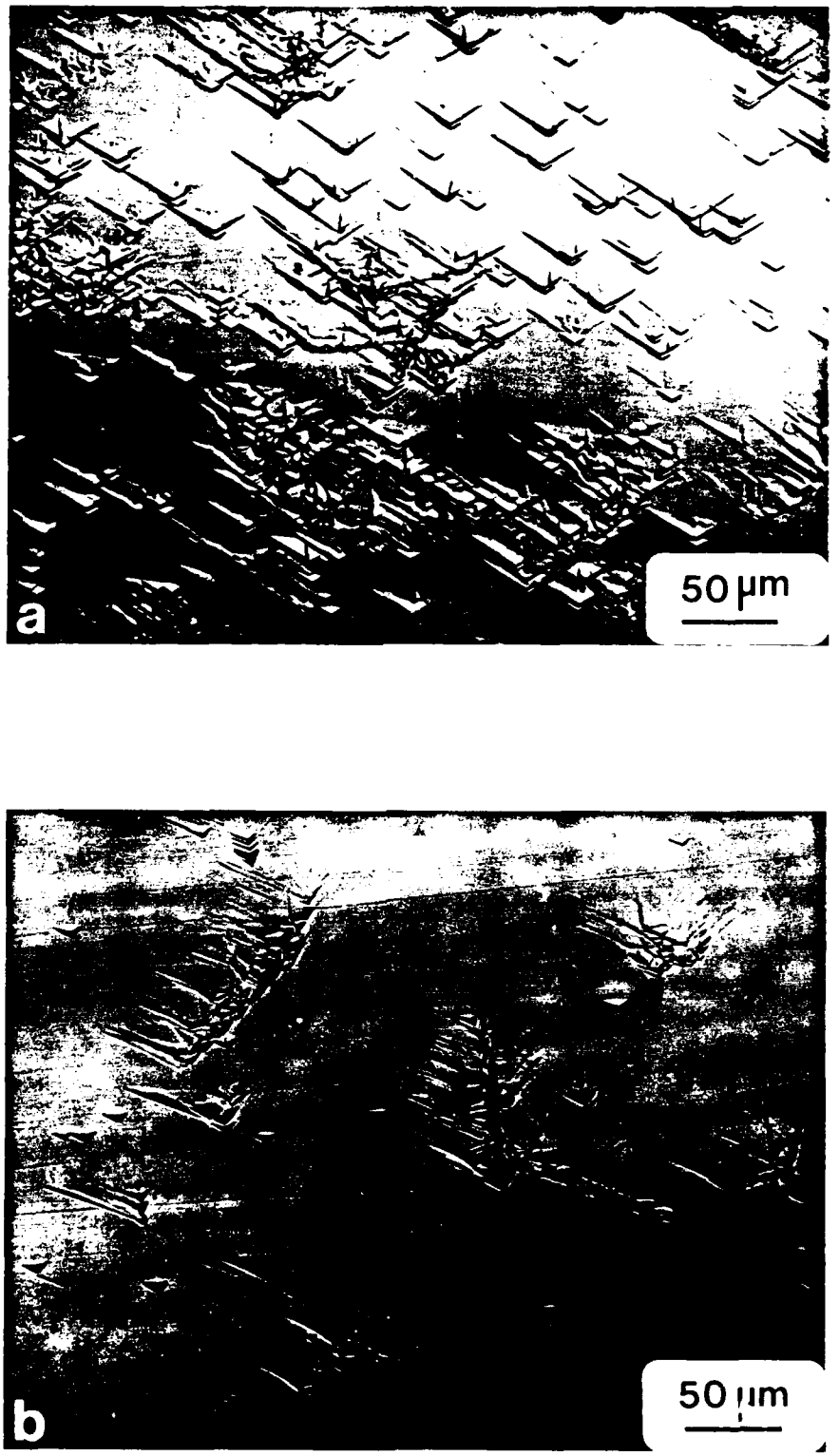

Figure 3: Optical micrographs of surface morphologies of 6H-SiC films grown on an off-axis (0001) Si face of 6H-SiC substrates. The growth temperatures were (a) 1623K, (b) 1673K, (c) 1723K, (d) 1773K and (e) 1823K.

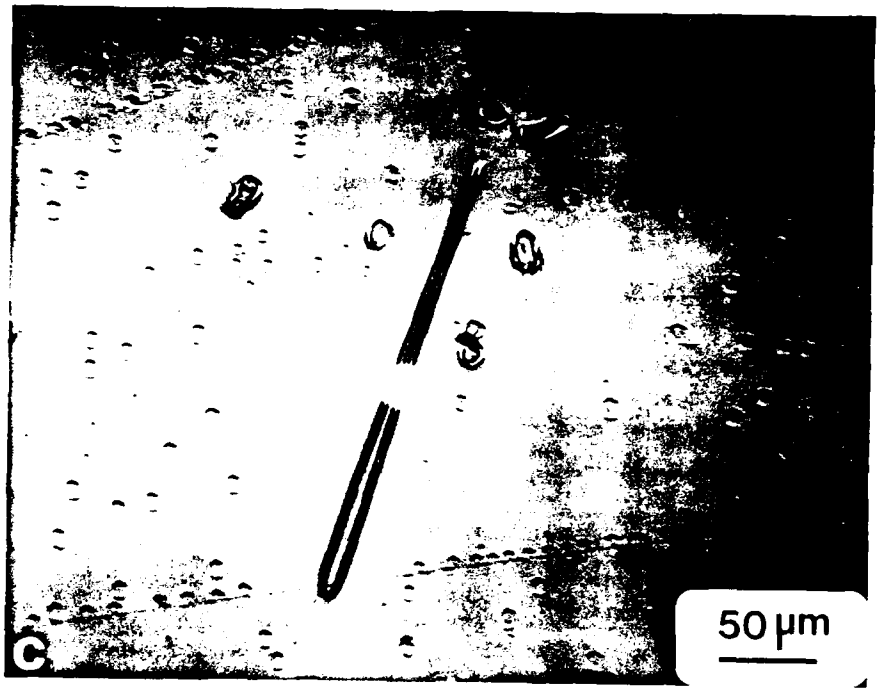
c
50 µm

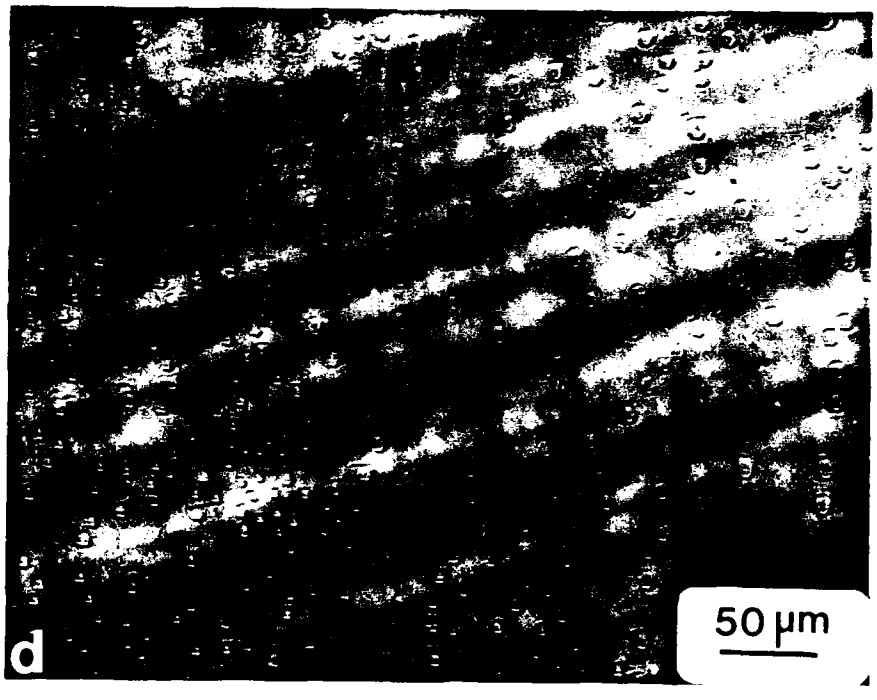
d
50 µm

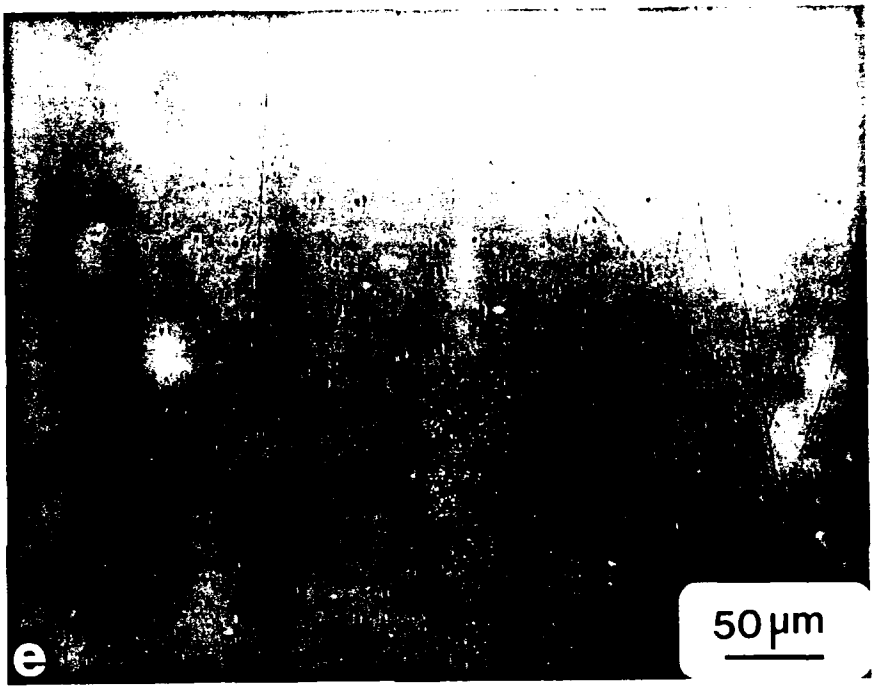
e
50 µm

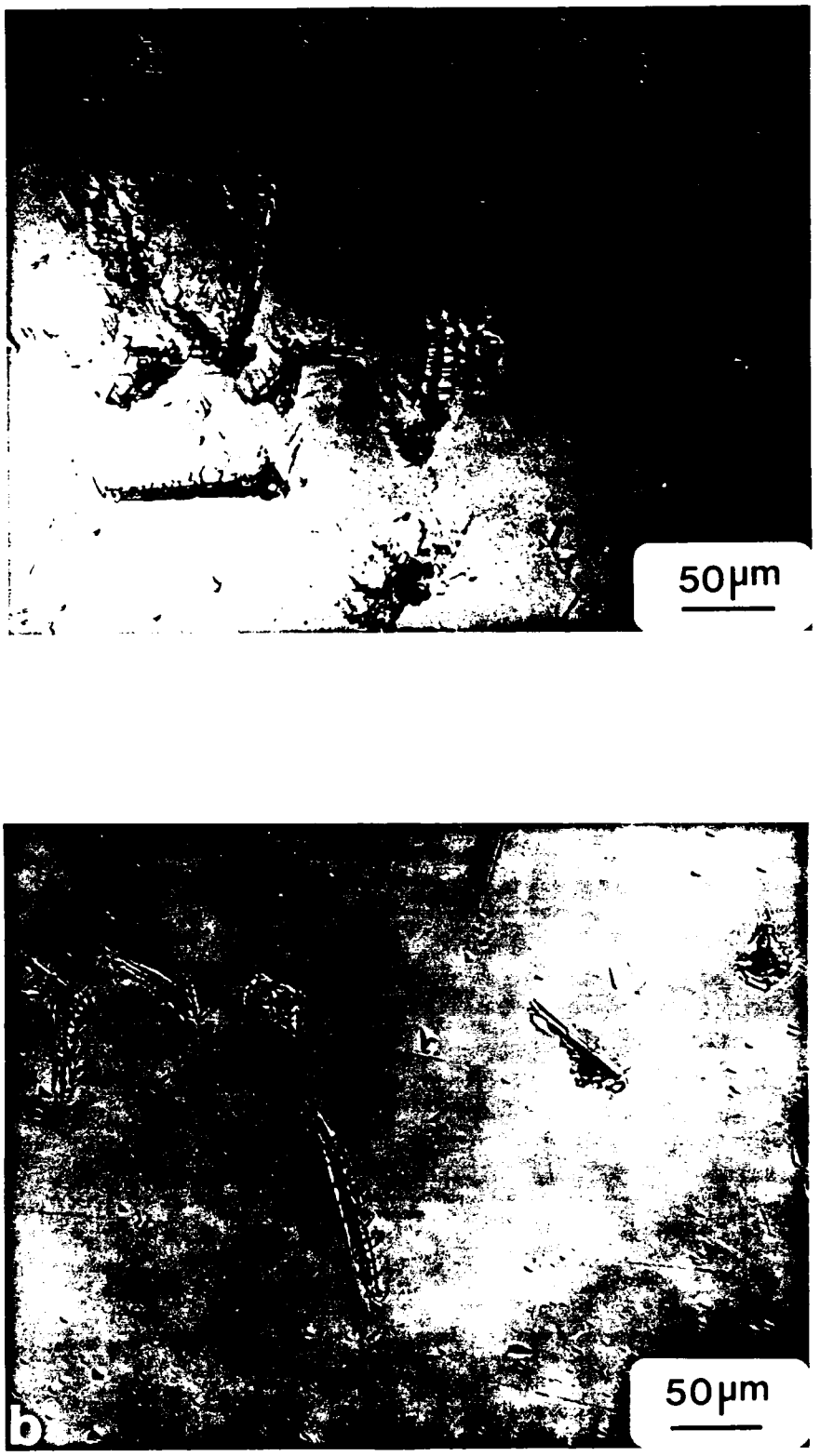

Figure 4: Optical micrographs of the surface morphologies of 6H-SiC films grown on off-axis (000$\bar{1}$) C face of 6H-SiC substrates. The growth temperatures were (a) 1623K, (b) 1673K, (c) 1723K, (d) 1773K and (e) 1823K.

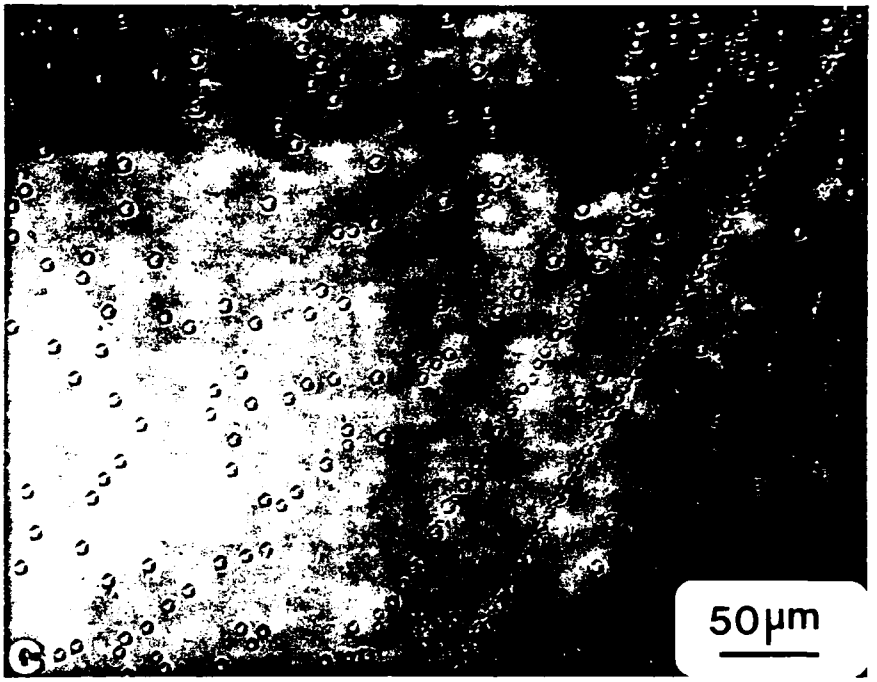
50µm

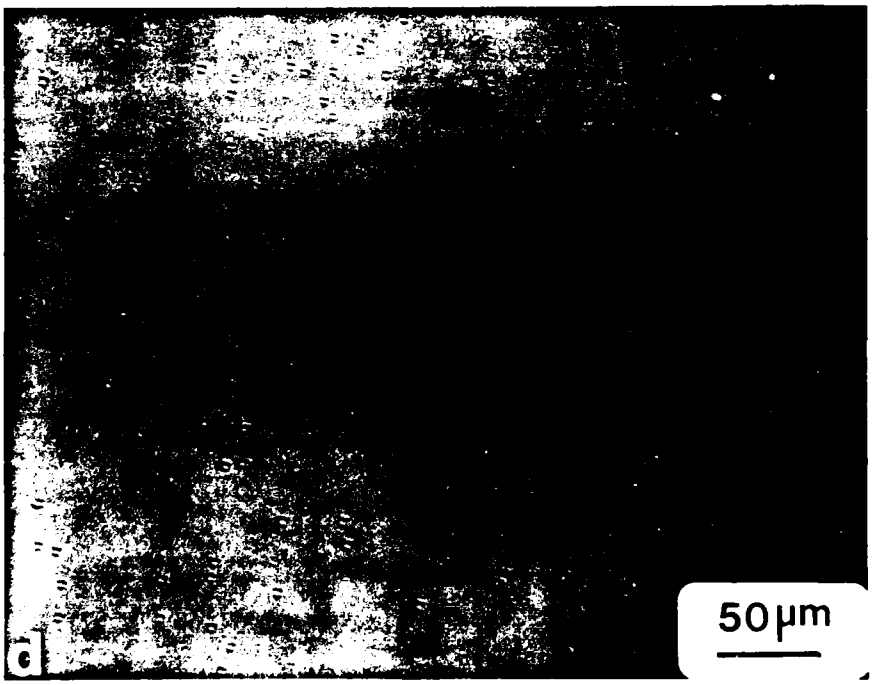
50µm


e
50µm

were grown at 1623K (a), 1673K (b), 1723K (c), 1773K (d) and 1823K (e) with a $(SiH_4 + C_2H_4)/H_2$ gas flow rate ratio of 1:3000. The higher temperatures yielded a smoother surface on both the Si face and the C face. However, the surfaces of the films on the C face had fewer features than those on the Si face grown at the same temperatures. Therefore, the optimum growth temperature range for a film grown on a C face substrate can be wider than that for a Si face, which is 1723-1823K in the present CVD system, while that for Si face is 1773-1823K.

The dependencies of the surface morphologies on the source gases/carrier gas flow rate ratio are shown in Fig. 5 and 6 for the films grown at a temperature of 1773K on the Si face and the C face, respectively, of the 6H-SiC substrates. The gas flow rate ratios of $(SiH_4 + C_2H_4)/H_2$ were 1:3000 (a), 1.5:3000 (b), 2:3000 (c), 2.5:3000 (d) and 3:3000 (e). The surfaces of the films grown on the Si face showed less change, although more surface features appeared with increasing flow rate ratio. However, the surfaces of the films on the C face changed drastically when the flow rate ratio increased to 2.5:3000 and above. The film became a mixture of a 6H-SiC matrix containing β-SiC particles (see triangular feature in Fig. 6 (d)). Further increasing the flow rate ratio increased the size of the β-SiC particles but reduced the density of the particles (Fig. 6 (e)). Two types of triangular particles with opposite orientations, as shown in Fig. 7, indicated that double positioning boundaries (DPB) would form in the film if further growth occurred.

The effect of the degree of off-axis orientation on the surface morphology of the films deposited on both the Si face and the C face of the 6H-SiC substrates is shown in Figs. 8 and 9. The off-axis orientations of the [0001] toward the $[11\bar{2}0]$ of the substrates were 3° (a), 5.5° (Fig. 8 (b), Si face only), 8.5° (Fig. 9 (b), C face only), 11.5° (c) and 14.5° (d). In both the Si and C faces, the surface roughness increased with increasing degrees of off-axis orientation. The defects in the high degrees of off-axis orientation will be studied in the near future by transmission electron microscopy (TEM).

III. IN SITU DOPING OF 6H-SiC VIA CVD

A. Theoretical Considerations

Dopant species are presumed to follow Henry's law when introduced, but not electrically activated (ionized), into SiC. This statement is based on the equilibrium solubility model of Rai-Choudhury and Salkovitz[15] which incorporates dilute solution thermodynamics. The solute

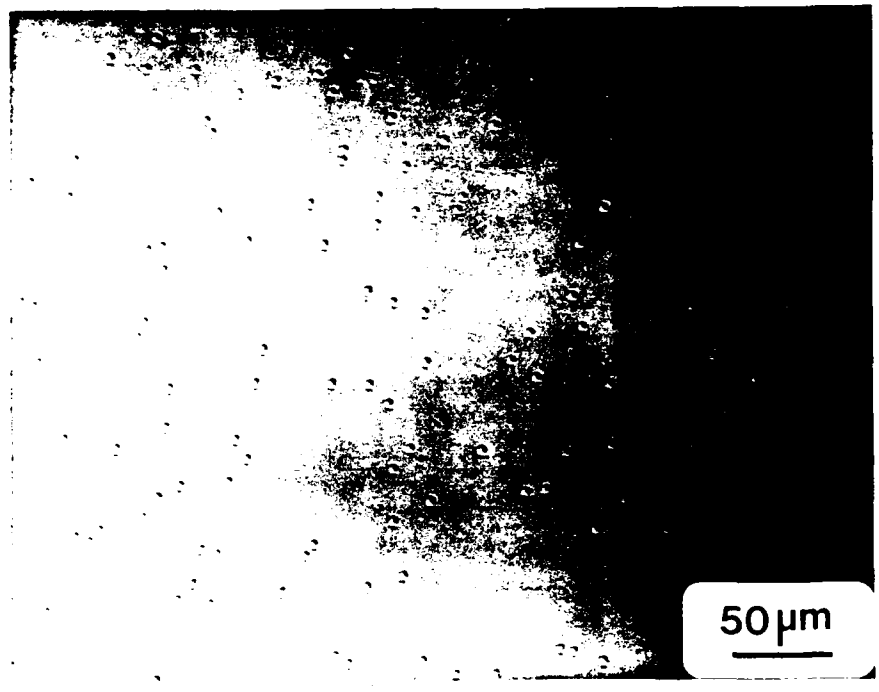

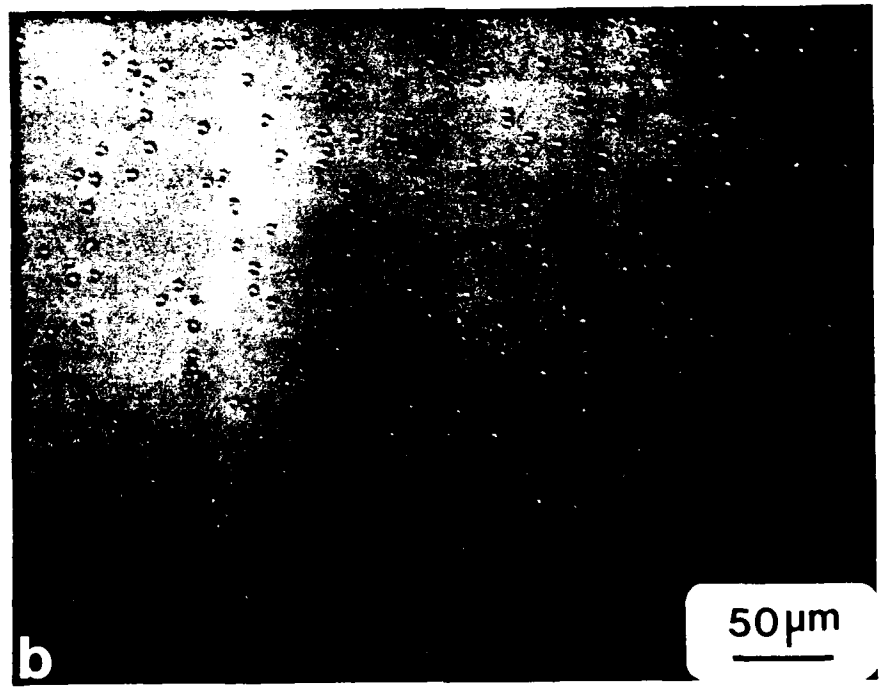

Figure 5: Optical micrographs of surface morphologies of 6H-SiC films on off-axis, (0001) Si face 6H-SiC substrates. The films were grown at 1773K and (SiH_4/C_2H_4)/H_2 gas flow rate ratio of (a) 1:3000, (b) 1.5:3000, (c) 2:3000, (d) 2.5:3000, (e) 3:3000.

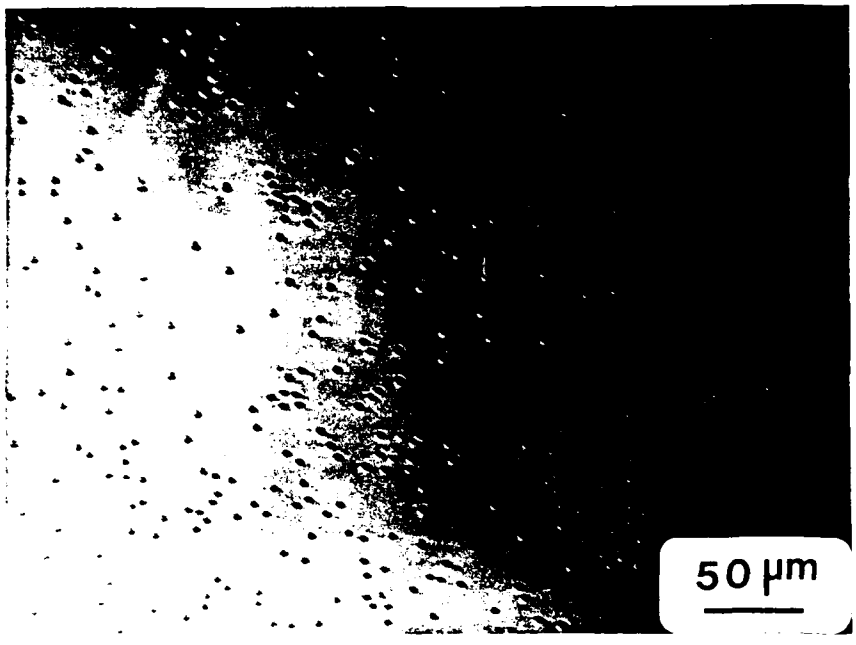
50 µm

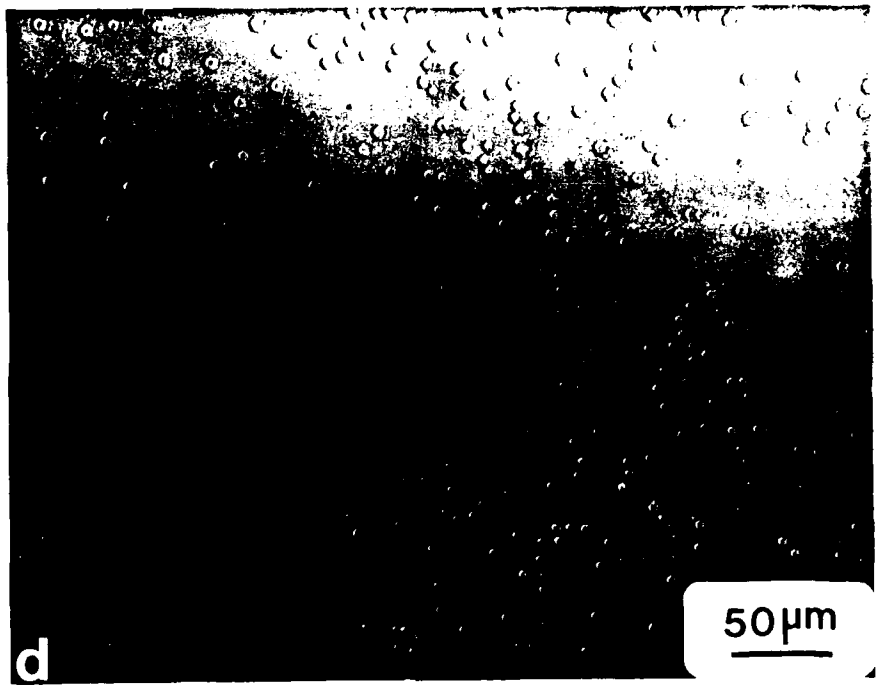
50µm
d

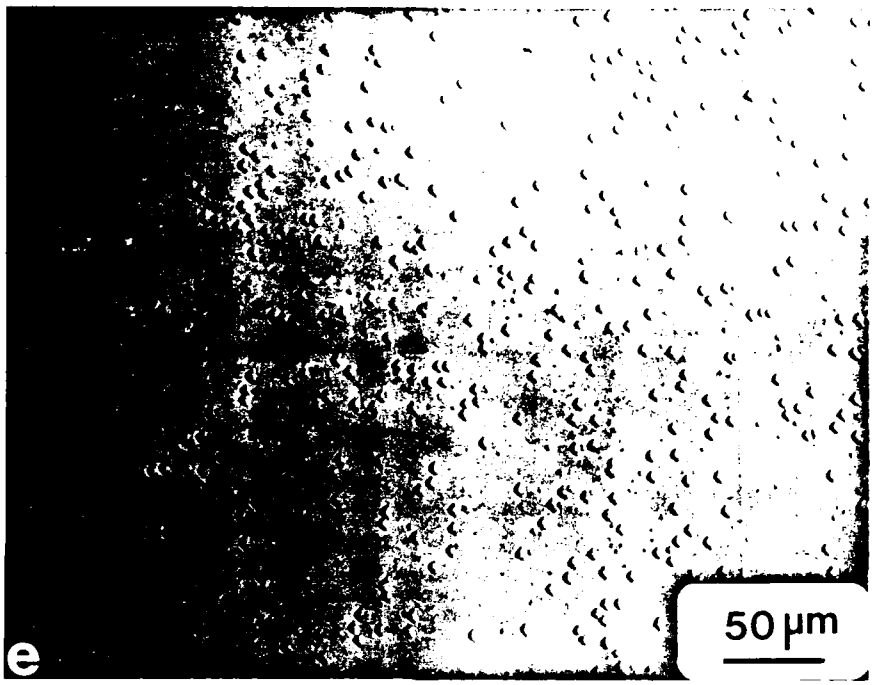
e
50 µm

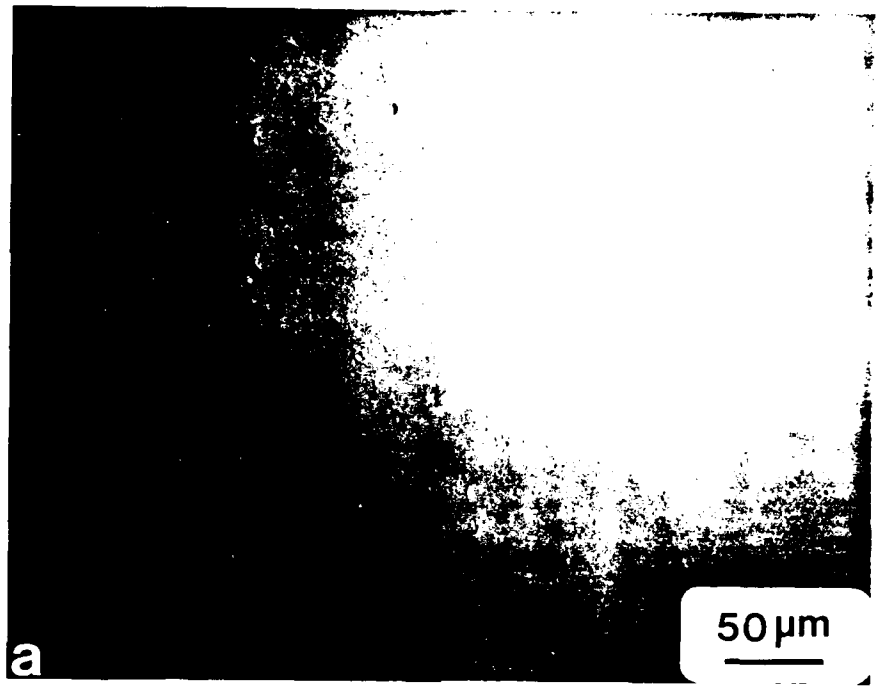

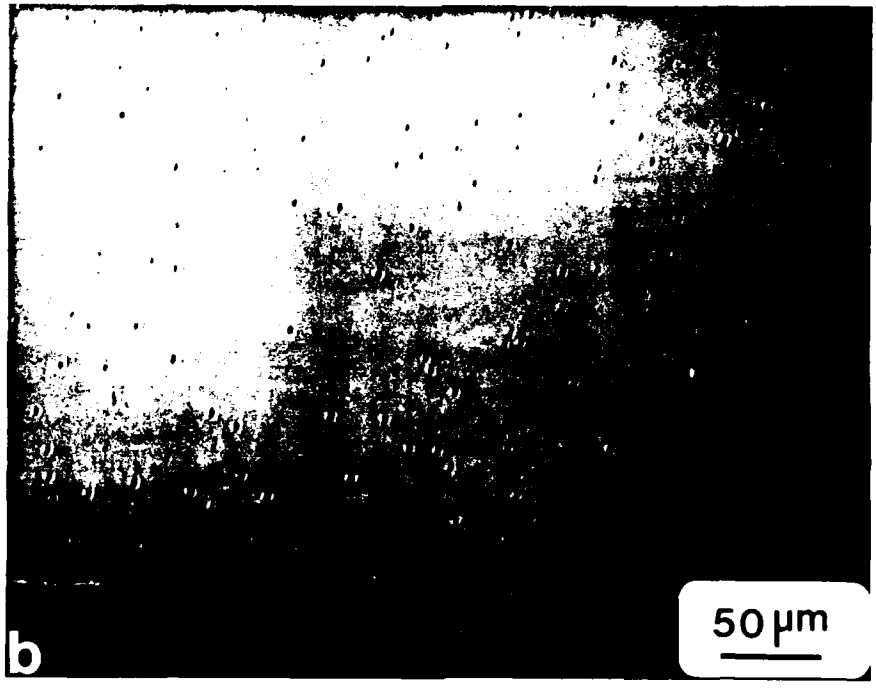

Figure 6: Optical micrographs of surface morphologies of 6H-SiC films on an off-axis $(000\bar{1})$ C face of 6H-SiC substrates. The films were grown at 1773K and (SiH_4 + C_2H_4)/H_2 gas flow rate ratios of (a) 1:3000, (b) 1.5:3000, (c) 2:3000, (d) 2.5:3000, (e) 3:3000.

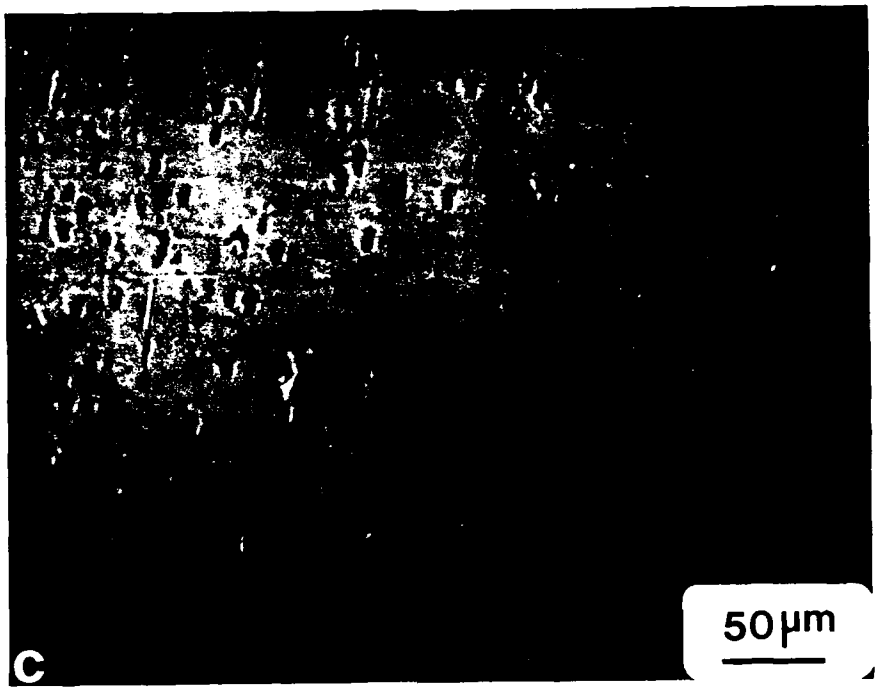
50 µm
c

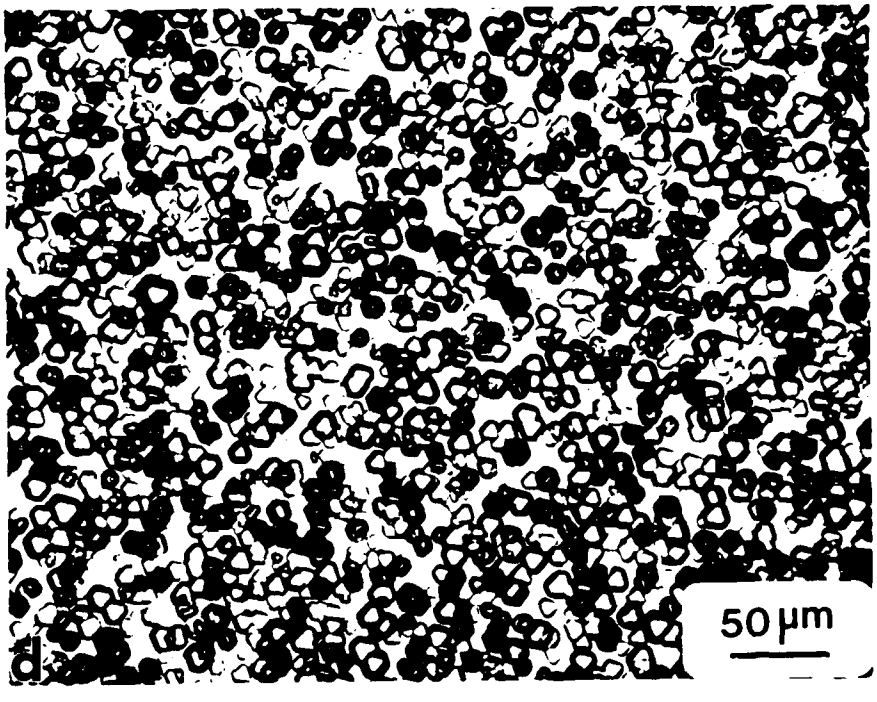
50 µm
d

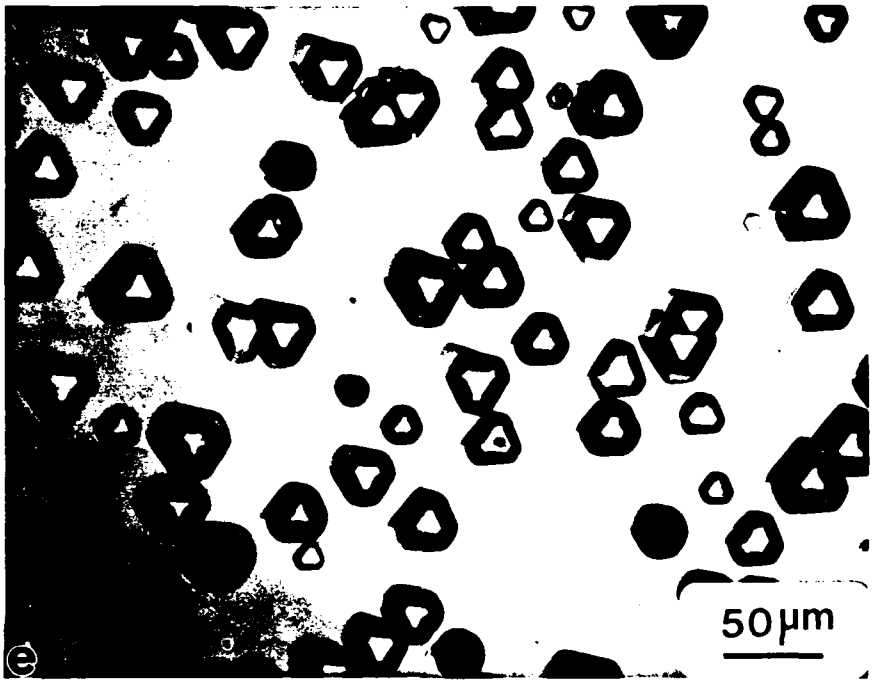
50μm
e

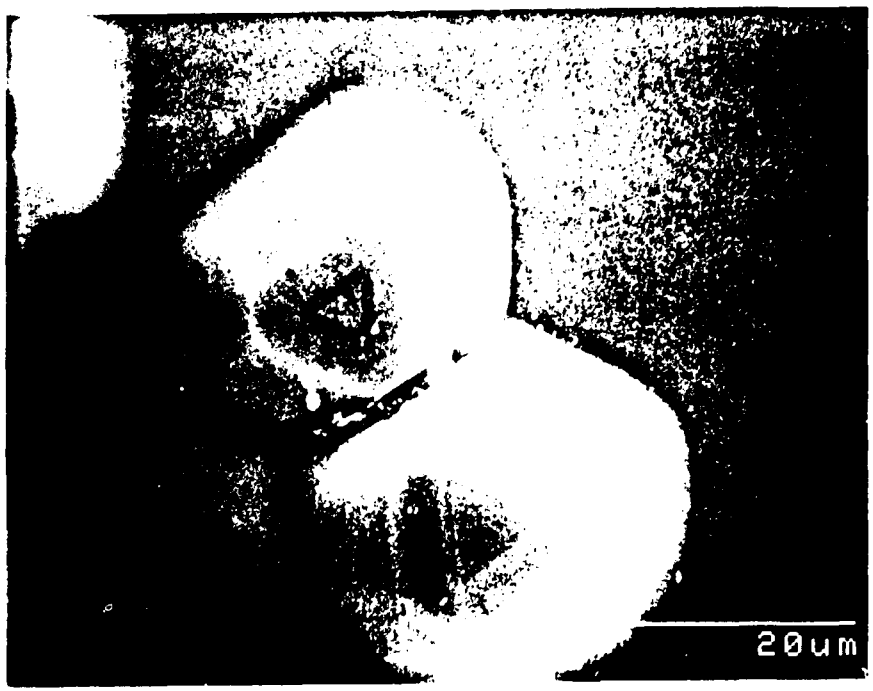

Figure 7: SEM micrograph showing two types of triangular particles in the off-axis $(000\bar{1})$ C face 6H-SiC film grown at a temperature of 1773K and a $(SiH_4+C_2H_4)/H_2$ gas flow rate ratio of 3:3000.

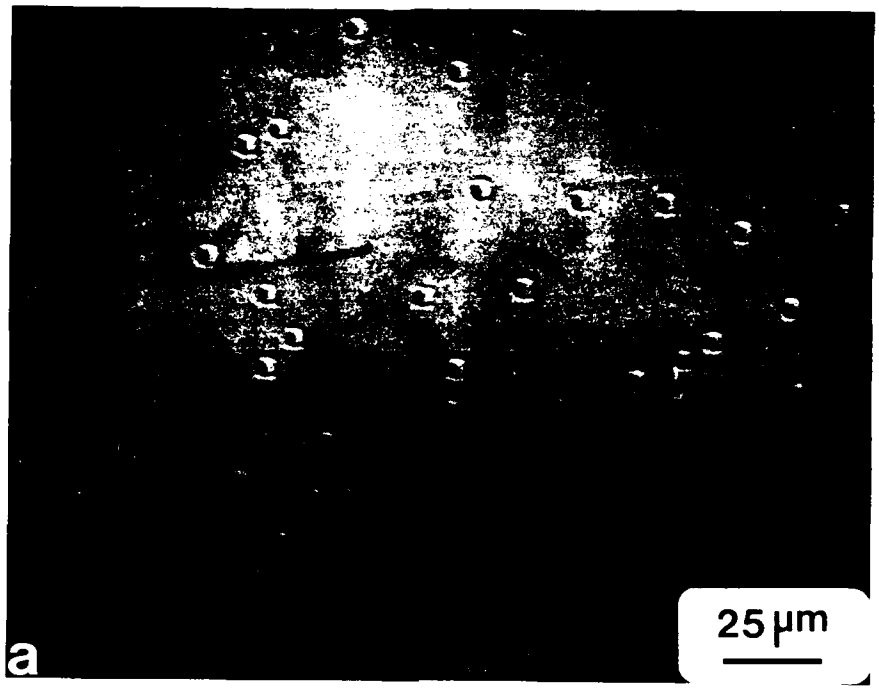

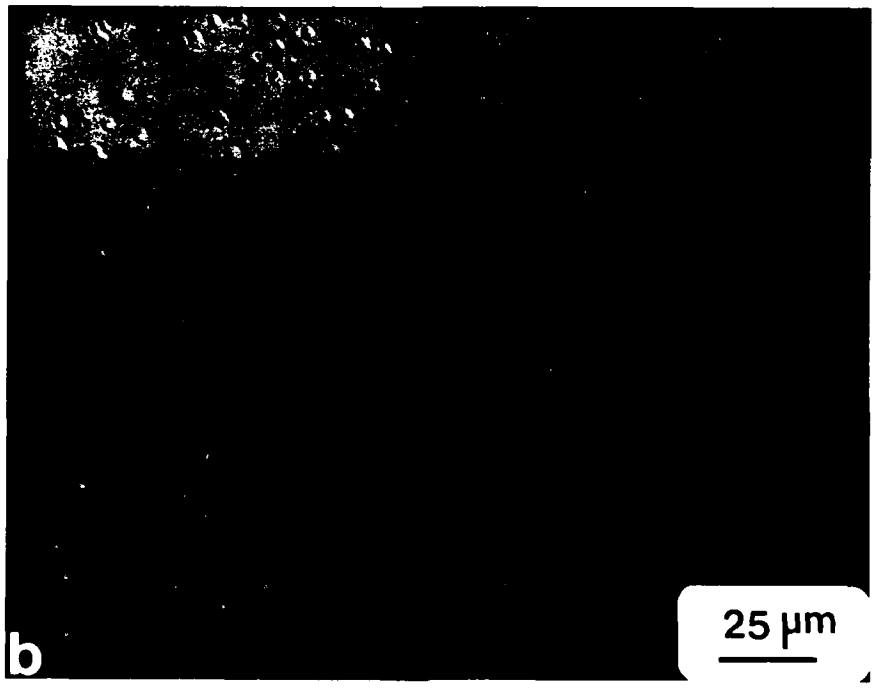

Figure 8: Optical micrographs of surface morphologies of 6H-SiC films grown on an off-axis (0001) Si face of 6H-SiC substrates. The substrates were (a) 3°, (b) 5.5°, (c) 11.5°, and (d) 14.5° off (0001) toward [$11\bar{2}0$] axis, respectively.

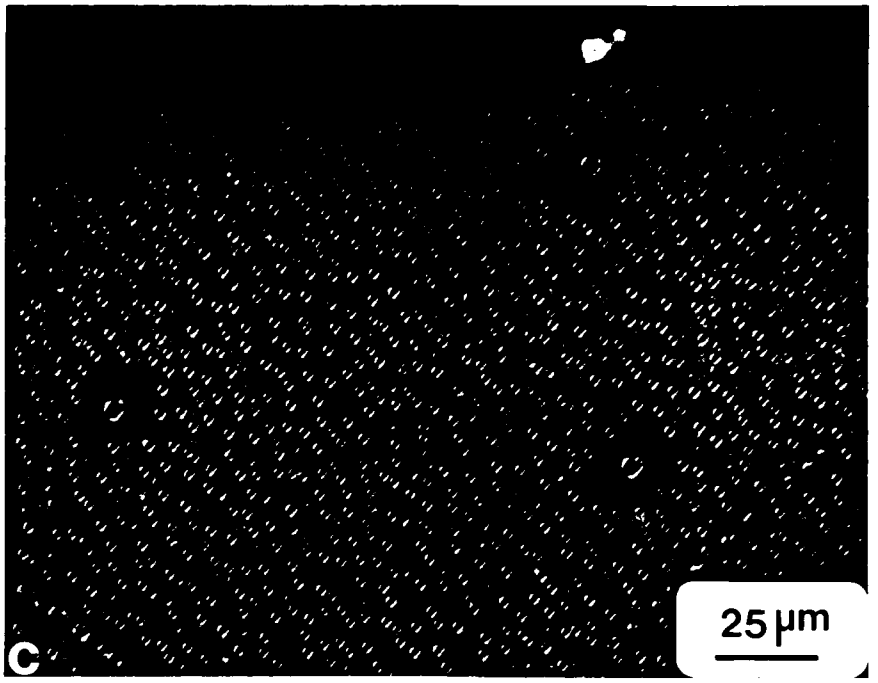
25 µm
c

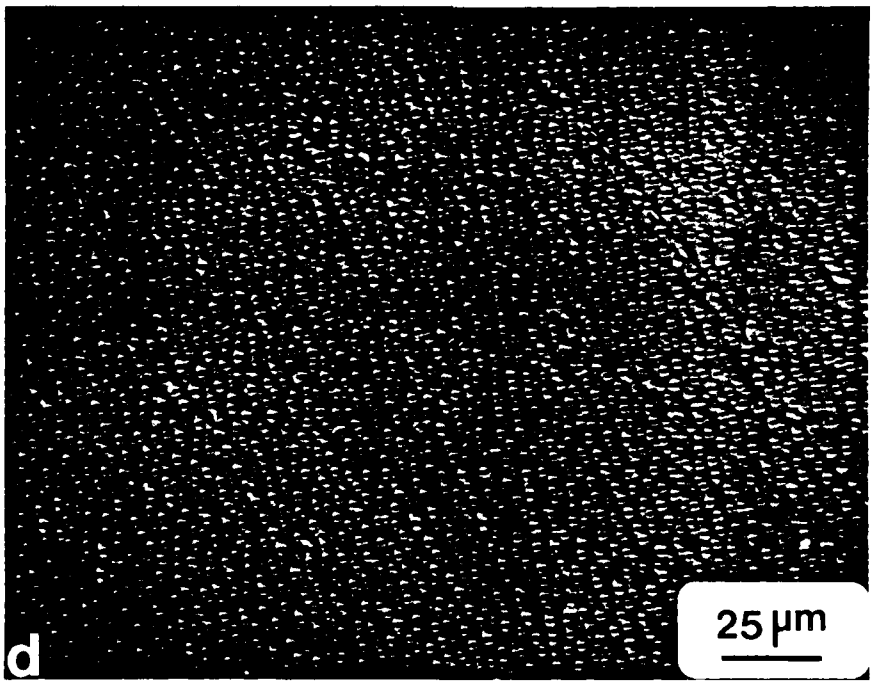
25 µm
d

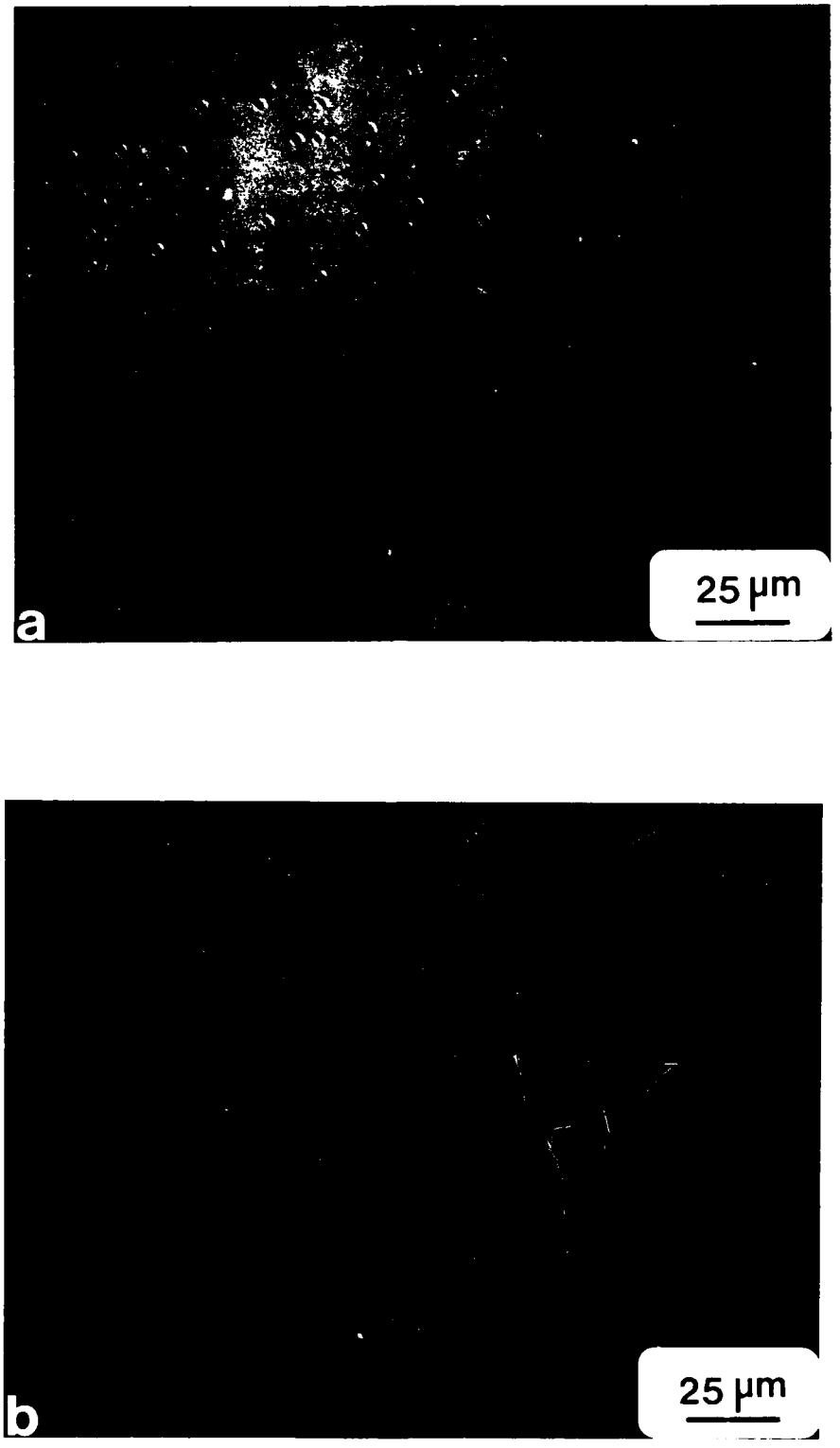

Figure 9: Optical micrographs of surface morphologies of 6H-SiC films grown on off-axis $(000\bar{1})$ C face 6H-SiC substrates. The substrates were (a) 3°, (b) 8.5°, (c) 11.5° and (d) 14.5° off $(000\bar{1})$ toward $[11\bar{2}0]$ axis, respectively.

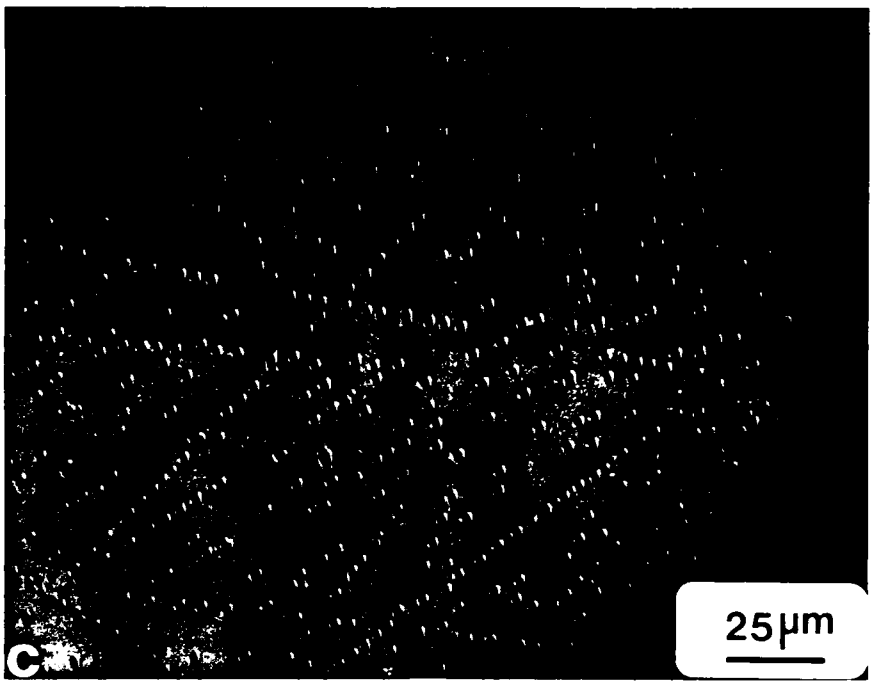
25μm
c

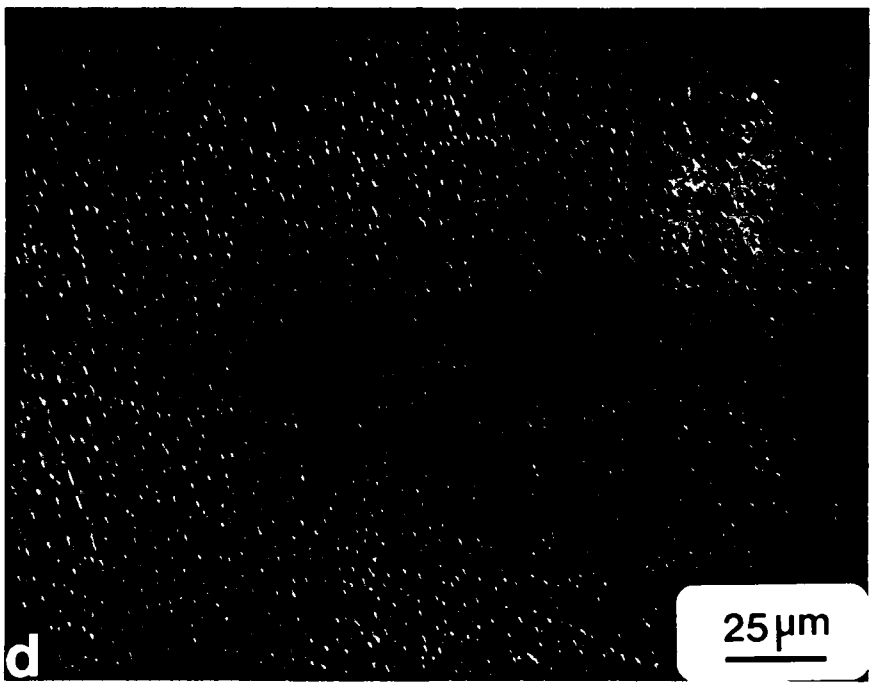
25μm
d

atoms are considered to exist in monoatomic form. The overall reaction fort the dopant species entering into the solution in the SiC is

$$D_y(g) = yD \text{ (in the SiC crystal)} \quad [1]$$

where D_y is the dopant gas species, y is the number of dopant atoms per molecule of the dopant gas species and D is the single dopant atom in the SiC crystal.

The equilibrium constant of the reaction may be expressed as

$$K = \frac{\alpha_{Dy}}{P_{Dy}} = \frac{Y_D{}^Y N_D{}^Y}{P_{Dy}} \quad [2]$$

where α_D is the activity of the dopant species, P_{Dy} is the partial pressure of the dopant species, D_y, $Y_D{}^Y$ is a proportionality constant (it is the activity coefficient if N_D is the mole fraction of dopant species), and N_D is the concentration of dopant in the SiC crystal.

Since we assume that Henry's law is followed, at constant temperature,

$$N_D = \frac{K^{1/y}}{Y_D} P_{Dy}{}^{1/y} = K' P_{Dy}{}^{1/y} \quad [3]$$

where K' is a new proportionality constant. By taking the logarithm of both sides of Eq. 3, one obtains

$$\log N_D = \log K' + (1/y) \log P_{Dy} \quad [4]$$

The ratio of the ionized dopant concentration to the total dopant concentration in the SiC crystal may be defined as follows

$$\gamma' D = \frac{N_i}{N_D} \quad [5]$$

where N_i is the ionized dopant concentration at some actual N_D. Combining Eqs. 3 and 5, one obtains

$$N_i = K' \gamma_D' (P_{Dy})^{1/y} \quad [6]$$

By taking the logarithm of both sides of Eq. 6, it becomes

$$\log N_i = \log (K' \gamma_D') + (1/y) \log P_{Dy} \quad [7]$$

Assuming that K' and γ' are independent of the partial pressure of the given dopant species, Eqs. 4 and 7 predict that plots of log N_D vs. P_D and log N_i vs. log P_D should be linear and parallel with a slope of 1/y within the range of values of N_D where Henry's law is valid.

To obtain values of 1/y for the Al and N dopants, it is necessary to experimentally introduce these dopants at several known partial pressures into the growth chamber during deposition and to subsequently measure their atomic and carrier concentrations in the resultant 6H-SiC films.

B. Experimental Procedure

Black 6H-SiC crystals obtained from an industrial Acheson furnace and green, transparent crystals grown by the Lely method were used as the substrates for the in situ doping with Al and N, respectively. Both types of substrates were lapped such that the $[000\bar{1}]$ was off-axis 3° towards the $[11\bar{2}0]$ orientation and polished using 0.1 μm diamond paste. Each 6H-SiC substrate was then oxidized at 1473K in flowing dry oxygen to remove approximately 50 nm of subsurface damage caused by the mechanical polishing. The oxide layer on each substrate was removed with an HF acid solution immediately prior to loading on a SiC-coated graphite susceptor which held the samples during growth. A cold wall, vertical barrel-type, rf-heated system, evacuated to 10^{-6} Torr before growth to remove air and moisture, was used for the deposition (Ref. 13).

Al and N dopant gases were incorporated directly into the primary gas stream containing SiH_4, C_2H_4 and H_2 for the deposition of 6H-SiC under the growth condition of 1773K and 1 atm total pressure. The flow rates of SiH_4, C_2H_4 and H_2 were 2, 1 and 3000 sccm, respectively. Nitrogen in a H_2 gas mixture and liquid trimethylaluminum ($Al(CH_3)_3$, TMA) were used as the sources of the N and Al dopants, respectively. The concentration of TMA in the gas stream was altered both by changing the flow rate of H_2 over the TMA and by changing the temperature of the bath containing the bottle of TMA (temperature controlled within ± 0.1K). The vapor pressure of TMA at a specific temperature was calculated by using the equation[16]:

$$\log P_V = 7.3147 - \left(\frac{1534.1}{T-53}\right)$$

where P_V is the vapor pressure of TMA in mmHg and T is the temperature in degrees Kelvin. Equation 8 is effective in the temperature range of 290-370K. The number of moles of TMA carried into the reaction chamber by H_2 per unit time as a result of its flow through the TMA bottle was calculated by using the ideal gas equation

$$n = \frac{PV}{RT}$$

where n is the number of moles of TMA introduced into the reaction chamber per unit time, P is the vapor pressure of TMA obtained from Eq. 8, V is the volume occupied by TMA per unit time, which was obtained from the flow rate of H_2 from the TMA, T is the temperature of the bath containing the bottle of TMA and R is the gas constant.

The amounts of Al or N introduced into the epitaxial 6H-SiC films has been analyzed quantitatively as a function of depth using secondary ion mass spectrometry (SIMS). Oxygen was used as the primary ion with a beam size of 250 μm. The atomic concentration of Al or N at each point in the SIMS profile was obtained by multiplying a conversion factor by the value of the Al/Si or N/Si count ratio at this point. The conversion factor was determined from the product of the Al/Si or N/Si count ratio and the theoretically calculated atomic concentration at the peak of an Al and N implanted profile standard.

The amounts of ionized Al or N (carrier concentration) in the epitaxial 6H-SiC films were determined by the differential capacitance-voltage technique. In this method, the capacitance of each 6H-SiC film was measured as a function of a reverse voltage by using a 590CV analyzer with a Hg-probe which produced both Ohmic and Schottky-barrier contacts on the surface of the epitaxial layer. The carrier concentrations of the layers were then calculated from the differential capacitance-voltage relationship.

The as-grown surfaces of the Al- and N-doped 6H-SiC films were examined by OM and /or SEM.

C. Results and Discussion

Figure 10 shows the results of the SIMS and CV measurements for the Al atomic and carrier concentrations as functions of the partial pressure of TMA. The linear and parallel character of both curves was predicted by Eqs. 4 and 7. The slope (1/y) in the atomic concentration curve is 0.92 with a correlation coefficient of 0.98. The slope of ~ 1 indicates that the Al is in dilute solution in the 6H-SiC films and that pure Al and/or a complex containing only on Al atom are the principal species which contribute to the introduction of this dopant. The ratio of the carrier concentration to the atomic concentration was 0.02 at all partial pressures of TMA employed.

The N atomic and carrier concentrations are also parallel and linearly proportional to the partial pressure of N_2 (Fig. 11). The slope of the atomic concentration curve is 0.92 with a correlation

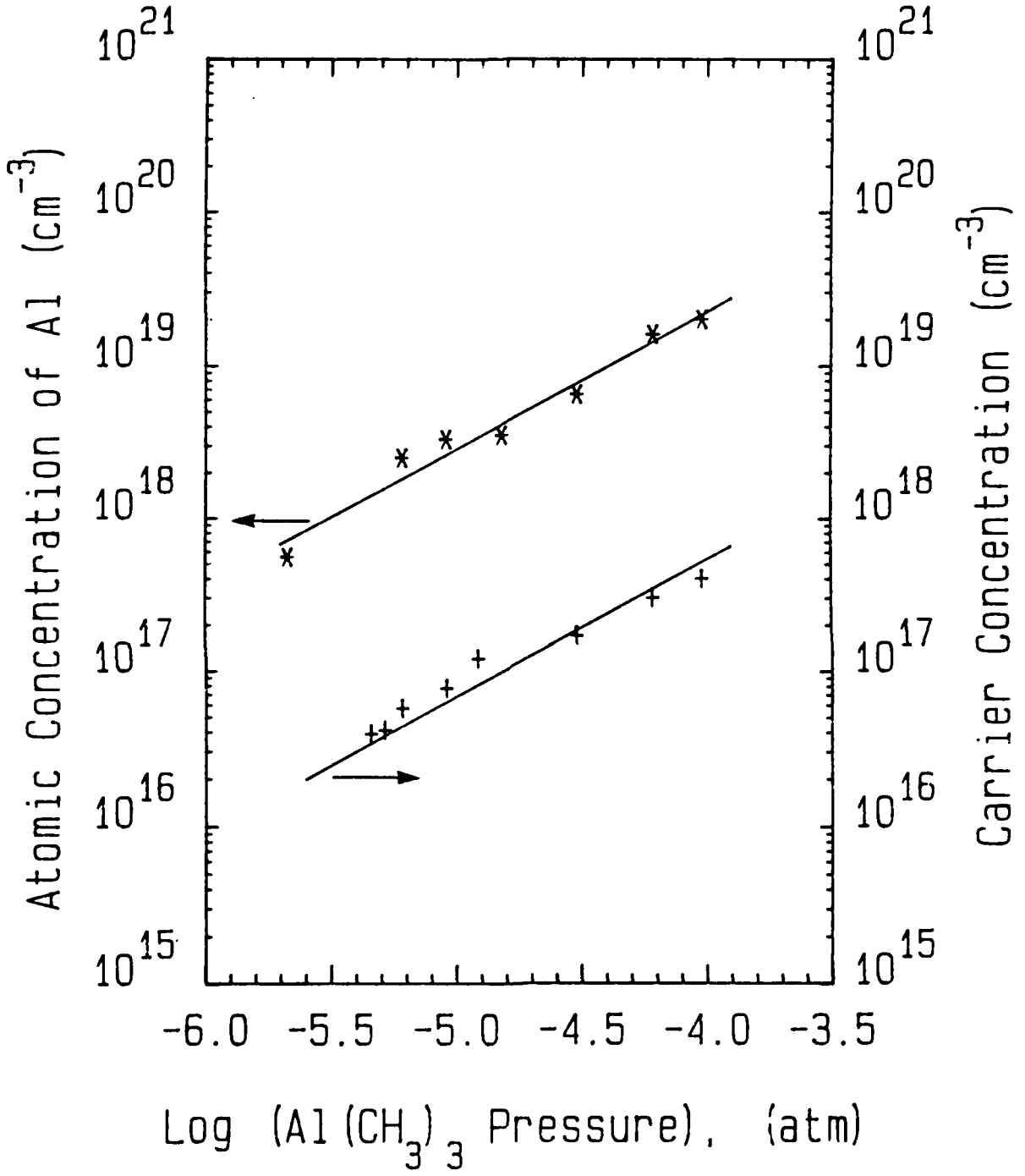

Figure 10: Aluminum atomic and carrier concentrations in Al-doped 6H-SiC on off-axis 6H-SiC as a function of Al dopant (TMA) partial pressure.

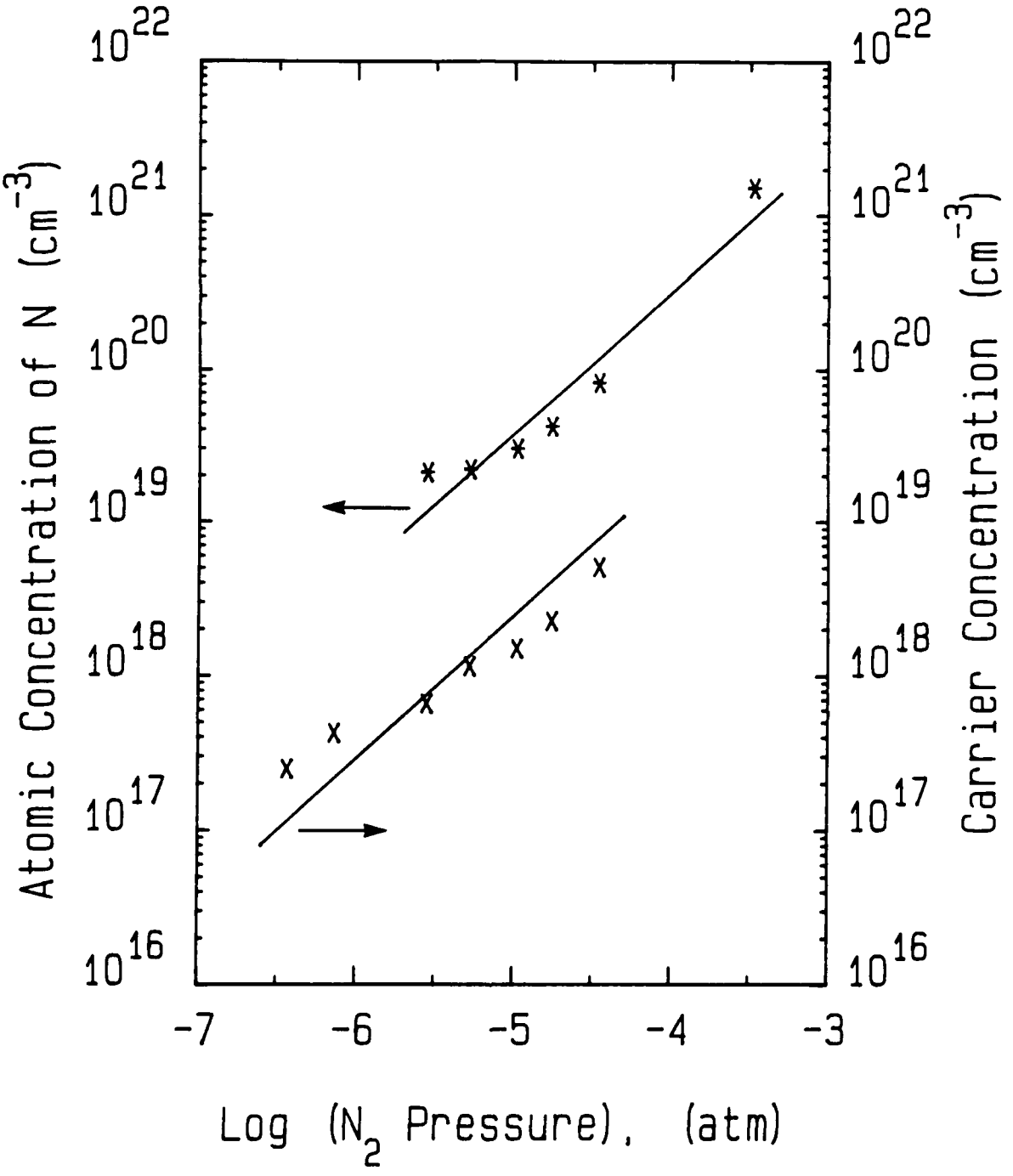

Figure 11: Nitrogen atomic and carrier concentrations is N-doped 6H-SiC on off-axis 6H-SiC as function of nitrogen dopant (N_2) partial pressure.

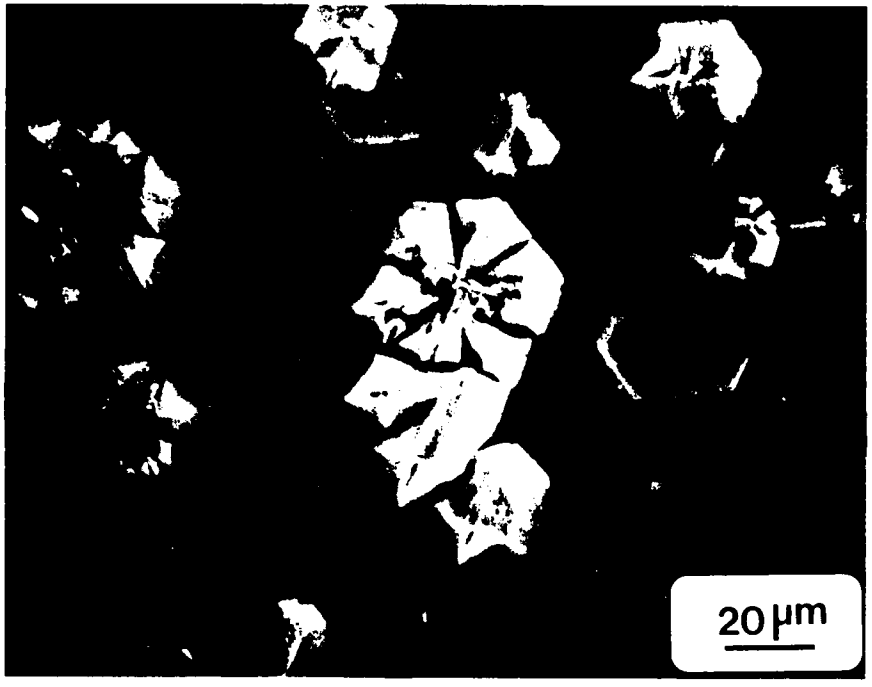

Figure 12: SEM micrograph showing the flower-like particles in an Al doped 6H-SiC film.

coefficient of 0.96. This 1/y value of ~ 1 is twice the expected value and implies that incorporation of the N species occurs to a greater extent than would be expected from equilibrium calculations based on dilute solution theory. The ratio of the carrier concentration to the atomic concentration in the N-doped films is 0.06.

The surface morphology of the N-doped films examined by OM is the same as that of the undoped films. But the surface morphology of the Al-doped films is related to the Si/C ratio during growth. Particularly , when higher doping levels were employed, it was necessary that the flow rate ratio of SiH_4 to C_2H_4 be adjusted in the Si-rich direction in order to obtain a film with good surface morphology. For example, the SiH_4/C_2H_4 flow rate ratio was changed from 2 to 2.25 while the partial pressure of TMA increased from 6.08×10^{-6} atm to 3.04×10^{-1} atm. Otherwise, the films obtained at a SiH_4/C_2H_4 flow rate ratio of 2 had a surface containing many flower-like particles, as shown in Fig. 12. Such surface features may be caused by the incorporation of the carbon component in TMA during film deposition.

IV. Electrical Contacts on Silicon Carbide Thin Films

A. Au Contacts of Beta-SiC

1. Fabrication

To prepare the surface for diode fabrication, the grown films were polished with 0.1 μm diamond paste for 48 hr. The mounting wax residue was removed with hot concentrated H_2SO_4. A final cleaning was conducted in a 1:1 mixture of $H_2SO_4 : H_2O_2$ followed by a 2 min buffered oxide etch. In order to remove the damage caused by the polishing process, an ~1000Å thick oxide layer was thermally grown in a dry oxygen ambient at 1200°C. The oxide layer was etched and a layer of gold, ~2000Å in thickness, was thermally evaporated onto the samples to form a metal-semiconductor contact. Active diode areas, 100 μm diameter, were delineated by photolithography and gold etching in a $KI:I_2:H_2O$ solution, 4:1:40 by weight. The diodes were separated from the field region by a 100 μm wide annular ring. The structure of these diodes were similar to those reported by Ioannou *et al.* [IEEE Trans. Electron Devices, ED-34, 1694 (1987)]. The infinitely large area of the field-region ensured an adequate 'back contact' with required current handling capability. A measurement of I-V characteristics between the active device and the field

region was conducted using an HP 4145A Semiconductor Parameter Analyzer. Current-voltage measurements as a function of temperature between 25°C - 150°C were obtained for the diodes on NCSU 870626/1 (since these diodes did not exhibit ohmic conduction at low biases), in order to establish whether thermionic emission was the prevailing conduction mechanism. This procedure was also expected to yield the barrier height and the modified Richardson's constant. However, at temperatures of 50°C and above, ohmic conduction at low forward biases was observed indicating the non-thermionic character of the contact diodes.

2. Characteristics

Logarithmic plots of the I-V characteristics in the forward direction indicate space charge limited current conduction through the active volume of the diodes. The β-SiC films grown on nominally (100) oriented substrates show the presence of two deep levels located approximately between 0.26 eV and 0.38 eV below the conduction band edge. In some films on nominal (100) substrates, the I-V characteristics are also influenced by additional traps which are exponentially distributed in energy with a maximum occurring at the conduction band edge. In contrast, the films deposited on off-axis substrates have only one deep level located at approximately 0.49 eV for the 2° off (100) substrates and 0.57 eV for the 4° off (100) substrates. Previous microstructural analysis revealed that the nature and density of defects in the β-SiC heteroepitaxial films on both nominal and off-axis (100) silicon are similar except that the films on nominal (100) substrates have a high density of inversion(a.k.a. antiphase) domain boundaries. Therefore, the presence of the shallower deep-level states observed in the β-SiC films grown on nominal (100) substrates is speculated to be due to the electrical activity of antiphase domain boundaries. These results have been presented at the Fall 1989 meeting of the Materials Research Society. A preprint of the paper is included in Appendix 1. A detailed version of the paper has been accepted for publication in the Journal of the Electrochemical Society.

B. Platinum Contacts on Beta SiC

Platinum contact diodes were formed by sputtering a layer of platinum ~ 2000Å in thickness. A lift-off technique was used to define the active diode areas. The SiC was oxidized at 1200°C for 1 hr in order to grow a layer approximately 1000Å in thickness. The metal contact areas were opened, using the mask that was employed for defining the Au pattern (see section

2.1). A pattern reversal process was then utilized with a positive resist and the dark-field mask. The oxide in the contact areas was subsequently etched in buffered oxide for 10min (this overetching ensures good contact with subsequently deposited metal film) and the samples baked at 120° C for 10 min. A layer of Pt ~ 2000Å in thickness was sputtered onto the sample and a contact pattern defined by photoresist lift-off in acetone with ultrasonic agitation. Finally the samples were cleaned in acetone followed by a methanol rinse.

The as-deposited Pt contact diodes were near ohmic, however, rectification was observed on annealing at 400°C for 30min. The annular space between the active device and the field region was protected by a thermally grown layer of oxide. The oxide layer appeared to eliminate edge effects, thereby contributing to characteristics in some ways superior to Au contact diodes. In particular Pt diodes are not degraded as a result of bias stressing, although for -5V to 5V operation, Pt diodes have a higher leakage current than Au diodes. The device structure and current voltage characteristics are shown in Figs.13 and 14, respectively. Interaction between Pt and SiC appears to introduce a distribution of deep-level states in the band-gap of the semiconductor resulting in a slow rise in the forward current. It is speculated that these deep states also serve as the origin of the high reverse-leakage. It is considered that a sandwich-type structure composed of a layer of silicon between the SiC and Pt would provide the Si needed for the interface reaction and thereby contribute to a better contact than Pt alone.

C. Platinum Silicide Contacts on Beta-SiC

Platinum silicide contacts were formed by depositing a layer of CVD polycrystalline silicon and reacting with a sputtered layer of platinum at a temperature of 450°C. The active diode areas were defined by a triple masking sequence employing a single bright-field mask involving a mask-reversal stage. The complete devices have the same dimensions as the Au contact diodes except that the annular area between the active diode and the field region is protected by a layer of thermally grown oxide, as shown schematically in Fig. 15. A preliminary study of I-V characteristics, as shown in Fig. 16, indicates that these present diodes are potentially superior to those formed by sputtered layers of platinum alone. A sputtered layer of Si followed a layer of Pt had the advantage of a single mask process. However, the thickness of the layers and anneal treatment have to be optimised. A detailed study is being conducted currently.

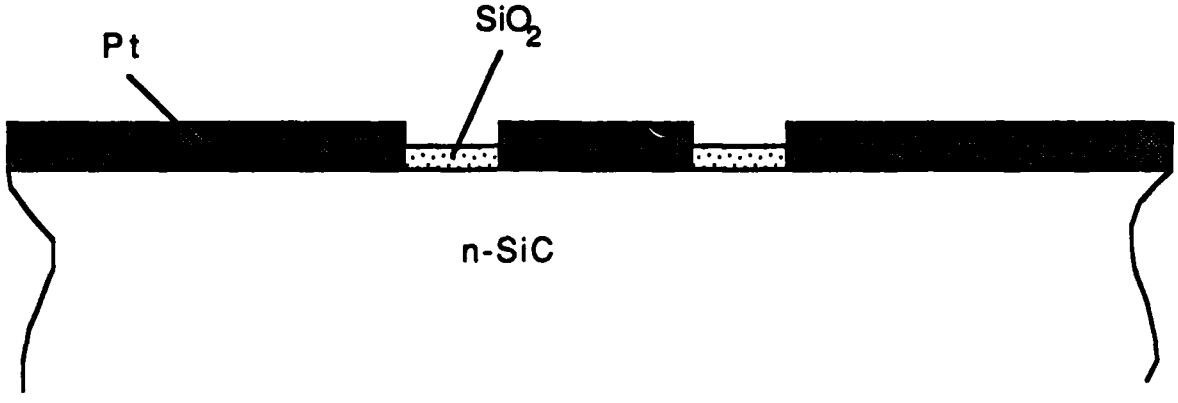

Fig. 13: Schematic of the Pt/SiC contact diode.

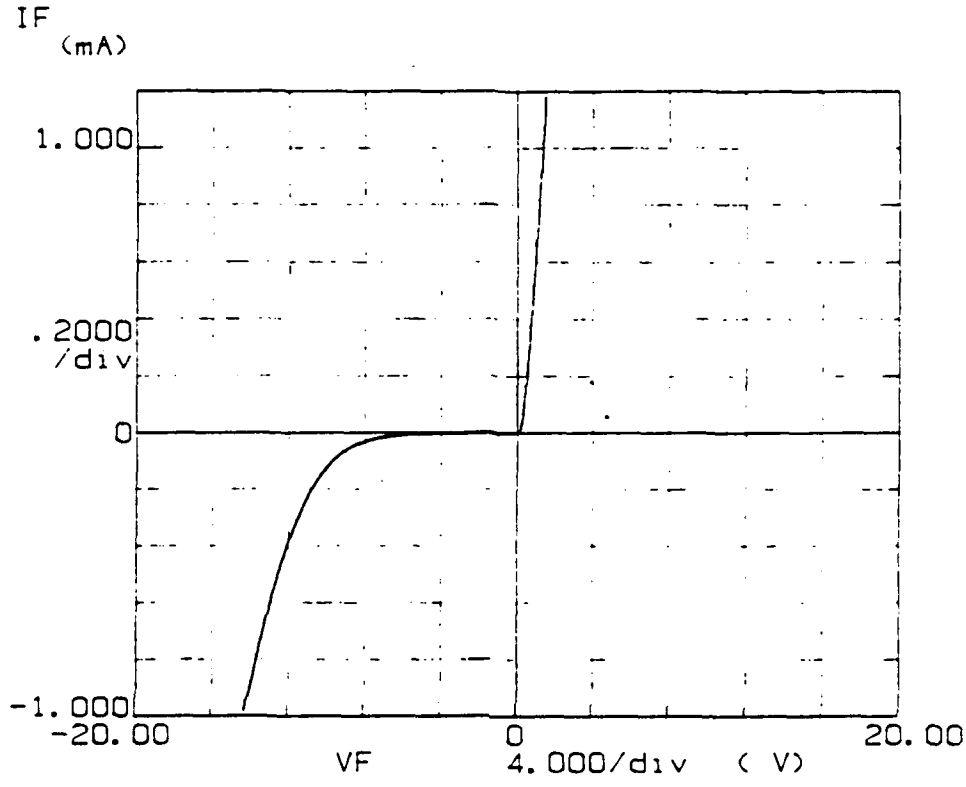

Fig. 14: Current-voltage characteristics of the Pt/SiC contact diode

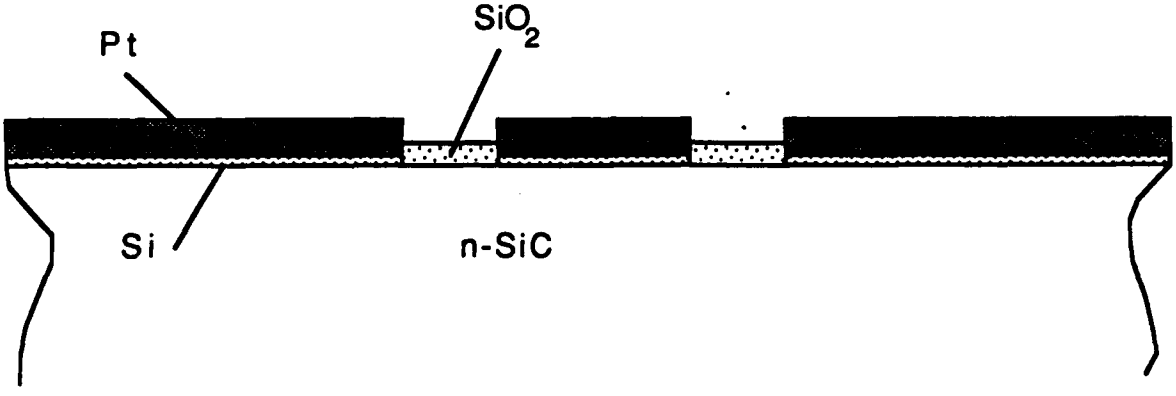

Fig. 15: Schematic of the Pt/Si/SiC contact diode.

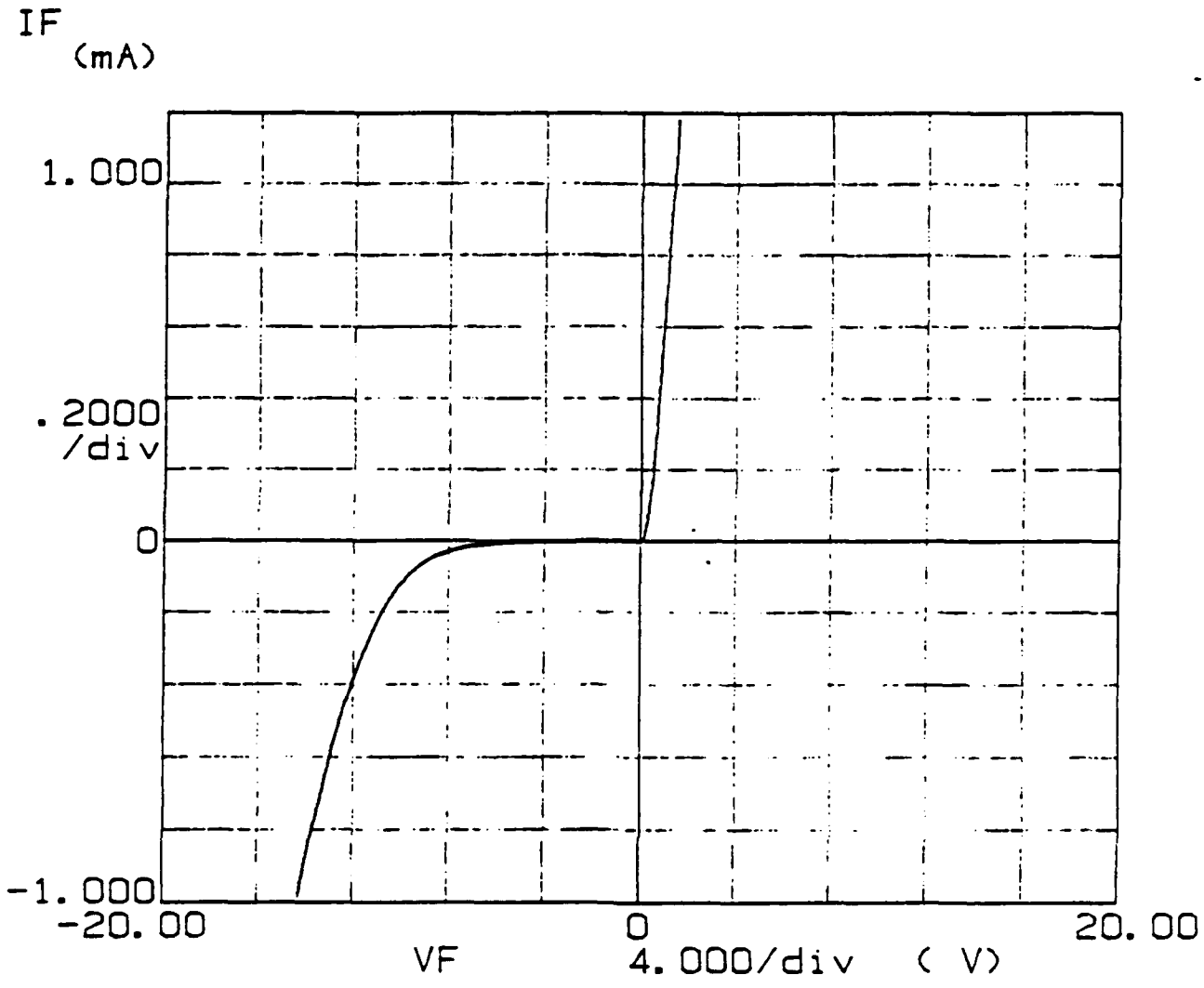

Fig. 16: Current-voltage of the Pt/Si/SiC contact diode.

D. Ohmic Contacts on Alpha-SiC

Preliminary work on ohmic contacts on n-type α-SiC has been performed. Process steps similar to those described in Sections 2.1 and 2.2 were employed for the fabrication the test devices. It was observed, as reported by other workers, that ohmic contacts can be formed with sputter-deposited Ni subsequently annealed at a temperature between 1035°-1050°C at a pressure of ~ 5 x 10^{-5} torr. Fig. 17 shows the I-V characteristics of an annealed Ni contact dot of 100 μm in diameter separated from a Ni field region by a 100 μm wide annular ring.

E. Rectifying Contacts on Alpha-SiC

Sputter-deposited Pt was found to form rectifying contacts. Process steps similar to those described in Sections 2.1 and 2.2 were employed for the fabrication the test diodes. Current-voltage characteristics of 100 μm diameter Pt dots as a function of temperature and following a 400°C anneal are shown in Fig. 18. Annealing of Pt contacts at temperatures in the range between 400°-600°C tends to degrade the forward characteristics. For both Ni and Pt contact studies, substrates with a carrier concentration of ~$2X10^{18}$ cm^{-3} were employed.

IV. DEVICE FABRICATIONS OF 6H-SiC FILMS

A. p-n Junction Diodes

1. Experimental Procedure

A 3 μm thick, undoped, n-type 6H-SiC layer followed by a 1.5 μm thick, Al-doped, p-type layer were deposited on a nitrogen doped, n^+-type 6H-SiC substrate from Cree Research, Inc. The $[000\bar{1}]$ direction of the substrate was oriented 3° off-axis toward the $[11\bar{2}0]$ axis. Silane (SiH_4) and ethylene (C_2H_4) were used as the source gases of Si and C, respectively, and hydrogen as the carrier gas. Trimethylaluminum was used as the source of Al for p-type layer growth. Both undoped- and Al-doped layers were grown at 1773K and total pressure of 1 atm.

A mesa structure with a junction area of 6.4 x 10^{-4} cm^2 was used for the diode fabrication. The sample was oxidized in dry oxygen at 1473K to produce an approximately 1000Å oxide layer for passivation of the as-grown surface. Aluminum and nickel were used as ohmic

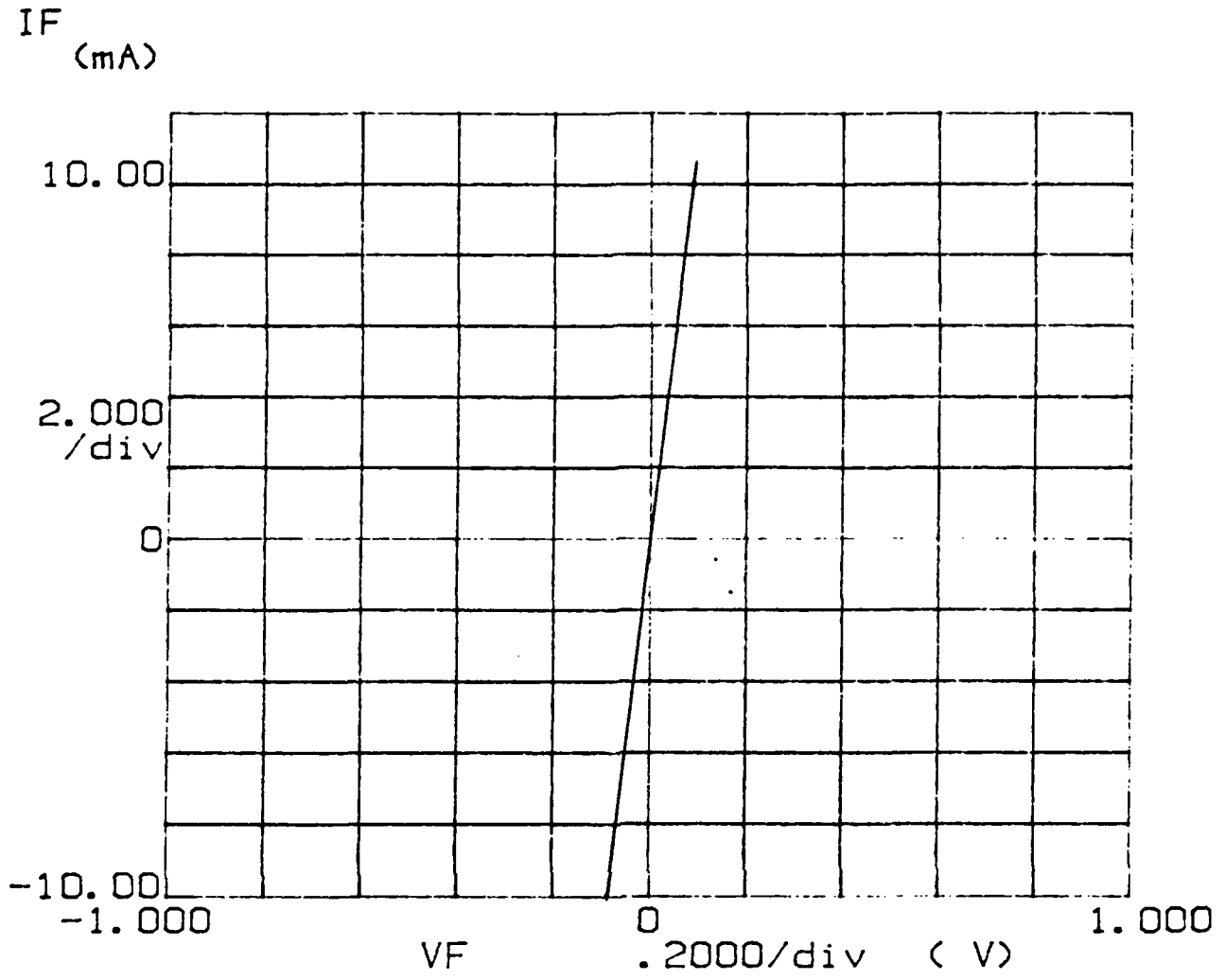

Fig. 17: Current-voltage characteristics of annealed Ni contacts on n^+ α SiC

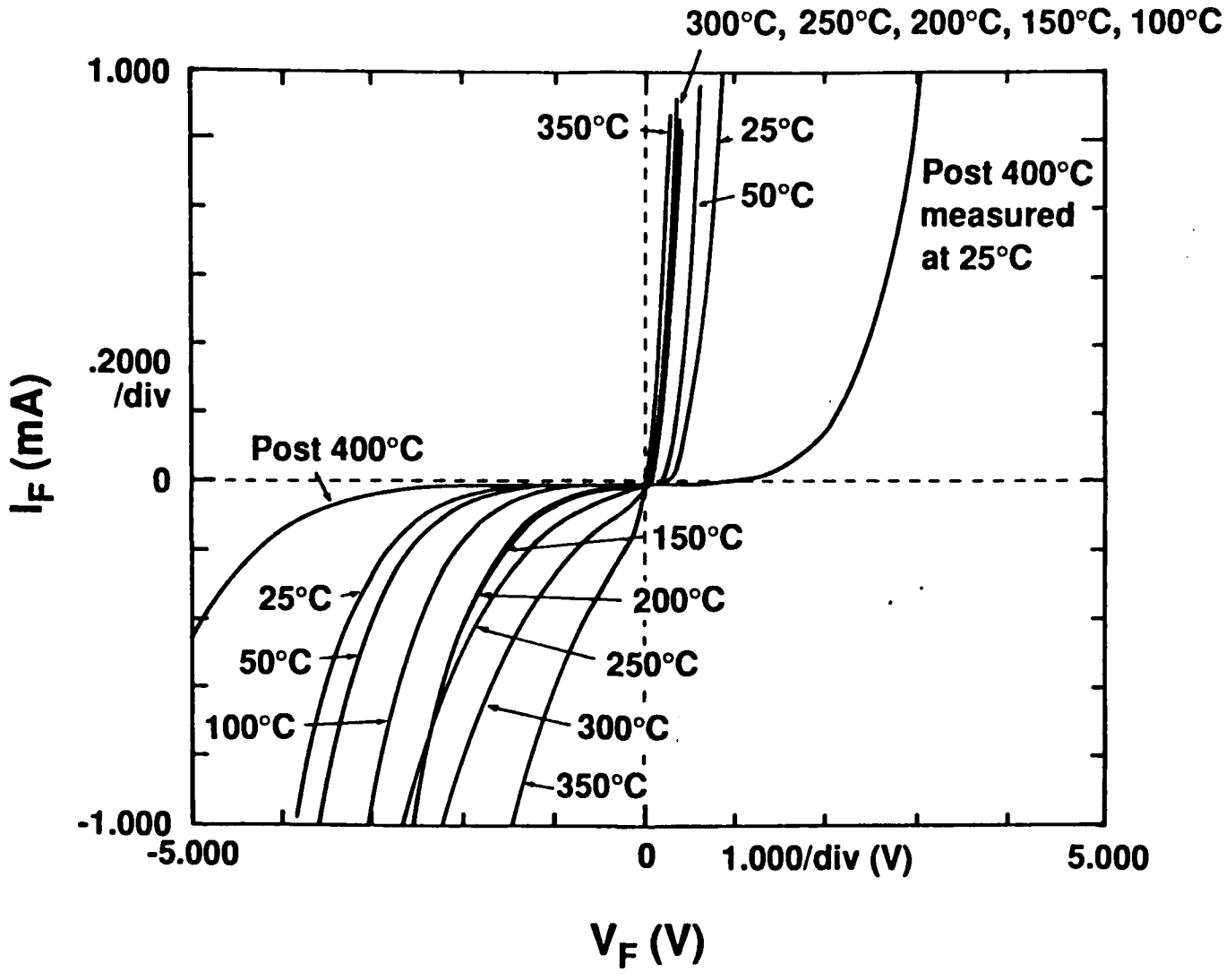

Fig. 18: Rectifying characteristics of Pt contacts on n^+ α SiC as a function of temperature.

contacts. These contacts were producedby rf sputtering. Both contacts were 0.5 μm thick. The sample was then annealed at 1273K for 5 minutes. Fig. 19 shows a schematic cross-sectional view of the diode structure.

Carrier concentrations in the n- and p-type layers were measured by using a 590 CV analyzer with a Hg-probe. Current-voltage characteristics of the diodes were measured by a HP 4142-B system at both room and elevated temperatures.

2. Results

Fig. 20 shows the I-V curve of a 6H-SiC p-n junction diode at room temperature. The leakage current measured at 100 volts reverse bias was $3x10^{-4}$ A/cm^2. The turn-on voltage at forward bias was 2.2V. In Fig. 21, the I-V data presented in Fig. 20 are shown in a semi-logarithmic plot. From the slope of the linear portion of this latter plot, the ideality factor, n, was found to be approximately 2.5. The saturation current, I_s, determined from the extrapolated intersection of this plot with the current axis is $1.2x10^{-32}$ A/cm^2.

The I-V characteristics of the diode at elevated temperature up to 623K are shown in Fig. 22. The leakage current at 100 volts was $2x10^{-3}$ A/cm^2 at 623K. The forward turn on voltage reduced with increasing temperature, from 2.2V at 298K to 2.1 V at 423K and to 1.9V at 623K.

B. MESFETs

1. Experimental Procedure

MESFETs were fabricated in an n-type 6H-SiC thin film epitaxially deposited on a 2.5 μm thick, p-type 6H-SiC layer previously grown on an off-axis 6H-SiC substrate via CVD. The n-type layer was either doped with nitrogen or undoped. The p-type layer which confined the current to a thin n-type active region was doped with Al. All layers were grown at the same growth conditions as those used for the diodes described above.

Following the growth of the n-type layer, the sample was oxidized in dry oxygen to grow a 1000Å thick oxide layer for passivation of the surface. A two-level mask set employing a concentric ring geometry was used for fabrication of the MESFETs. The gate pattern completely enclosed the center (drain) contact which had a diameter of 100 μm. The gate

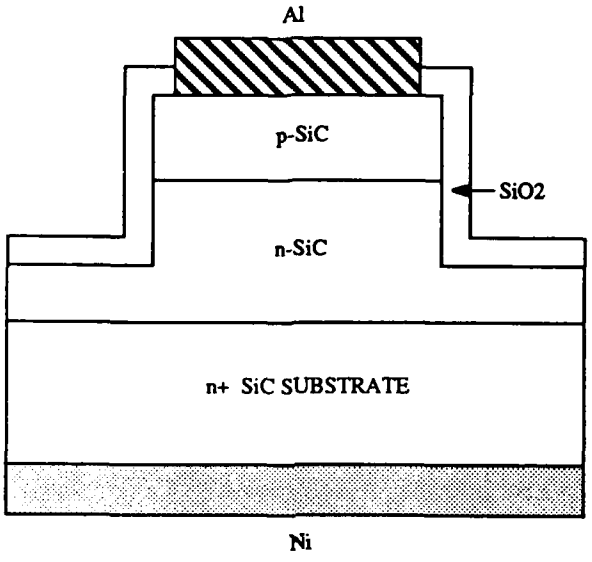

Figure 19: Schematic cross-sectional view of a 6H-SiC p-n junction diode.

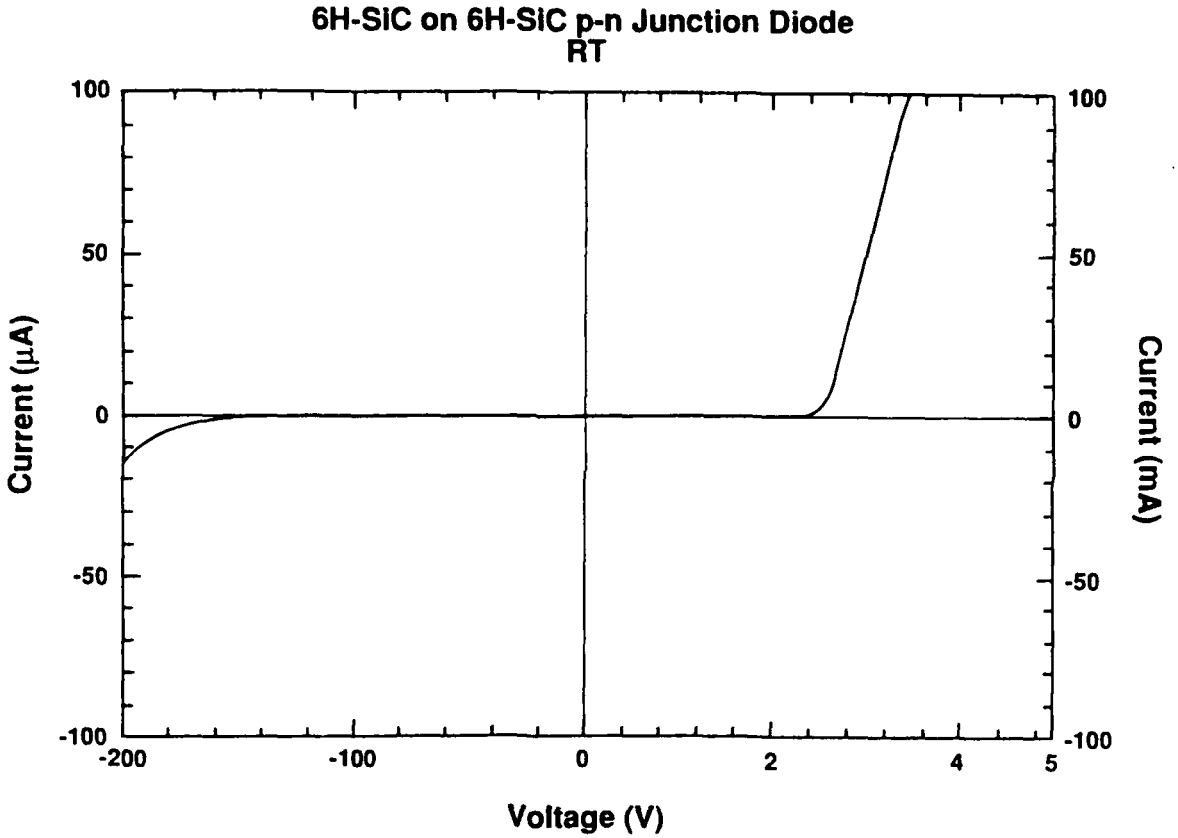

Figure 20: Current-voltage characteristics of 6H-SiC p-n junction diode at room temperature.

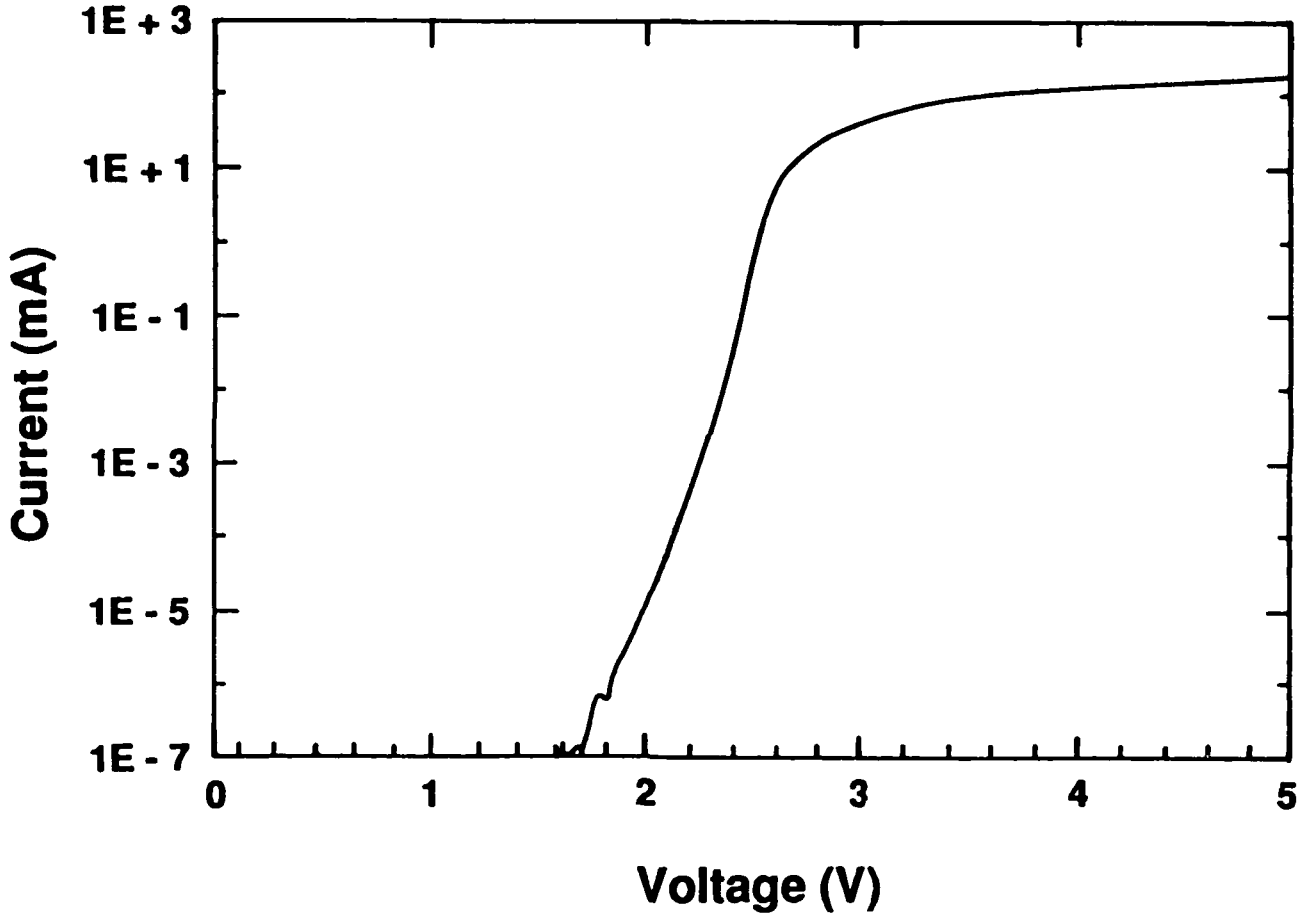

Figure 21: Log current vs. voltage for the diode shown in Fig. 20 under forward bias.

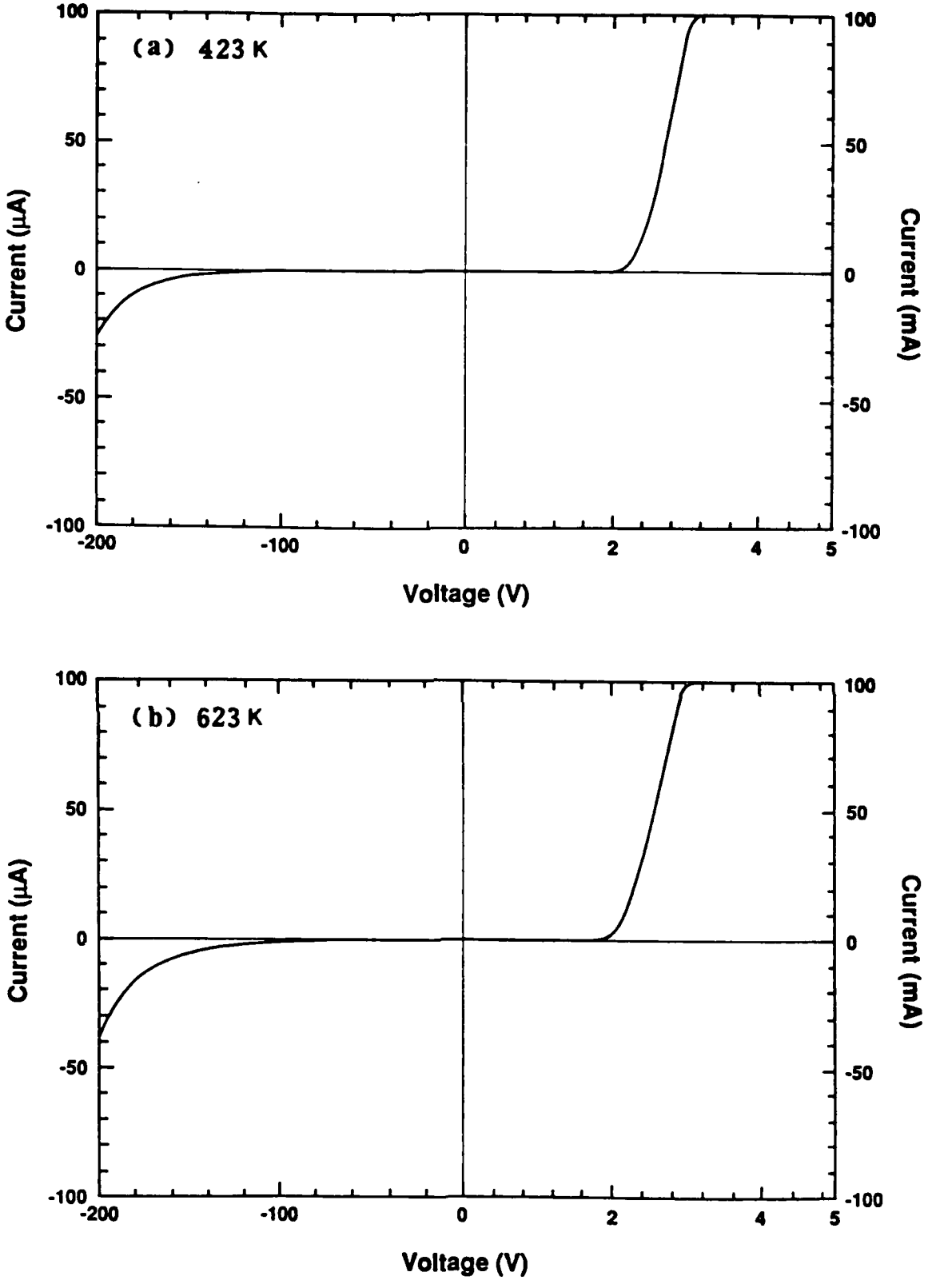

Figure 22: Current-voltage characteristics of the diode shown in Fig. 20 at temperatures of (a) 423K and (b) 623K.

contact pad was 100 μm on a side, and the outer (source) ring contact paid was 100 μm in diameter. Gate lengths of 3.5, 5, 10, 20 and 50 μm were used with the source contact-drain contact distances of 10.5, 15, 24, 34 and 70 μm, respectively. Sputtered nickel was used as the material for the source and drain contacts. After sputtering, the sample was annealed at 1373K to minimize contact resistance. Sputtered platinum was used as the gate Schottky contact. Two dark-field masks were used in conjunction with reversal photo resist in order to open the ohmic andSchottky contact windows in the oxide layer. A lift-off technique was used to remove excess Ni and Pt deposited on the SiO_2. The schematic illustration of the fabrication procedure is shown in Fig. 23.

Drain current-drain voltage characteristics of the MESFETs were measured by using a 4145 A semiconductor parameter analyzer.

2. Results and Discussion

i. MESFETs with Undoped n-type active layer. Figure. 24 shows the I_D-V_D curves of a MESFET with an undoped n-type layer at room temperature. The gate length of this device is 10 μm. Excellent saturation and a small leakage current were achieved to a drain voltage of 60 volts. Fig. 25 shows the high temperature performance of the same MESFET to a temperature of 698K. Although the drain current saturation was still good at relatively high drain voltage, the leakage current increased significantly at 698K. The maximum transconductance for all MESFETs with an undoped n-type layer was small. The maximum value measured on a MESFET with 3.5 μm gate length was 4.3×10^{-2} mS/mm at room temperature.

The possible reasons for such small maximum transconductance are as follows: (1) Low carrier concentration in the n-type active layer (for this sample, the n layer carrier concentration was estimated to be in the range of $4\text{-}6 \times 10^{-6}/cm^3$) and/or (2) the n-type layer was too thin (approximately 0.4 μm) for this low carrier concentration.

To improve the properties of MESFETs, a nitrogen doped, n-type active layer was grown instead of an undoped layer, as discussed below.

ii. MESFETs with Nitrogen Doped n-type Active Layer. The n-type layer of these MESFETs had a carrier concentration of $2 \times 10^{17}/cm^3$, measured by using the 590 CV analyzer, and a thickness of 0.35 μm.

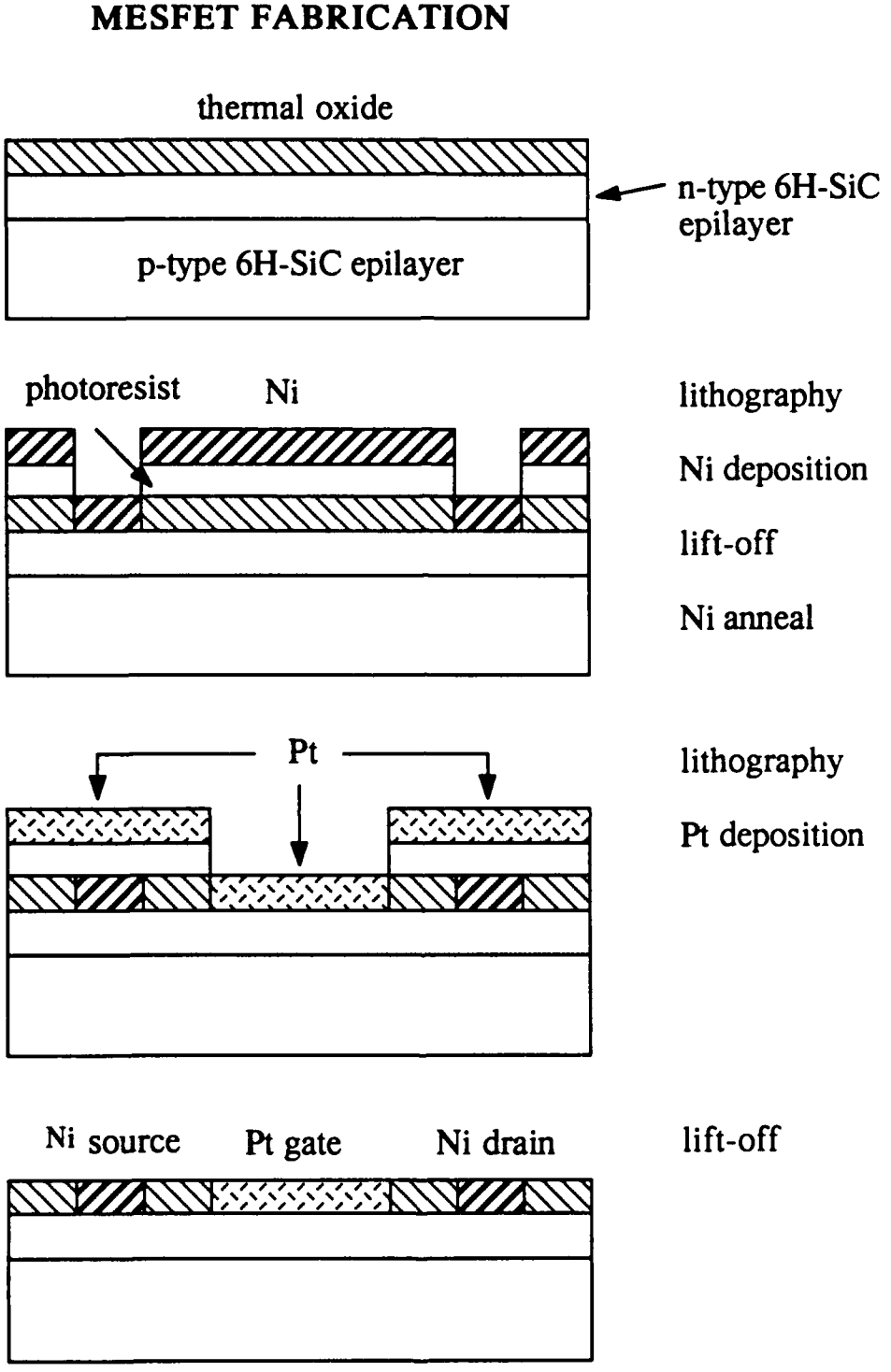

Figure 23: Cross-sectional view of the processing steps for the MESFETs.

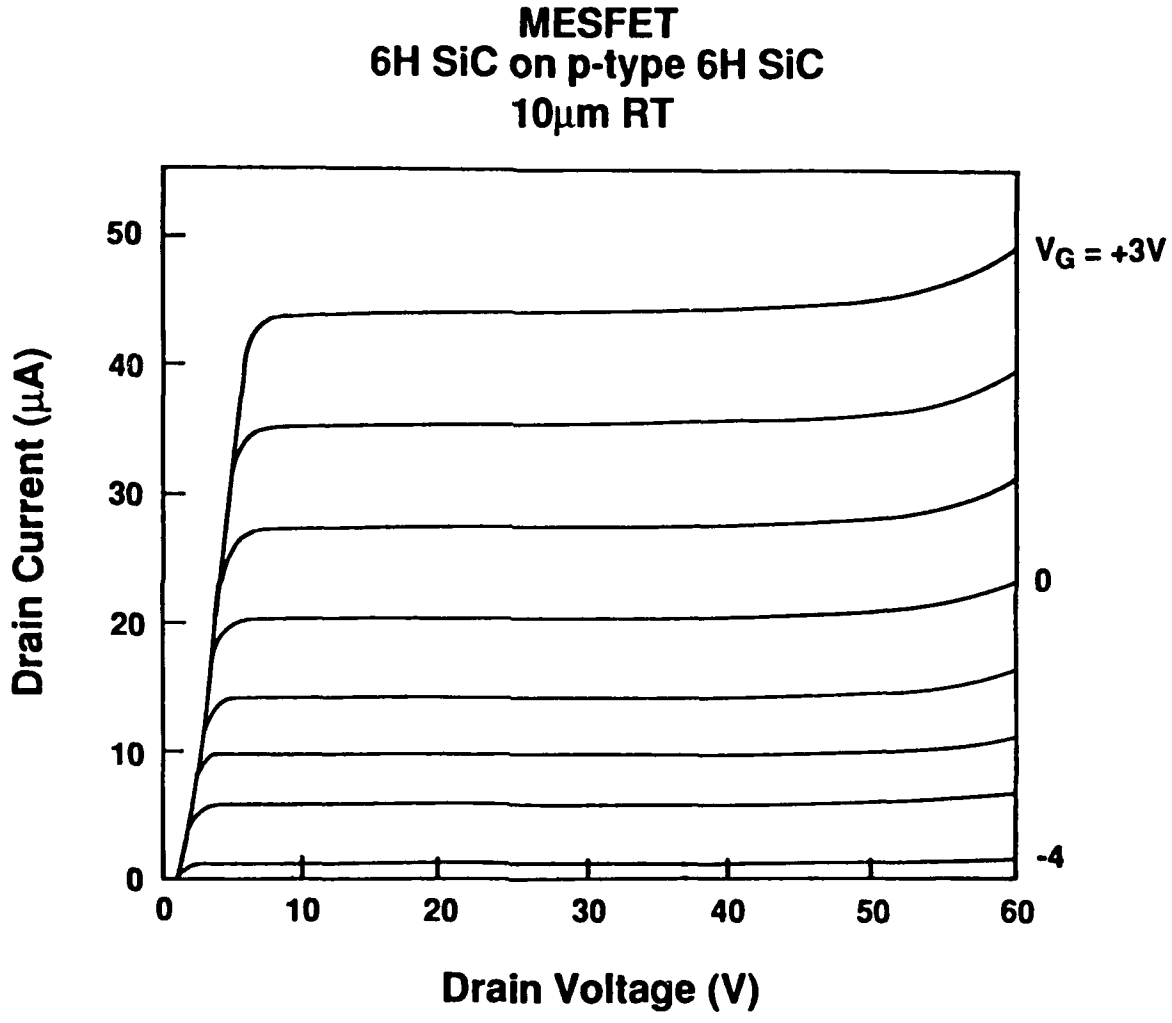

Figure 24: Drain current-voltage characteristics of a 6H-SiC MESFET with undoped n-type active layer at room temperature. The gate length is 10 μm.

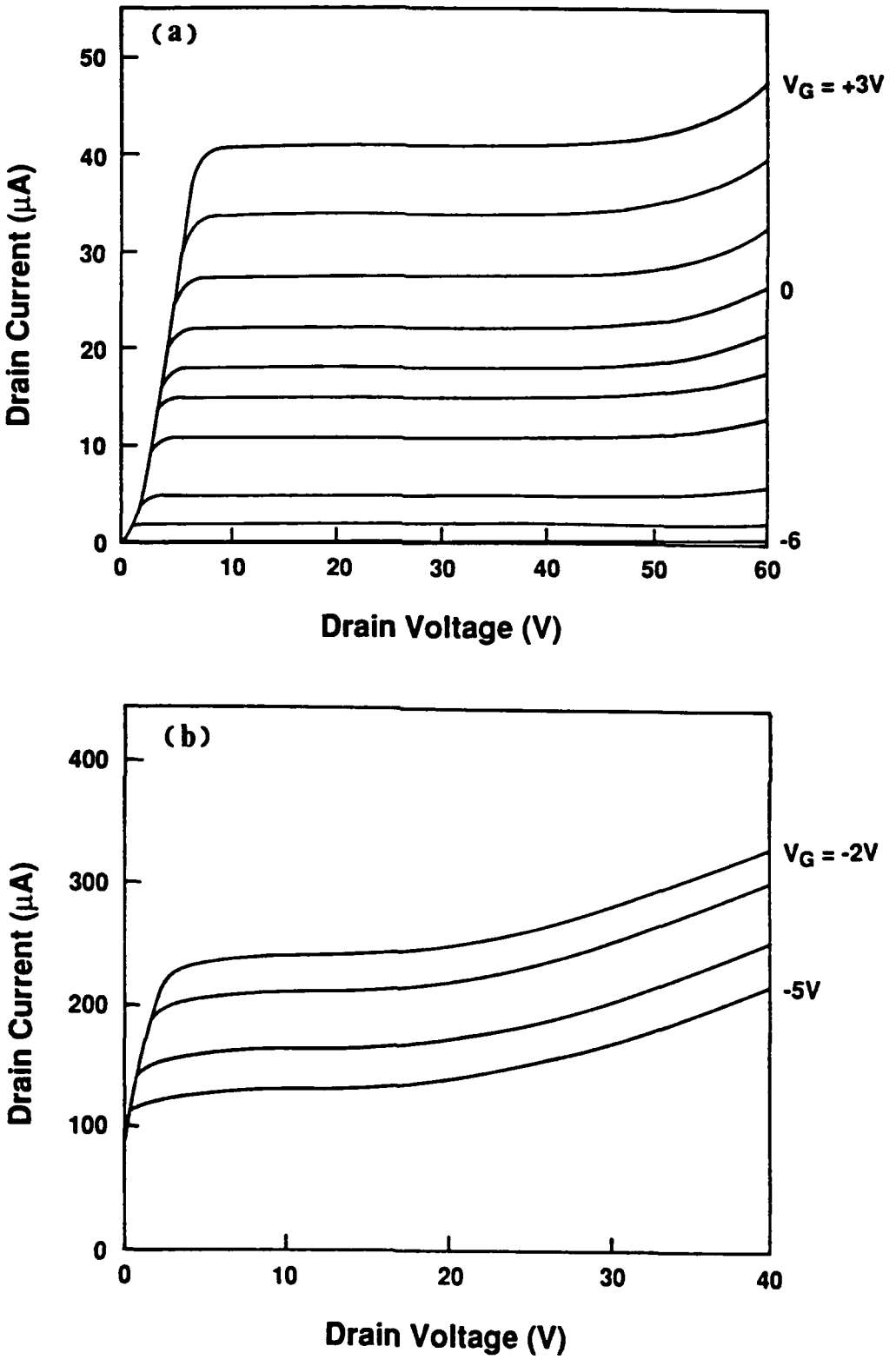

Figure 25: Drain current-voltage characteristics of the MESFET shown in Fig. 24 at temperatures of (a) 398K and (b) 698K.

As expected, the maximum transconductance was greatly increased. A typical value measured on a 5 μm gate length device is 5 mS/mm, which is two orders of magnitude higher than that obtained before. The I_D-V_D characteristics of the MESFET is shown in Fig. 26. Good saturation was still achieved, but the leakage current was larger than that measured on previous MESFETs. From the gate-to-drain I-V curve of the same device, shown in Fig. 27(a), the Schottky diode was relatively leaky, compared with that measured on a same gate size MESFET with an undoped n layer (Fig. 27 (b)). The larger leakage current in the Schottky diode indicated that the surface leakage current was dominant, which may be attributed to the redistribution of N in the n layer surface due to oxidation.

C. MOSFETs

1. Experimental Procedure

MOSFETs was produced in undoped ($n \approx 5x10^{16}$ cm^{-3}) 6H-SiC films grown by conventional CVD by Wang at NCSU on p-type ($P \approx 10^{17}$ cm^{-3}) 6H-SiC substrates provided by Cree Research, Inc., RTP, NC.

The MOSFET consisted of a concentric ring design with a 100 μm center dot for the source, a surrounding gate ring attached to a 100 x 100 μm square contact pad and a semicircular drain contact attached to 100 μm diameter circular contact pad. There were 5 gate lengths on the mask set: 3.5, 5, 10, 20 and 50 μm with corresponding gate widths of 347, 361, 390, 431 and 534 μm.

The gate oxide layer was thermally grown on the SiC epitaxial film using a resistively heated tube furnace. Growth conditions were 1200°C in flowing dry O_2 for ≈ 20 minutes for C-face samples to produce ≈ 60 nm of SiO_2.

Approximately 500 nm of polycrystalline silicon was deposited by low pressure CVD at 893K. The polysilicon was then degenerately doped using $POCl_3$ to deposit a phosphorus glass at 900°C for 10 minutes followed by a drive-in (diffusion) step at 900°C for 11 minutes. It was subsequently etched in BOE to remove the glassy surface generated by the doping process.

The gate was photolithograhically defined with positive photoresist. Polysilicon was wet etched using Allied Poly Etch containing ~50 wt% nitric acid and ~1 wt% hydrofluoric acid.

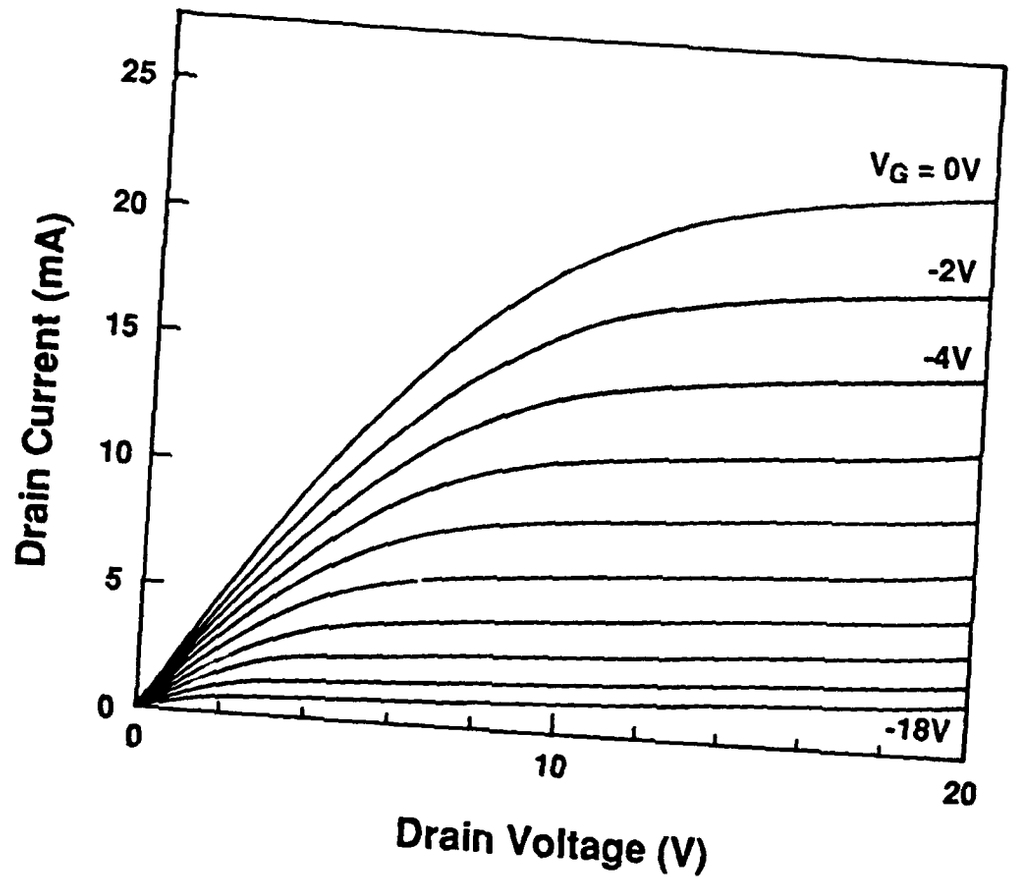

Figure 26: Drain current-voltage characteristics of a 5 μm gate length MESFET with N doped n-type active layer at room temperature.

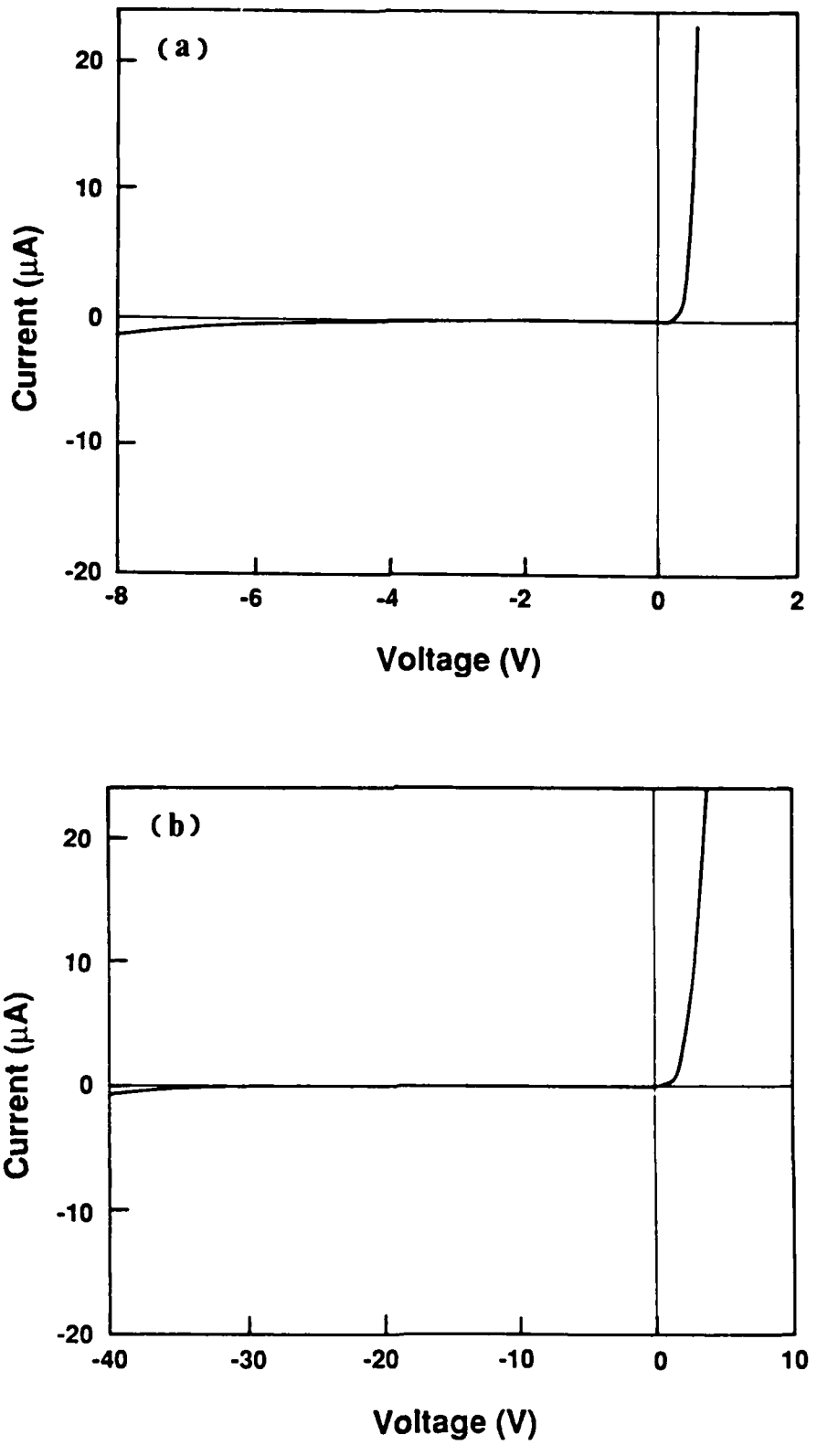

Figure 27: Gate-drain current-voltage characteristics of the MESFETs with (a) N doped n-type active layer and (b) undoped n-type active layer.

Etching times were typically 1 to 3 minutes and the endpoint was usually visually determined by watching the progression of the interference fringes. The photoresist was stripped from the sample after etching with acetone for 10 minutes followed by a DI water rinse.

The source and drain were photolithographically defined with image reversal photoresist. Windows were opened in the oxide by wet etching with BOE followed by a DI water rinse. Etch times were calculated for the measured oxide thickness and a 100% overetch was used.

Nickel was deposited via RF sputtering as the ohmic source and drain contacts. The photo resist was lifted off by dissolution in acetone. As-deposited Ni is rectifying, thus all ohmic contacts were annealed for 1 to 5 minutes in a resistively heated, SiC coated graphite boat under vacuum ($\approx 5x10^{-6}$ ion). Contacts formed on nominally undoped 6H-SiC were not truly ohmic and exhibited a large contact resistance, even after anneals at temperatures up to 1100°C.

In order to improve the contacts to the active layer, the sample was dual implanted with N^+ at 70 keV and 40 keV using doses of $5x10^{14}$ cm^{-2} and $3.35x10^{14}$ cm^{-2}, respectively. The sample was implanted at 600°C and the poly-Si gate served as an implant mask to self-align the gate channel. The projected range of the implants was 0.1314 μm and 0.0738 μm producing a shallow N^+ layer of estimated peak atomic concentration of $5x10^{19}$ N/cm^{-3} and, with 10% activation, an estimated carrier concentration of $\approx 5x10^{18}$ cm^{-3}. Ni contacts sputtered onto ion implanted samples showed ohmic behavior with good current carrying capability.

2. Results and Discussion

The MOSFETs were tested for ohmic contacts, drain current saturation, field effect transistor active and gate leakage using an HP4145 Semiconductor Parameter Analyzer. A plot of the forward drain current versus drain voltage is shown in Figure 28 for a 10 μm gate length device at some temperature. The current saturates up to source-to-drain voltages in excess of 60V. The apparent transistor action is not accurate, as significant gate leakage current was measured. The quality of the gate oxide is suspect in the high leakage devices. Initial measurements before the ohmic contact anneal step, however, showed gate leakages of < 1 nA at 10V. Therefore, some compromise between the high temperature anneal for good ohmic contacts and the degradation of the gate oxide/electrode must be made.

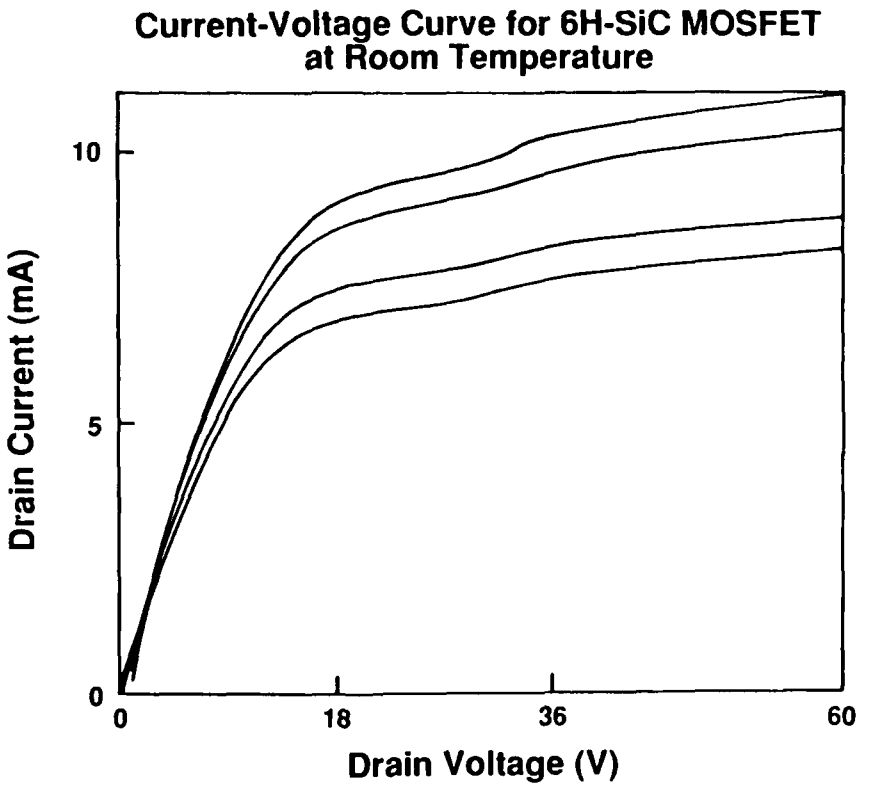

Figure 28 Current-voltage characteristics under forward bias of a depletion mode MOSFET produced in an n-type 6H SiC epitaxial film (0.4 μm) grown on p-type 6H SiC bulk sublimation wafer. Gate voltage is +8V to -4V in 4V increments. Gate electrode was P-doped polysilicon and the source and drain contacts were Ni.

D. IMPATTs

IMPATT diodes are two terminal devices which operate with the bias holding the device at the edge of breakdown. Increases in bias generate huge increases in current if the breakdown is truly steep avalanche breakdown. IMPATT diodes having the structure seen in figure 29 were designed by Dr. Trew's group at NCSU to operate near 10 GHz. Initial attempts to produce IMPATTs in 3C SiC films grown on Si was unsuccessful due to the difficulties in handling the μm thick films and getting Au beam leads to adhere. There was also the question of operation due to the "soft" breakdown observed in the highly defective 3C SiC films. Fabrication was restarted using 6H-SiC films grown on n^+ 6H-SiC substrates with a 3.5 mil diameter Pt dot as the Schottky contact to the undoped layer and Ni as the ohmic contact to the n^+ layer. The devices were annealed at 900°C for 1 minute and exhibited some adhesion problems. An IV plot before and after annealing are shown in figures 30 and 31 and exhibits excellent rectifying character and a reverse bias breakdown greater than -100V (the equipment limit) before annealing and > 60V after annealing. A plot of the forward characteristics log I versus V gives a linear region over 0.1V to 0.5V with a slope of 3.47 and extrapolated intercept at V=0 of -7.54 which gives an I_s (reverse bias estimated current as 28 nA).

E. High Power Diodes

After the success of using Pt as a Schottky contact to 6H-SiC (see Section IV), the idea of producing higher power diodes capable of withstanding high reverse bias voltages was realized. The methods used to increase the reverse bias breakdown voltage have been well developed for use in Si technology and the two simplest are field plates and guard rings. For this experiment, field plates around larger diameter contacts was chosen as a method of increasing both the reverse bias breakdown voltage and the forward bias current capacity.

The maximum reverse bias breakdown strength (V_B) of Schottky diode of a metal-undoped semiconductor-doped semiconductor structure is related to the doping (N_B) of the undoped layer by

$$V_B = \frac{\varepsilon E_c^2}{2qN_B}$$

where q is the electronic charge, ε is the dielectric constant and E_c is the critical field strength of the semiconductor material. The undoped layer thickness (W_c) can then be determined at breakdown

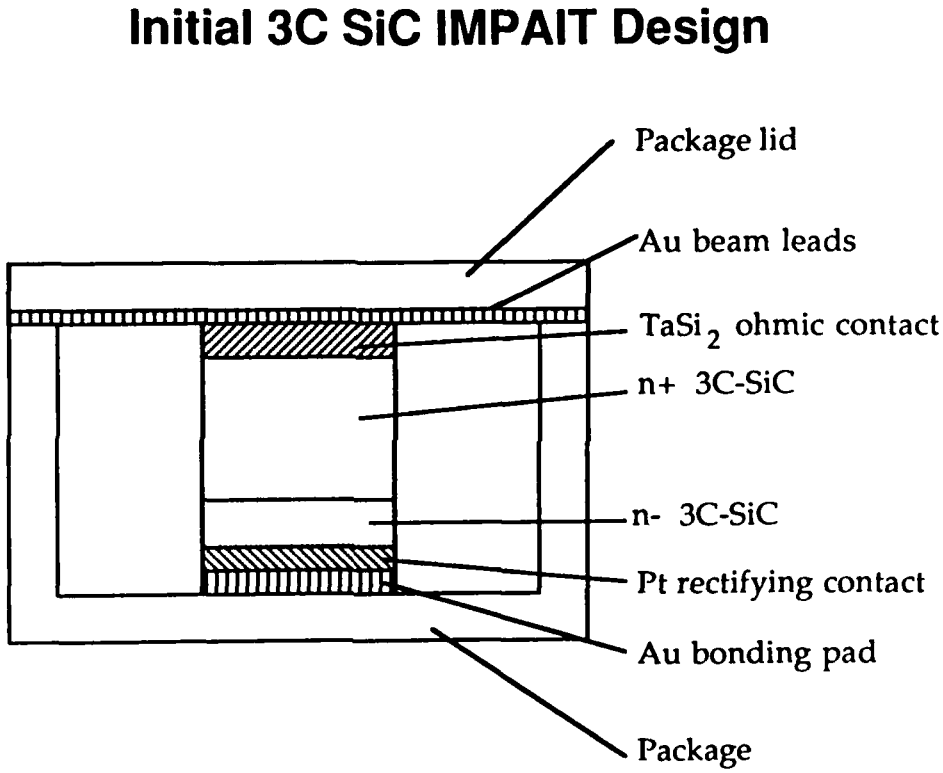

Figure 29 Schematic of the IMPATT diode design for 3C SiC. A similar design is used for 6H SiC, but package on a diode header.

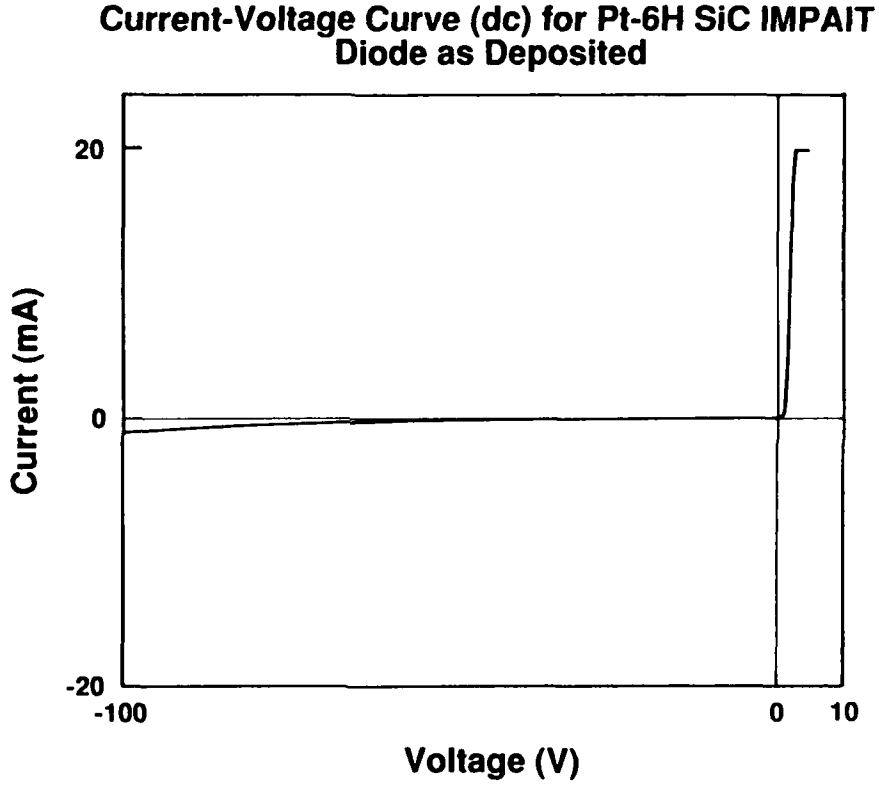

Figure 30 Current-voltage characteristic of 6H SiC IMPATT diodes in dc bias conditions at room temperature. Notice the reverse bias breakdown is > 100V and the forward current reaches 20mA at under 5V forward bias.

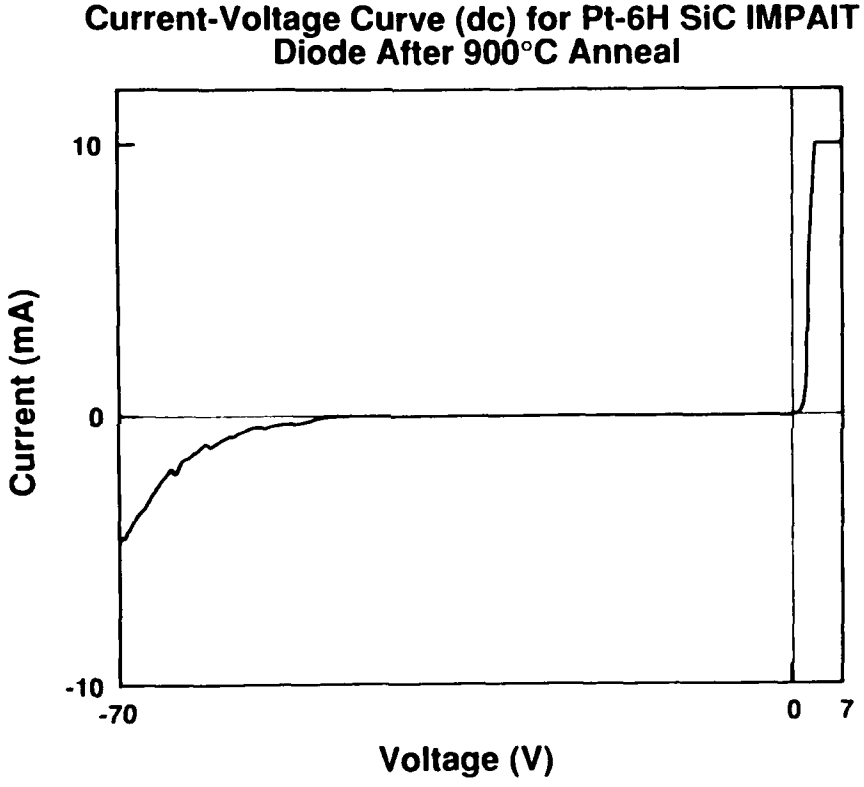

Figure 31 Current-voltage characteristic of IMPATT diodes in dc bias conditions at room temperature after the diode has been annealed in vacuum at 900°C. Notice the reverse bias breakdown is now less than 70V and appears 'soft', while the forward characteristics remain unchanged.

as $W_c = ZV_B/E_c$. Using $E_c = 2x10^6$ V/cm, $\varepsilon = 10\ \varepsilon_o$ and $N_B = 10^{17}$ cm^{-3}, the best breakdown voltage is calculated as 110.6V for an undoped layer 1.1 μm thick. The value of N_B was chosen as one consistently producible by current CVD techniques. As the quality of the films improves, the theoretical breakdown strength will also improve.

This value of V_B is not usually obtained due to the edge effects around metal-semiconductor contacts, as was seen in the reverse bias brealdown in Pt dots on 6H-SiC at 60V or less. In order to apply the field plate concept,the oxide layer must be of a thickness to reduce the depletion region in the semiconductor to almost the oxide/semiconductor interface. This is necessary to reduce the crowding of the electric field lines at the termination. The relationship of $r_j = t_{ox}\ \varepsilon_{SiC}/\varepsilon_{SiO_2}$ where r_j is the depletion depth under the metal at breakdown and t_{ox} is the oxide thickness determines the required t_{ox} to be ≈ 420 nm. Therefore, the higher breakdown device — a vertical diode with a field plate Pt contact on top of undoped layer of 6H-SiC grown on an n^+ layer of 6H-SiC with an Ni ohmic contact — is shown in figure 32. This device was fabricated in several steps. The epilayers were grown on n^+ 6H-SiC substrates for Cree Research, Inc. The surface was oxidized to 420 nm. The back side was etched in HF to remove the oxide, sputtered with Ni and annealed at 1100°C for 3 minutes. The topside was patterned with photoresist and a 480 μm dot was etched through the oxide. The photoresist was stripped and reapplied and a 5440 μm dot was patterned surrounding the hole in the SiO_2. Pt was sputtered and the photoresist shipped to leave the field plate diode. The IV characteristics are shown in figure 33 and even with the large leakage due to the large area contact, the diode shows good rectifying characteristics. Figure 34 details the low voltage portion of the curve, emphasizing the exponential forward current.

VI. MOLECULAR BEAM EPITAXY OF SILICON CARBIDE

A. Introduction

A system for the growth of SiC films by the technique of gas-source molecule beam epitaxy has been designed, purchased, and is currently under construction. The technique of molecular beam epitaxy (MBE) allows for precise control of growth parameters and minimization of sample contamination. Monocrystalline SiC films will be grown at relatively low temperatures using minute amounts of gas introduced into the system by leak valves. Pressures within the chamber during growth will be in the 10^{-5} torr range. As the mean free path of molecules at this pressure is

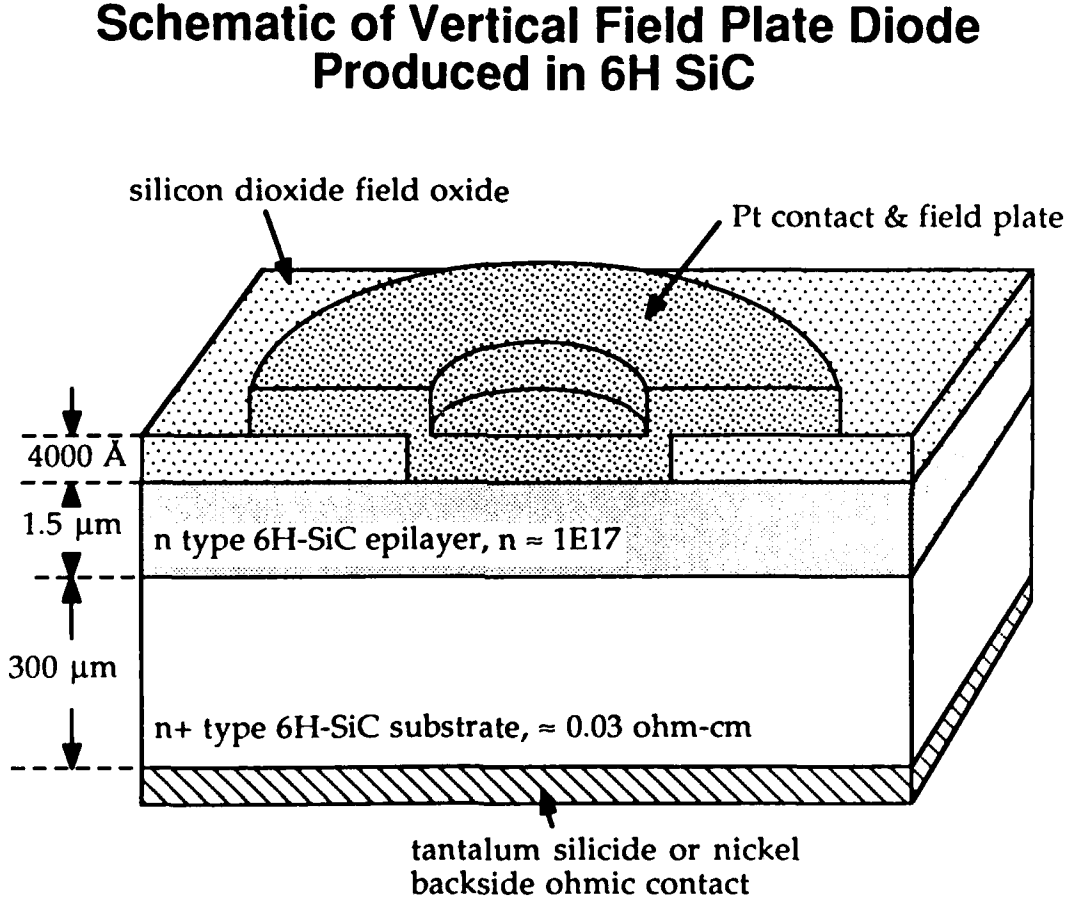

Figure 32 Schematic cross-section of a vertical rectifying diode with a field-plated Pt Schottky contact and a Ni ohmic back contact produced in n-type 6H SiC.

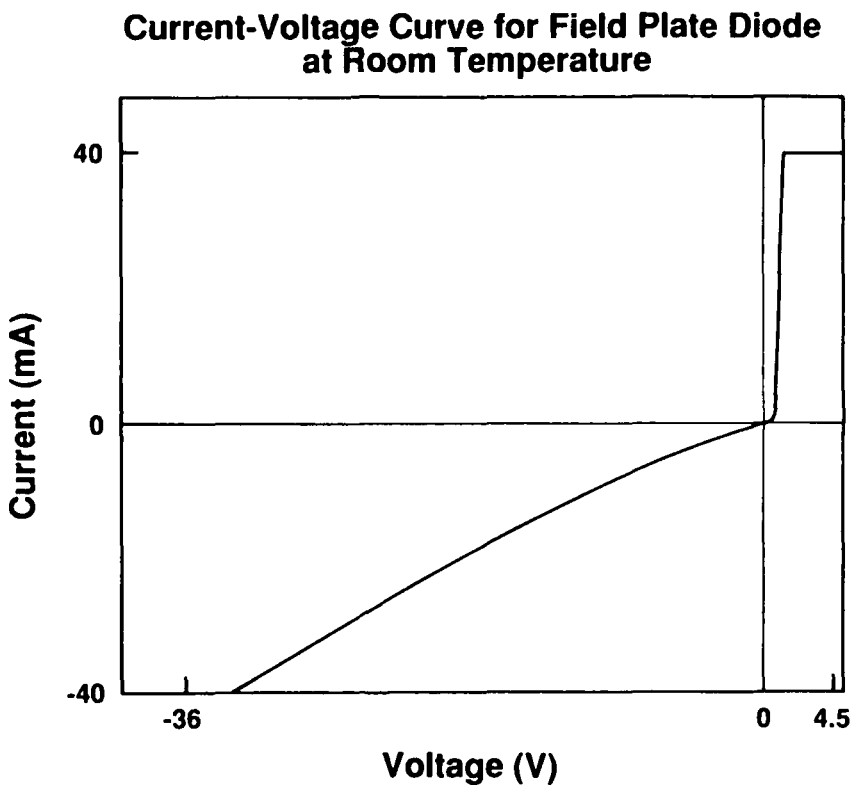

Figure 33 Current-voltage characteristics of the field-plated vertical diode described in Figure 32, biased from -40V to +5V at room temperature.

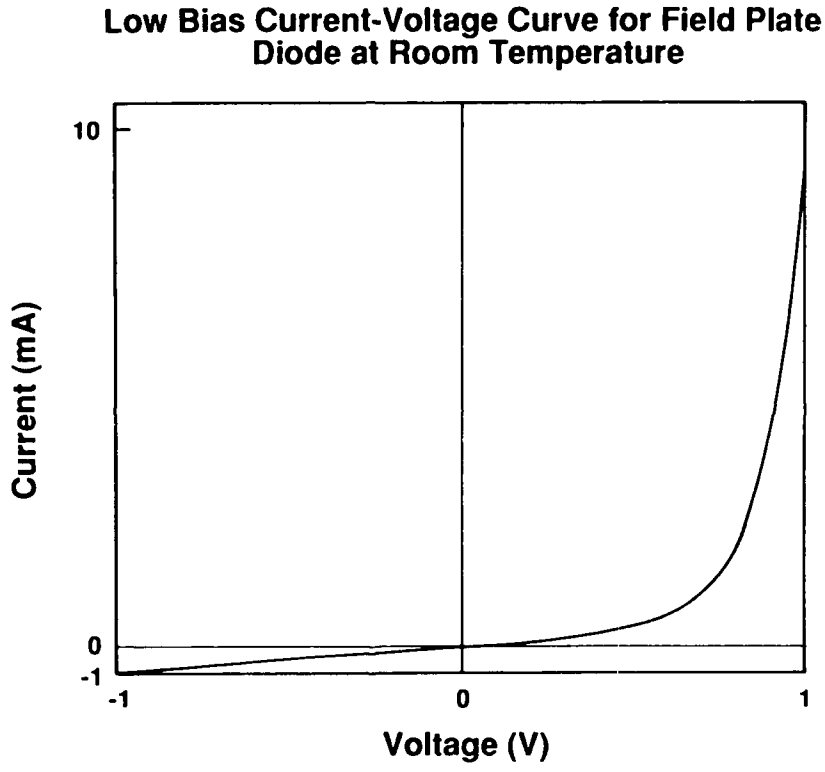

Figure 34 Low bias current-voltage characteristics of the vertical field plated diode from -1 to 1V at room temperature. Note the forward bias curvature and a threshold voltage of approximately 0.7V.

much longer than the dimensions of the growth chamber, the source gas molecules reach the sample surface without collisions. Thus a great deal of control over growth conditions can be achieved using this technique. This deposition system will be used for low defect-density growth of monocrystalline SiC thin films, SiC/AlN solid solutions , and SiC/AlN pseudomorphic structures.

B. Growth System

A schematic of the system is shown in figure 35. Samples will be introduced into a small load lock chamber, which will be subsequently evacuated. The samples will then be transferred to the heating stage in the growth chamber. The load lock is used in order to increase sample throughput, as well as to keep the main deposition chamber under vacuum. It is pumped by a turbomolecular pump backed by a rotary vane pump. The load lock is fully constructed, and pressures of 1×10^{-6} torr or below are reached within 30 minutes after pumping begins.

The growth chamber will be utilized for both *in situ* sample cleaning and deposition. Substrates will be cleaned prior to deposition by using Ar plasma to produce H^+ radicals from H_2 introduced into the system downstream from the plasma. The Ar plasma will be obtained using an electron cyclotron resonance plasma source developed in our laboratory by Sitar. This source should be completed within two months. To date, no published work has been performed on plasma cleaning of α-SiC. However H^+ plasma cleaning of silicon using this method has been performed at 300°C [1].

The growth chamber has been designed to maximize versatility and minimize sample contamination. It has the capability of using gaseous sources introduced into the chamber using automatic variable control leak valves. The leak rates can be varied precisely and automatically as a function of time, or flow can quickly be shut off and on using solenoid valves. As a result, growth species can be reproducibly controlled. This is necessary for the growth of novel structures, such as the SiC/AlN layered structures. Solid MBE sources (either Knudsen cells or electron-beam sources) can also be installed along the source flange and used as desired.

The electron cyclotron resonance (ECR) source used for H^+ plasma cleaning will also be used for the production of activated nitrogen species from N_2 for n-type doping of SiC. During cleaning and deposition, the sample sits at a 45° tilt from upside down in order to avoid contamination on itself from falling particulates as well as to avoid contamination of the solid

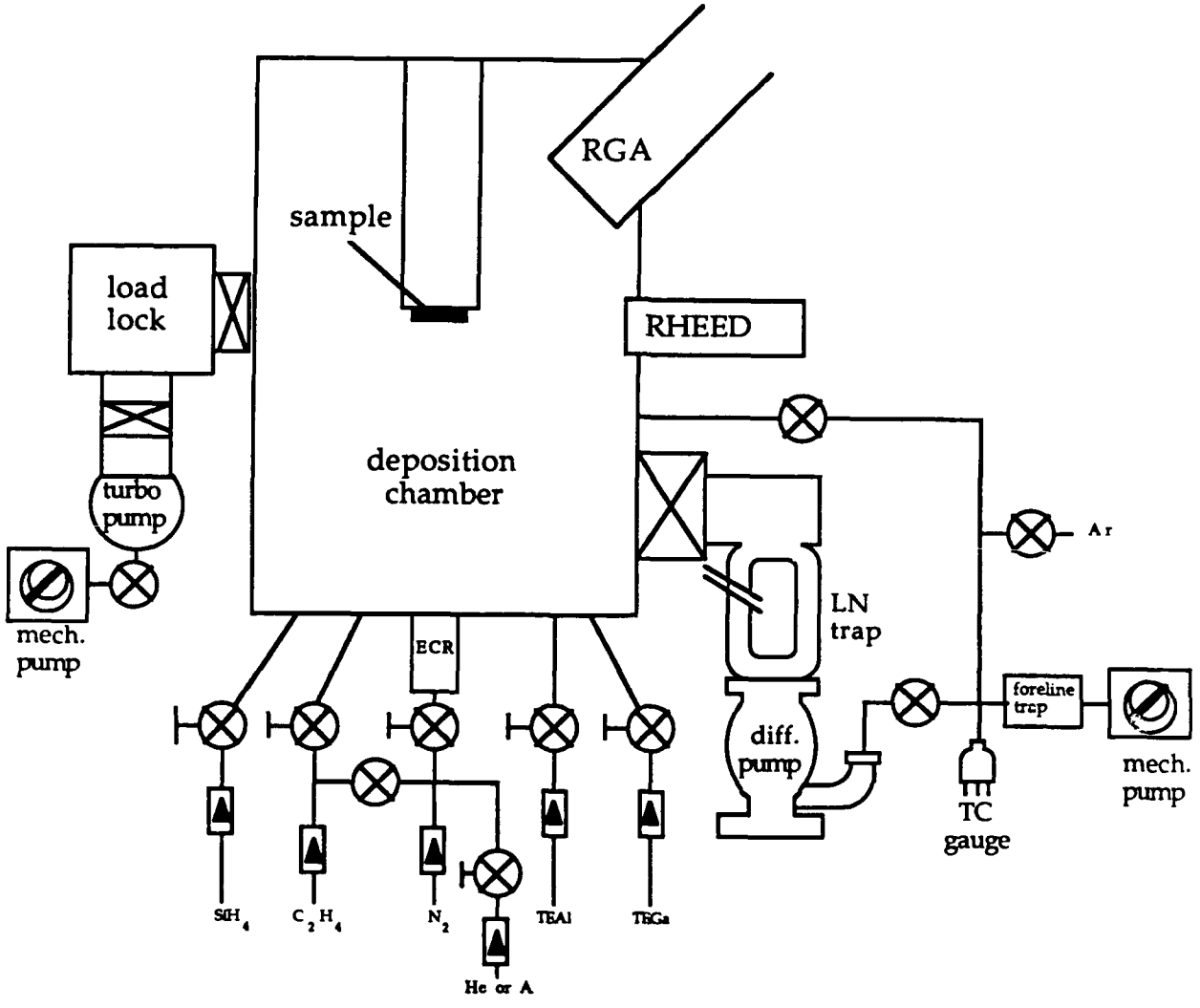

Figure 35: Schematic of the Molecular Beam epitaxy System for the deposition of silicon carbide.

sources from falling particulates generated on the sample holder and/or sample. The chamber will also have equipment for residual gas analysis in order to determine species present in the chamber during growth. Characterization of films using RHEED during growth is planned, but this equipment has yet to be purchased. The system will be pumped using a 2400 *l*/s diffusion pump with a Vacuum Generators UHV liquid nitrogen cold trap backed by a rotary vane pump. Background pressures of 10^{-10} torr are expected in this system. All components of this system mentioned above are either on order or have been received.

Samples will be heated using a heater specially designed for this system. Exposure of the sample to materials containing electrically active impurities, such aluminum, has been minimized. All components in contact with the sample will be high purity SiC-coated graphite. Heat is produced by resistive heating of a coiled tungsten filament within a SiC-coated graphite cylindrical heating cavity lined with tungsten heat shielding. A high-purity pyrolitic BN disk is used as an insulating plate for holding the W coil. The heater will be capable of temperatures of well over 1000°C, which is necessary for this research.

C. Experimental Details

Low temperature growth of high-purity, low defect-density, monocrystalline SiC layers on α-SiC substrates is the primary goal of this project. These SiC films will be grown on α-SiC substrates obtained from Cree Research. Gases initially to be used for growth of SiC are silane (SiH_4) as the Si source and ethylene (C_2H_4) for the carbon source. An emphasis has been placed on finding a solid carbon source for the production of monomolecular carbon species, as decomposition of hydrocarbons requires fairly high temperatures. The growth temperature of SiC can be substantially lowered if the energy required for this decomposition can be decreased. Plasma decomposition is a proven method for low-temperature decomposition of gaseous species, though the process control necessary for monocrystalline growth is not easily achieved.

The feasibility of a heated graphite filament for carbon doping of GaAs in a MBE system has recently been demonstrated [17]. A large percentage of monomolecular C has been produced by resistive heating of graphite to temperatures of about 2500°C. This carbon source is very simple and effective and has potential as a solid source for carbon in SiC. Though the carbon flux from the graphite filament must be much greater for SiC than for doping of GaAs. the use of a filament with a larger cross-section and greater power should give a sufficiently large carbon flux. Other methods of producing a flux of C, such as modified electron beam evaporation to produce

monomolecular species, are also being considered. Dopants to be used for SiC are Al (p-type) obtained by thermal decomposition of triethylamuminum(TEA) and N obtained by the Decomposition of N_2 using the ECR source noted above. Growth temperatures will be in the range of 1000-1200°C.

In addition to SiC films, SiC/AIN pseudomorphic layers and solid solutions will also be grown as a part of this research. Research conducted in the U.S. and the Soviet Union indicates that a wide range of solid solutions exists in the SiC/AIN system. A solid solution between these materials would undoubtedly have interesting electrical properties, such as the effective bandgap as a function of AlN in the solid solution.

In addition, the lattices of the hexagonal polytypes of SiC and AIN have an effective mismatch in the axial direction of less than 1%. Layers of these materials below a certain thickness will elastically strain to accommodate each other. If the layers are monocrystalline, this will produce a pseudomorphic structure. This structure will undoubtedly have novel properties. For example, a pseudomorphic structure with SiC (an indirect bandgap material) and AIN (a direct bandgap material) may have a direct bandgap intermediate between the two materials. The same could be true of a SiC/AIN solid solution in certain composition ranges. These structures may prove to have many useful applications. Experimental work to produce these novel structures and examine their effects on material properties will take place in future research.

REFERENCES

1. G.A. Slack, J. Appl. Phys. 35, 3460 (1964).
2. H.R. Philipp and E.A. Taft, in "Silicon Carbide, A High Temperature Semiconductor", edited by J.R. O'Connor and J. Smiltens (Pergamon Press, New York, 1960) p.366-376.
3. W.V. Muench and I. Phaffeneder, J. Appl Phys. 48, 4831 (1977).
4. B. Wessels, H.C. Gatos, and A.E. Witt, in "Silicon Carbide—1973", edited by R.C. Marshall, J.W. Faust, Jr., and C.E. Ryan (University of South Caroina Press, Columbia, 1974), p. 25-36.
5. S. Nishino, H. Matsunami, and T. Tanaka, J. Cryst. Growth 45, 144 (1978).
6. W. von Muench and I. Phaffeneder, Thin Solid Films 31, 39 (1976).
7. J.A. Powell and H.A. Will, J. Appl. Phys. 44, 177 (1976).

8. P. Rai-Choudhury and N.P. Formigoni, J. Electrochem. Soc. 116, 1440 (1969).

9. I. Berman, C.E. Ryan, R.C. Marshal, and J.R. Littler, "The Influence of Annealing on Thin Films of Beta SiC," AFCRL-72-0737, 1972.

10. R.W. Bartlett and R.A. Mueller, Mater. Res. Bull. 4, S341 (1969).

11. H.S. Kong, J.T. Glass, and R.F. Davis, Appl. Phys. Lett. 49, 1074 (1986).

12. H.S. Kong, J.T. Glass, and R.F. Davis, J. Appl. Phys. 64, 2672 (1988).

13. P. Liaw and R.F. Davis, J. Electrochem. Soc. 132, 642 (1985).

14. H.S. Kong, J.T. Glass and R.F. Davis, J. Mater. Res. 4, 204 (1989).

15. P. Rai-Choudhury and E.I. Salkovitz, J. Cryst. Growth 7, 353 (1970).

16. R. Rudder, G. Fountain and R. Markunas, J. Appl. Phys. 60, 3519 (1986).

17. R. J. Malik, R. N Nottenberg, E. F. Schubert, J. F. Walker, and R. W. Ryan, Appl. Phys. Lett. 53, 2661 (1988).

APPENDIX 1

DEEP-LEVEL DOMINATED ELECTRICAL CHARACTERISTICS OF Au CONTACTS ON β–SiC

K. DAS, H.S. KONG, J.B. PETIT, J.W. BUMGARNER, L.G. MATUS* AND R.F. DAVIS
Department of Materials Science and Engineering, North Carolina State University, Raleigh, North Carolina 27695-7907
*National Aeronautics and Space Administration, Lewis Research Center, Cleveland, Ohio 44135

ABSTRACT

Current-voltage characteristics of Au contacts formed on β-SiC films grown heteroepitaxially on both nominally (100) oriented and off-axis (100) silicon substrates have been investigated. Logarithmic plots of the I-V characteristics in the forward direction indicate space charge limited current conduction through the active volume of the diodes. The β-SiC films grown on nominally (100) oriented substrates show the presence of two deep levels located approximately between 0.26 eV and 0.38 eV below the conduction band edge. In some films on nominal (100) substrates, the I-V characteristics are also influenced by additional traps which are exponentially distributed in energy with a maximum occurring at the conduction band edge. In contrast, the films deposited on off-axis substrates have only one deep level located at approximately 0.49 eV for the 2° off (100) substrates and 0.57 eV for the 4° off (100) substrates. Previous microstructural analysis revealed that the nature and density of defects in the β-SiC heteroepitaxial films on both nominal and off-axis (100) silicon are similar except that the films on nominal (100) substrates have a high density of antiphase domain boundaries. Therefore, the presence of the shallower deep-level states observed in the β-SiC films grown on nominal (100) substrates is speculated to be due to the electrical activity of antiphase domain boundaries.

INTRODUCTION

Rectifying metal-semiconductor contacts (Schottky-barrier diodes) on SiC, a wide band-gap semiconductor that is emerging as a material for high-temperature [1], high-power and high-frequency devices [2], have been studied by a relatively small number of workers [3]. In all these studies Au was the metal of choice for these contacts. In the present study, values of the ideality factor, *n*, between 1.3 and 3.5 were observed from the apparently linear portion of the semi-logarithmic I-V plots for diodes fabricated in several different β-SiC films. The deviation of *n* from 1.0 in these crystals and the detailed structure of the forward characteristics appear to be caused by a space charge limited current (SCLC) conduction mechanism. Observations of SCLC conduction in both alpha-and beta-SiC have been reported previously [4,5]

Considering the potential importance of SiC as an electronic device material, a detailed study of Au/β-SiC contacts on both nominal and off-axis (100) silicon substrates has been conducted and is reported here. A detailed analysis of the fine-structure in the observed I-V characteristics has revealed information pertaining to the deep states present in the material studied. It appears that certain deep-level states which are likely to affect device performance are characteristically associated with given types of crystallographic defects.

THEORETICAL CONSIDERATIONS

Space charge limited current flow in insulators and wide band gap semiconductors has been considered in detail by Lampert and Mark [6]. Representative I-V characteristics obtainable from such materials are shown in Fig. (1). Ideal SCLC conduction is characterized by a square-law dependence on voltage (Fig. 1 (a)). Initially, ohmic behavior is observed if thermally generated free carriers are present (Fig. 1(b)). For traps above the Fermi level, termed "shallow-traps" by Lampert and Mark, a trapped square law behavior is observed at a lower bias (Fig. 1 (c)). When these traps are filled, current rises rapidly to true SCLC square law regime. If deep traps located

below the equilibrium Fermi level are present, ohmic behavior will be observed until all the trap levels are filled. At this point a sharp rise followed by square law behavior will be observed in the I-V curve (Fig. 1 (d)). An *n* value much greater than 1 is obtained if the sharp rise in current is interpreted as an exponential function given by, $I \propto e^{qV/nkT}$.

The "trap-filled-limit" voltage at which the sharp rise in current occurs is designated by V_{TFL}, and is given by [6],

$$V_{TFL} \approx \frac{qp_{to}L^2}{\varepsilon\varepsilon_o} \tag{1}$$

where p_{to} is the hole occupancy of the traps in the active region of the diode (i.e., the concentration of traps not occupied by electrons), L is the thickness of the active region (obtained from the measured zero-bias capacitance), q is the electronic change, ε is the dielectric constant, and ε_o is the permittivity of free space. The effective carrier concentration in the active region, n_o, is given by the relation [6]:

$$\frac{J(2V_{TFL})}{J(V_{TFL})} \approx \frac{p_{to}}{n_o} \tag{2}$$

where J is the current density. In the diodes studied, values of n_o range between 10^9 and 10^{13} cm^{-3}, whereas the bulk carrier concentration in the films is of the order of 10^{17} cm^{-3}. The apparently low effective carrier concentrations arise from carrier-transport through the active volume of the diode that is partially depleted at low biases. The effective carrier concentration determines the position of the quasi-Fermi level. The position of the deep level is taken as being within kT of the quasi-Fermi level [6]. As such, p_{to} is the concentration of the unoccupied states located approximately at the calculated quasi-Fermi level.

Traps distributed in energy may occur due to a high density of defects [7]. Current voltage characteristics, in the presence of traps distributed in energy, may not exhibit all the features of SCLC discussed above. In particular, the sharply rising regime in current may not be evident, although an exponent of greater than one is likely to be observed. This super-linear behavior can be conveniently described by an exponential distribution of traps given by $N(E) = N_o e^{-E/\Delta}$, where N_o is the density of trap states at the conduction band edge, N(E) is the density of trap states at an energy E below the conduction band-edge, and Δ is a thermal energy parameter characterizing the trap distribution [7].

The SCLC is then given by

$$I_{SCLC} = A\, q\, \mu\, N_c \left(\frac{\varepsilon\varepsilon_o}{qN_o\Delta}\right)^{\Delta/kT} \left(\frac{V^{\Delta/kT+1}}{L^{2\Delta/kT+1}}\right) \tag{3}$$

where $\Delta/kT+1$ is equal to m, the observed exponent of the experimental I-V curve (i.e., $I \propto V^m$). A characteristic temperature, such that $\Delta = kT_t$, has been defined [7]. However, the physical significance of temperature T_t is not clear [6].

EXPERIMENTAL

β-SiC films were epitaxially grown on nominal (100) and on off-axis <100> oriented (2-4° toward <011>) silicon substrates by chemical vapor deposition (CVD). Details of the CVD reactor systems and growth procedures employed were previously published [8-10].

These layers were not doped intentionally; however, a net electron concentration of ~1×10^{17} cm^{-3} was measured in these films. To prepare the surface for diode fabrication, the grown films were polished with 0.1 μm diamond paste for 48 hr. The mounting wax residue was removed with hot concentrated H_2SO_4. A final cleaning was carried in a 1:1 mixture of H_2SO_4 : H_2O_2 followed by a 2 min buffered oxide etch. In order to remove the damage caused by the polishing process, an ~1000Å thick oxide layer was thermally grown in a dry oxygen ambient at 1200°C.

The oxide layer was etched and a layer of gold, ~2000Å in thickness, was thermally evaporated onto the samples to form a metal-semiconductor contact. Active diode areas, 100 μm diameter, were delineated by photolithography and gold etching in a $KI:I_2:H_2O$ solution, 4:1:40 by weight. The diodes were separated from the field region by a 100 μm wide annular ring. The structure of these diodes were similar to those reported by Ioannou *et al.* [3]. The infinitely large area of the field-region ensured an adequate 'back contact' with required current handling capability. A measurement of I-V characteristics between the active device and the field region was conducted using an HP 4145A Semiconductor Parameter Analyzer. Current-voltage measurements as a function of temperature between 25°C - 150°C were obtained for the diodes on NCSU 870626/1 (since these diodes did not exhibit ohmic conduction at low biases), in order to establish whether thermionic emission was the prevailing conduction mechanism. This procedure was also expected to yield the barrier height and the modified Richardson's constant [11]. However, at temperatures of 50°C and above, ohmic conduction at low forward biases was observed indicating the non-thermionic character of the contact diodes.

RESULTS

The current-voltage characteristics of the metal-semiconductor contact diodes fabricated in β-SiC on nominal (100) and off-axis (100) silicon substrates are shown in Fig. 2. The linear plots in Fig. 2 (a) show asymmetric (rectification) behavior. The diodes in films deposited on the nominally (100) oriented substrates have higher reverse currents. The semi-logarithmic plots of the measured data are shown in Fig. 2 (b). Values of n range between 1.23 and 3.5. No improvement in the n values was obtained when the measured I-V data was corrected for the effective series resistance of the contact diodes. An effective resistance of 125 Ω was obtained from I-V measurements on $TaSi_2$ metallized representative samples of β-SiC having the same active area as the Au contact diodes. Tantalum silicide forms an ohmic contact on n-type β-SiC with a contact resistance of 2.0×10^{-2} Ω-cm^{-2}[12].

In silicon junction devices at the early stages of the technology, surface recombination and surface channel effects resulted in n values greater than 2 [13]. In the present β-SiC material, studies of MOS devices indicate that the surface is reasonably well-controlled, permitting the fabrication of high-quality MOS transistors in the material [14]. The observed low reverse currents in the off-axis films are considered to be an indication of the absence of any significant surface leakage component. Although the role of the surface in determining the characteristics of the Au-contact diodes is not clear, it appears that under identical conditions of surface preparation and metal deposition the observed effects and differences in the various films studied are bulk-dominated.

The high values of n indicated a mechanism other than thermionic emission dominating current transport in these devices. An ohmic slope at low biases (0.01V-0.1V), as seen in the logarithmic plots of Fig. 2 (c), is a clear indication of non-thermionic behavior. Features in the I-V characteristics which strongly indicate SCLC conduction in the presence of deep-level states became evident at higher biases(1-5V). The diode in films deposited on off-axis substrates also exhibit ohmic behavior at an elevated temperature of 50°C, but not usually at room temperature. The exceptions are discussed later in this section.

In the nominal (100) plot shown in Fig. 2 (c), the transition from an ohmic regime to a sharply rising current regime is an indication of the presence of deep traps. Normally a sharp rise to a true SCLC level is obtained when all the deep traps are filled. From the estimated value of V_{TFL} given by Eqn. (1) (see Fig. 2 (a) and Fig. 3, plot 1), the concentration of unoccupied states, p_{to} is obtained. The effective carrier concentration, n_o, is obtained from Eqn. (2). The approximate location of the deep-level states is at the quasi-Fermi level determined by n_o.

In the diodes fabricated in films on off-axis substrates, the current at low forward biases is independent of bias as shown in Fig. 2 (c). The voltage at which the sharp rise in current occurs is taken as V_{TFL}. A given choice of V_{TFL} determines the value of p_{to}, but the position of the deep-level is primarily determined by the slope of the sharply rising regime in current.

A single discrete deep level is normally observed in the diodes in the off-axis material. In the 2° off-axis material, NASA 816/4, the deep level is located at 0.49 eV and in the 4° off-axis, NCSU 870626/1, 0.57 eV below the conduction band with respective concentrations of unoccupied states of 5.0×10^{15} and 5.2×10^{15} cm^{-3}.

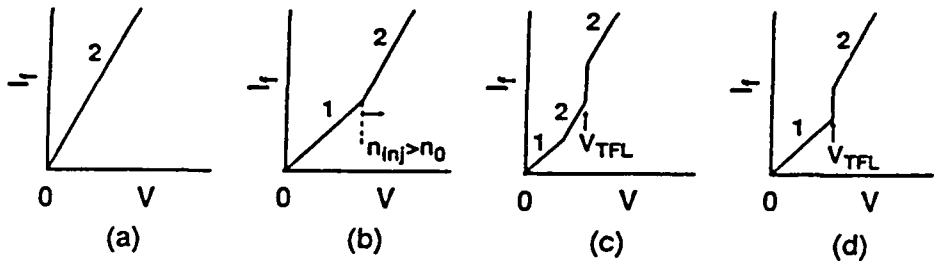

Fig. 1. Logarithmic dependence of current on voltage for: (a) Ideal SCLC conduction in an insulator. (b) Trap-free insulator with thermally generated free carriers. The slope changes from 1 to 2 when the injected carrier density exceeds the free carrier density. (c) An insulator with shallow traps and free carriers. (d) An insulator with deep-traps and thermal carriers.

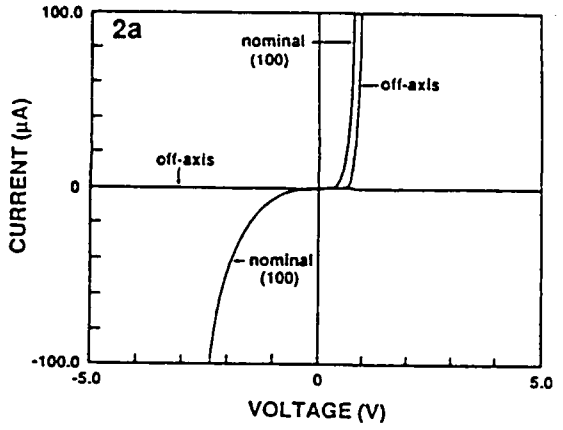

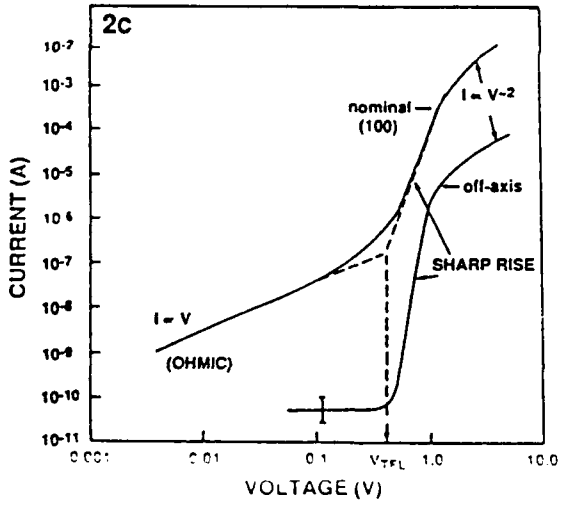

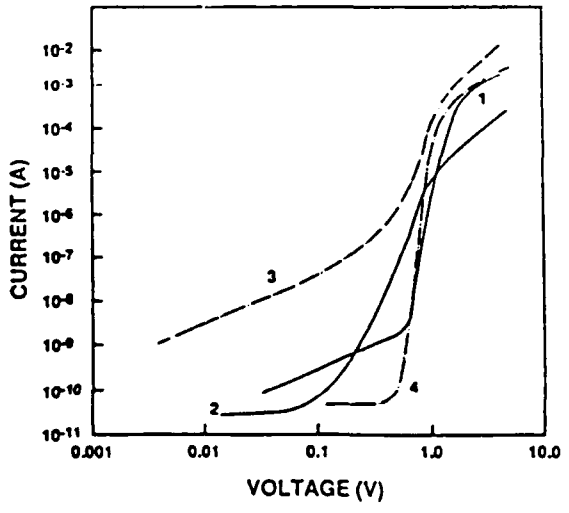

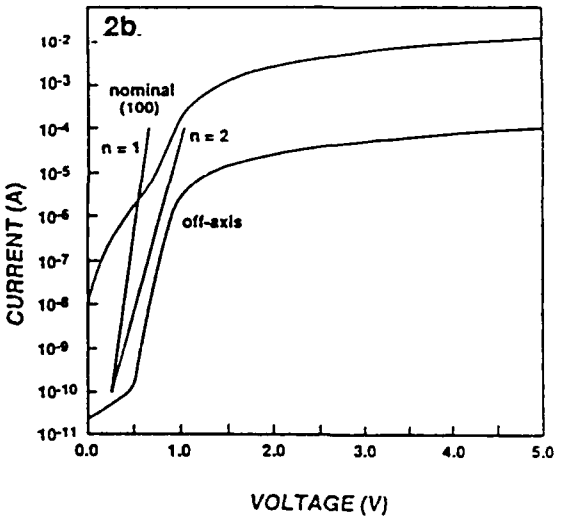

Fig. 2. (a) Linear plots of I-V characteristics for Au/β- SiC diodes on nominally (100) oriented (NASA 816/2) and off-axis <100> oriented (2° toward <011>) (NASA 816/6) silicon substrate. (b) Semilogarithmic plots of the forward characteristics presented in (a). (c) Logarithmic plots of the forward characteristics presented in Fig. 1. (a). Error bar represents maximum noise amplitude at low currents

Fig. 3. Logarithmic plots of the forward characteristics of different diodes showing effects of localized nonuniformities in the carrier concentration and deep-level contributions. (1): 4° off-axis (100) Si (NCSU 870715), shows effect of higher carrier concentration than normal. (2): 2° off-axis (100) Si (NASA 721/6), shows effects of two closely located deep-levels. (3) Nominal (100) Si (NASA 816/2). (4) 4° off-axis (100) Si (NCSU 870626/1).

In a number of diodes in films on the off-axis substrates, a change in slope is observed at the end of a sharply rising current regime, as shown in Fig. 3, plot 2. This change in slope is interpreted to be due to the filling of two sets of closely located deep level traps. In NASA 721/6 these traps are 0.33 eV and 0.4 eV below the conduction band with concentration of unoccupied states of 1.2×10^{15} and 2.5×10^{15} cm^{-3}, respectively. A small number of diodes in 8707/5 also showed an ohmic regime at room temperature, as shown in Fig. 3, plot 1. Nonuniformities in defect distribution and carrier concentrations are suspected to be the origin of these observed features. At low forward biases, diodes fabricated in films on nominal (100) substrates conduct a much higher current than those on off-axis substrates. In a number of cases, an ohmic regime is initially observed (NASA 816/2) and the rise in current following V_{TFL} is not very sharp. In this case, $I \propto V^3$. This is considered to be an indication of smearing of the states due to electrical activity of crystallographic defects in the material [14]. However, for the simple analysis using Eqns. (1) and (2) only one discrete level is considered. In NASA 816/2, this level is located at 0.26 eV below the conduction band with a concentration of unoccupied states of 6.6×10^{15} cm^{-3} , whereas in NCSU 870130 a similar level is located 0.32 eV below the conduction band with 3.8×10^{15} cm^{-3} unoccupied states. When the shallower distributed traps are filled, the current rises sharply, and the characteristics are dominated by a deeper level at 0.38 eV in both NASA 816/2 and NCSU 870130 with concentration of unoccupied states as 3.8×10^{15} and 3.0×10^{15} cm^{-3}, respectively. In NCSU 870130, the current initially is proportional to $V^{1.6}$. This super-linear behavior appears to be due to an exponential distribution of traps. A value of N_o of 3.1×10^{16} cm^{-3} eV^{-1} is obtained with eqn. (3) using the following: $\Delta = (m - 1)kT = 0.0156$ eV, $I = 1 \times 10^{-9}$A, $V = 0.054$V, $A = 7.8 \times 10^{-5}cm^2$, $\mu = 200$ cm^2/V sec, and $N_c = 1.5 \times 10^{19}$ cm^{-3}. The slope of the SCLC part of the I-V characteristics following trap-filling varies from 1.5 to 1.9. It is probable that a resistive component or high-level injection effects degraded the ideal slope of 2.0.

A previous microstructural study established the presence of antiphase domain boundaries (APB's) in the heteroepitaxial β-SiC films deposited on nominal (100) Si substrates. These faceted boundaries also contain a high density of dislocations. These defects are mostly eliminated by depositing β-SiC on off-axis (100) oriented Si substrates [9,15]. The density of defects other than APB's, mainly stacking faults and microtwins, is comparable in heteroepitaxial films grown on both nominal and off-axis substrates. The high density of deep level states distributed in energy below the conduction band is attributed to the electrical activity of the APB related defects. The observed deep-level states located 0.57 eV below the conduction band-edge in films grown on off-axis substrates appear to be native to β-SiC considering its close agreement to the theoretically predicted state associated with isolated Si vacancy at 0.61 eV [16].

CONCLUSIONS

Gold deposited on heteroepitaxial β-SiC films grown both on nominal (100) and off-axis (100) silicon forms rectifying contact diodes. Very low reverse leakage currents are observed in diodes fabricated in films grown on off-axis silicon substrates. Although the I-V and C-V characteristics indicate the presence of a barrier, the I-V characteristics are dominated by bulk effects rather than by thermionic emission over the barrier.

Logarithmic plots of the I-V characteristics in the forward direction indicate space charge limited current conduction through the active volume of the devices. The β-SiC films grown on nominally (100) oriented substrates show the presence of two deep levels located between 0.26 eV and 0.38 eV below the conduction band edge. In some films on nominal (100) substrates, the I-V characteristics are also influenced by some additional traps which are exponentially distributed in energy with a maximum occurring at the conduction band edge.

In contrast, β-SiC films deposited on off-axis substrates have only one deep level located approximately 0.49 eV below the conduction band edge for the 2° off (100) substrates and 0.57 eV for the 4° off (100) substrates. The shallower distributed deep states in the β-SiC on nominal (100) silicon substrates are attributed to the presence of antiphase domain boundaries in these films. The deep-level states located 0.57 eV below the conduction band-edge in films grown on

off-axis substrates appear to be native to β-SiC considering its close agreement to the theoretically predicted state associated with an isolated Si vacancy at 0.61 eV. The shallower discrete levels observed are believed to be related to crystallographic defects other than APBs.

ACKNOWLEDGEMENTS

The program was partially supported by NASA Lewis Research Center (Grant No. NAG 3-782) and the Office of Naval Research (Contract No. N00014-85-K-0182 P005). Stimulating discussions with Dr. R. W. Hamaker, Department of Electrical and Computer Engineering, North Carolina State University, are highly appreciated.

REFERENCES

1. J.W. Palmour, H.S. Kong, and R.F. Davis, Appl. Phys. Lett. **15**, 2028 (1987).
2. B.J. Baliga, IEEE Electron Device Lett. **EDL-1**, 200 (1989).
3. D.E. Ioannou, N.A. Papanicolaou and P.E. Nordquist, Jr., IEEE Trans. Electron Devices, **ED-34**, 1694 (1987).
4. V. Ozarrow and R.E. Hysell, J. Appl. Phys. **33**, 3013 (1962).
5. J.A. Edmond, K. Das and R.F. Davis, J. Appl. Phys. **63**, 922 (1988).
6. M.A. Lampert and P. Mark, "Current Injection in Solids", (Academic, New York, 1970).
7. H.P.D. Lanyon, Phys. Rev. **130**, 134 (1963).
8. P. Liaw and R.F. Davis, J. Electrochem. Soc. **132**, 642 (1985).
9. H.S. Kong, Y.C. Wang, J.T. Glass and R.F. Davis, J. Mat. Res. **3**, 521 (1988).
10. J. A. Powell, L.G. Matus and M.A. Kuczmarski, J. Electrochem Soc., **134**, 1558 (1987).
11. S. M. Sze, "Physics of Semiconductor Devices", 2nd ed. (Wiley, New York, 1981).
12. J. A. Edmond, J. Ryu, J. T. Glass, and R. F. Davis, J. Electrochem. Soc., **135**, 359 (1988).
13. C-T Sah, IRE Trans. Electron Devices, **ED-9**, 94 (1962).
14. J. W. Palmour, H. S. Kong, and R. F. Davis, J. Appl. Phys. **64**, 2168 (1988).
15. J.A. Powell, L.G. Matus, M.A. Kuczmarski, C.M. Chorey, T.T. Cheng and P. Pirouz, Appl. Phys. Lett. **51**, 823 (1987).
16. Y. Li and P. J. Lin-Chung, Phys. Rev. B, **36**, 1130 (1987).

Distribution List

Address	No. of Copies
Mr. Max Yoder Office of Naval Research Electronics Program – Code 1114 800 North Quincy Street Arlington, VA 22217	2
Ms. Marta Morris ONR Resident Representative Office of Naval Research 1314 Kinnear Road Columbus, OH 43212-1194	1
Director, Naval Research Laboratory ATTN: Code 2627 Washington, DC 20375	6
Defense Technical Information Center Building 5 Cameron Station Alexandria, VA 22314	14
Dr. G. L. Harris Electrical Engineering Howard University Washington, DC 20059	1
Dr. J. Anthony Powell NASA Lewis 2100 Brookpart Road Cleveland, OH 44135	1
Dr. Ray Kaplan Code 6834 Department of the Navy Naval Research Laboratory Washington, DC 20375	1
Dr. P. Klein Naval Research Laboratory Code 6820 Washington, DC 20375	1
Dr. Steve Bishop Naval Research Laboratory Code 6870 Washington, DC 20375	1
Dr. J. Parsons Hughes Research Laboratory 3011 Malibu Canyon Road Malibu, CA 90265	1
Dr. J. Zeidler Naval Ocean Systems Laboratory Electronics Division - Code 7601 San Diego, CA	1